

Review of performance metrics of spin qubits in gated semiconducting nanostructures

Peter Stano^{1,2} and Daniel Loss^{1,3,4}

¹*RIKEN Center for Emergent Matter Science (CEMS), Wako, Saitama 351-0198, Japan*

²*Institute of Physics, Slovak Academy of Sciences, Dubravská cesta 9, 845 11 Bratislava, Slovakia*

³*RIKEN Center for Quantum Computing (RQC), Wako, Saitama 351-0198, Japan*

⁴*Department of Physics, University of Basel, Klingelbergstrasse 82, CH-4056 Basel, Switzerland*

(Dated: August 4, 2022)

This Technical Review collects values of selected performance characteristics of semiconductor spin qubits defined in electrically controlled nanostructures. The characteristics are envisioned to serve as a community source for the values of figures of merit with agreed-on definitions allowing the comparison of different spin qubit platforms. We include characteristics on the qubit coherence, speed, fidelity, and the qubit-size of multi-qubit devices. The focus is on collecting and curating the values of these characteristics as reported in the literature, rather than on their motivation or significance.

I. SCOPE, FORMAT, AND AIM OF THIS REVIEW

Spin qubits are among platforms pursued to serve as quantum computing hardware. In this Technical Review we focus on spin qubits hosted in semiconducting nanostructures controlled and probed electrically. Their prospect for scalability stems from their compatibility with modern silicon industrial fabrication. Even restricted to gated nanostructures, the field of spin qubits is vast. There is a host of variants on the sample material and structure, device design, or qubit encoding. Although this versatility in the qubit types is beneficial for overcoming possible roadblocks, it also makes comparison of different spin qubits difficult. The main motivation for this Technical Review is to provide a basis for such a comparison and for an assessment of the progress of various spin-qubit types over time. We believe that for such tasks, a reliable database of figures of merit normalized to common definitions is of primary importance, and this is what we provide here.

The restriction to gated nanostructures suggests what is not covered in this Technical Review. We do not include other than solid-state qubits; within the solid-state, we do not include superconducting qubits and qubits based on optically-accessed impurities and self-assembled dots. We also skip qubits based on the spin of atomic nuclei, that is, hyperfine-spin qubits. Even though spin-related, we sacrifice these possible extensions to keep the review manageable in length and in the time of preparation. However, we include some characteristics of charge qubits, that is qubits with states encoded into the charge degree of freedom of a confined particle. One reason is that often the experimental devices are identical for both spin and charge qubit experiments. Another reason is that there are configurations where the spin and charge degrees of freedom are hybridized and tunable. With the character continuously tunable from fully spin- to fully charge-like, it would be difficult to decide objectively which cases to include and which ones not. Finally, we point out that this Technical Review is not meant as an overview of the physics of spin qubits, such as principles of their operation and measurements, the decoherence channels, and so on. The reader interested in these aspects can consult, for example, Refs. [46, 93, 98, 144, 154, 217, 219, 246, 252, 253, 272, 286, 292]. In particular, we point out the recent extensive review in Ref. [34] as an excellent complement, cover-

ing the aspects intentionally omitted here.

The core of this Technical Review are the plots and tables of selected qubit characteristics on the qubit coherence, operation speed, operation fidelity, quality factors, and the size of multi-qubit arrays. The related quantities are defined, and their values collected from the literature given, in Sections II–VI, respectively.

We hope that this Technical Review will become useful and used as a database for spin-qubit characteristics. To this end, it is crucial that the database is up-to-date, error-free, and contains relevant quantities. These goals can hardly be met without an active participation of the spin-qubit community. We encourage the members of the community to provide us with feedback on any errors, omissions, or suggestions for changes.

A. We present a database of values

Though not necessarily of a concern for the reader, we note that the presented collection reflects a formally defined database. This fact might be useful to understand certain nomenclature, details of the presentation, and requirements on the included values and possible extensions. Let us briefly explain these aspects.

Every ‘value’ given in this Technical Review belongs to a certain ‘attribute’. These two basic elements define the database and constitute keywords with precise meaning. The ‘attributes’ are used as headers in tables and axes labels in plots. For example, the second line of Table I contains the value ‘LD/e’ under the attribute ‘Qubit’. It means that the corresponding experiment used a qubit encoded into the spin of an electron. Whereas most of the attributes are self-explanatory, they are additionally listed alphabetically, together with their definitions, in Appendix D. To draw attention to their special role, we mark the attributes with single quotation marks. This distinction is done only in the this (first) section and Appendix D.

B. Spin-qubit types, device geometries, material choices

Before we discuss specific characteristics, we comment on their common aspects. These stem from the fact that each ‘value’ inherits a set of characteristics from the publication it was reported in and the experimental device it was measured with. We describe these common aspects below.

Every value given in this Technical Review (such as a coherence time of 10 ns) is a result of a measurement with a specific device and qubit type, reported in a published reference.¹ This means, first of all, that we include only numbers explicitly stated and directly measured. We do not include extrapolations to other conditions or materials. Also, we do not usually derive the values ourselves even if it would be possible. For example, if the reference gives the operation time and the dephasing time, but does not state the quality factor, we do not evaluate the latter ourselves. However, if a quantity is discussed and presented as a figure (for example, the operation time implied from oscillations displayed by a resonantly driven qubit), we might include a value read-off from the figure. In such cases, the table entry contains a ‘Note’ with keywords (*derived*) or (*estimated*), which are explained in Appendix D. With this requirement, every value given in this Technical Review should be easy to find using the reference, given under the attribute ‘Reference’, and within the reference as described by the attribute ‘Source’. An example of the latter is say “page 4 and Fig. 1b”. One possible difference between the value given here and in the original work is normalization. In that case, a ‘Note’ explains how the value was converted. Any additional information, for example, alerting on an unusual configuration or a specific method used in the experiment, is also given as a ‘Note’.

The second group of common characteristics concerns the details of the qubit. We found it useful to categorize the following: the sample material, the geometry of the host, and the qubit type. They belong to the attributes ‘Material’, ‘Host’, and ‘Qubit’, respectively. Whereas the value for material, for example, ‘Si/SiGe’, is self-explanatory,² in some figures we group several different materials under a common tag, such as ‘Si’. Concerning the host geometry, we discrimi-

nate (qubits based on gating) the structures which are (quasi-)‘2D’, for example, a 2D electron gas (2DEG), (quasi-)‘1D’, for example a nanowire, and quasi-zero-dimensional, denoted by ‘imp’, an example being an implanted impurity. Some of these are not clear-cut cases, for example the hut-wires with a flat cross-section [312], or some variants of CMOS devices [298]; nevertheless, we assign both to ‘1D’. Finally, perhaps the largest variation exists among the qubit types. We distinguish the charge carrier: conduction electron, valence hole, and atomic impurity; and the spin-encoding: spin-1/2 (‘LD’), singlet-triplet (‘ST’), and hybrid (‘HY’) qubits. We have not found beneficial to subdivide further the hybrid qubits: everything which is not a spin-1/2 or a singlet-triplet is assigned the value hybrid here. A note might give additional information on the qubit type. The reader would benefit from consulting Appendix D now, to understand the database organization through attributes and values.

C. The choice of values to collect is subjective

A disclaimer is in order here: assigning a single specific value for each characteristic is necessary for a meta-analysis such as done here. However, converting an experimental investigation into a single number is inevitably a drastic compression. The choice of the value to quote requires subjective judgement: in a typical experiment, the value of a given figure of merit is seldom a unique value, but rather spans a range, sometimes a very large range, such as several orders of magnitude. We tend to take the most beneficial values, but it does not mean we simply take the largest one. Especially when an experiment presents a set of values for different characteristics, we try to choose a representative set measured at a common setting. For example, in an experiment with three qubits, where each is measured for relaxation, dephasing, and the echo coherence time, we do not simply take the largest value seen among all experiments. We choose a qubit and quote the three numbers for this particular qubit. We proceed similarly when several characteristics are measured under various conditions. Our overall approach is to adopt values which are mutually consistent (such as the coherence time and the operation speed) as much as possible. Nevertheless, we warn the reader that all such choices are largely subjective. The final authority to judge the value meaning and importance is the original reference itself.

D. What we do and what we do not

We would like to reiterate our goals, since this work is not a standard review. Our primary target is to provide a database of figures of merit and make its content accessible. This includes downloadable tables and figures, including interface to produce figures and tables according to user’s design, and a public repository including the environment for feedback and discussions. This content is accessible through a public data depository [1]. The repository includes detailed instructions on how to provide feedback, though writing an email directly

¹ Note that whereas we count arXiv preprints as ‘published references’, the absolute majority of the entries are from peer-reviewed journal publications. The current bibliography for the database contains 12 arXiv preprints, only two of which were uploaded before year 2021, Refs. [41, 106].

² Qubits based on silicon-oxide structures is one case which needs a comment. A unique identification in this Technical Review for such structures is the value ‘Si/SiO₂’ of the attribute ‘Material’. The attribute ‘Host’ is typically also straightforward to assign, being either ‘2D’, for example for an epilayer, or ‘1D’ for finFETs or structures denoted as nanowires by their authors. One can often find further specifications for such devices, such as: [complementary-]metal-oxide-semiconductor([C]MOS), silicon-on-insulator(SOI), field-effect-transistor(FET), foundry-compatible, and similar, including their combinations. These specifications hint to the fabrication details and the degree of compatibility with the industrial silicon technology. However, they are sometimes used interchangeably, even within one laboratory. Since the fabrication details are not our focus, we do not include such additional specifications even if given in the original work.

to the corresponding author is also encouraged. However, giving subjective view of the spin-qubit field in the form of qubit-suitability judgements, interpretations, outlooks, summaries, recommendations, predictions, and similar, is not our target and the reader will not find much of such type of content here.

After these preliminaries, we will now present the spin-qubit figures of merit published until the end of year 2021.

II. COHERENCE TIMES

The largest amount of published data on spin qubits refers to their coherence times. Qualitatively, a coherence time extracted in an experiment has the meaning of a time during which state oscillations stemming from quantum mechanical superpositions can be observed.

A. Definition and meaning of experimentally-extracted coherence times

Additional specifications of the conditions under which such a superposition decay is observed lead to several variants of the coherence time. The inhomogeneous dephasing time T_2^* implies a Ramsey experiment, meaning the following se-

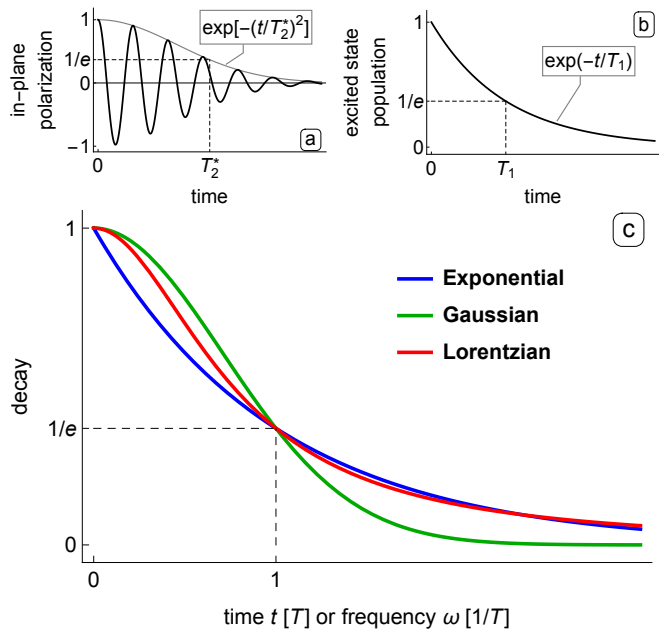


FIG. 1. Typical decay-curve envelopes. (a) Oscillations with a Gaussian decay envelope, typically appearing in Ramsey experiments measuring the inhomogeneous dephasing time T_2^* in the time domain. (b) Exponential decay typical for relaxation processes, reflecting the relaxation time T_1 . (c) Three curves are plotted for comparison. They are normalized to reach value 1 at the x-axis parameter equal to 0 and value $1/e$ at the x-axis parameter equal to 1. The Gaussian and Lorentzian, the Fourier transforms of the two envelopes given in (a) and (b), arise in probing the decay in the frequency domain. In that case, the horizontal axis on the figure is the frequency ω , see Eq. (7).

quence: the qubit is initialized to a state polarized within the equatorial plane of the Bloch sphere, for example along the x axis, and is left to precess freely for time t after which the in-plane polarization is measured; the evolution time t is varied, and for each value of t the sequence is repeated to gather enough statistics. A typical time-trace of the averaged signal fits a cosine with a Gaussian decay envelope $f(t)$,

$$P_x(t) = f(t) \frac{1 + \cos \omega t}{2} = \exp [-(t/T_2^*)^2] \frac{1 + \cos \omega t}{2}, \quad (1)$$

where ω is the precession frequency. This curve is plotted in Fig. 1(a).

The decay of a spin qubit in a Ramsey experiment described by Eq. (1) is often due to fluctuating nuclear spins. The strong effect of nuclei on the spin coherence was predicted in Refs. [139, 189] and confirmed experimentally in Ref. [231]. Because the dynamics of nuclear spins is slow, one can protect the spin-qubit coherence using the spin-echo techniques developed in the field of Nuclear Magnetic Resonance [266]. The simplest protecting protocol is the Hahn echo[96]. It means that the spin is flipped (rotated around an in-plane axis by angle π) in the middle of the free evolution, at time $t/2$, of the described Ramsey sequence. The coherence time measured under a Hahn echo is denoted in this Technical Review as T_2^{Echo} . Already in Ref. [231], the Hahn echo prolonged the spin qubit coherence by a factor of a hundred. There are more elaborate protocols, applying more echo pulses, which prolong the coherence further. Although there are several different variants of such protocols [2], here we assign any sequence containing more than a single echo under a common category, denoting the coherence time as T_2^{DynD} . A typical member of this family is the Carr-Purcell-Meiboom-Gill (CPMG) protocol, with which the coherence of a singlet-triplet spin-qubit was prolonged to almost a millisecond in Ref. [179].

All these protocols aim at prolonging the coherence of an idling spin qubit. The decay of a driven spin, meaning the decay of coherent Rabi oscillations, is another important time scale which is often reported. It is denoted here as T_2^{Rabi} . The understanding that the decay of coherence of a driven and idling spins can strongly differ goes back to Alfred Redfield (Ref. [238]) and has been demonstrated with a spin qubit [163]. Finally, we include also the time T_1 , called the relaxation time, to denote the decay of qubit energy. That it is a different type of process is denoted by its subscript ‘1’ as opposed to ‘2’ for the times describing the decay of phase. These subscripts refer to the notation usual in Bloch equations, where these two processes with distinct physical origin are called the ‘longitudinal’ and ‘transverse’ relaxation, respectively [15]. See Appendix A for the notation of various decay times.

Whereas we attributed the Gaussian decay in Eq. (1) to nuclei as an example, the coherence-times nomenclature applies in the same way, irrespective of the noise source. Low-frequency charge and high-frequency phonon noise, influencing the spins through spin-orbit interactions, are most relevant. More importantly for the coherence-time measurement, the functional form of the envelope $f(t)$ in Eq. (1) is often different from the Gaussian. Another typical case is an exponential,

$$f(t) = \exp(-t/T_1). \quad (2)$$

We have suggestively used T_1 for the time scale, as the energy relaxation is often described by such an envelope. The function is plotted in Fig. 1b. Because of the superimposed oscillations in Eq. (1), it is not easy to discriminate between the exponential and Gaussian decay envelopes. Although the functions differ strongly in their exponential tails, these tails are basically never resolvable, due to measurement errors and statistical fluctuations. If the discrimination is possible, it is based on the different shape of the two functions at small times: linear versus quadratic.

The discrimination becomes even more difficult in experiments where the qubit is probed in the frequency domain. A typical example is recording the amplitude and phase response of a resonant electrical circuit which the qubit is a part of. Both of these quantities are parametrized by the circuit reflection coefficient, a complex number. A standard result for it reads³

$$r(\omega_p) = \frac{\omega_r - \omega_p + i\kappa/2 + \chi(\omega_p)}{\omega_r - \omega_p - i\kappa/2 + \chi(\omega_p)}. \quad (3)$$

Here, ω_p is the frequency of the signal probing the circuit, ω_r is the circuit resonant frequency, κ is the circuit-field decay rate, and χ is the qubit response function, proportional to the Fourier transform of the decay envelope $-if(t)$. For a qubit described by an exponential decay, the latter becomes[53, 74]

$$\chi(\omega_p) = -\frac{g^2}{\omega_q - \omega_p - i\Gamma_2} D, \quad (4)$$

with $\hbar\omega_q$ the energy difference of the qubit excited and ground states, g the qubit–circuit coupling, D the difference of the population probability of the qubit ground and excited state, and $\Gamma_2 = \Gamma_1/2 + \Gamma_\varphi$ is defined in Appendix A. These formulas are also valid when the qubit itself is driven, the so-called two-tone spectroscopy[250]. In that case, all parameters on the right hand side of Eq. (4) should be replaced by the corresponding quantities in the rotating reference frame [118]. From Eq. (3), one can express the fraction of the reflected power, $|r|^2$, through the following formula

$$|r(\omega_p)|^2 - 1 = \frac{2\kappa \text{Im}\{\chi\}}{\left(\frac{\kappa}{2} - \text{Im}\{\chi\}\right)^2 + (\text{Re}\{\chi\} - \omega_p + \omega_r)^2}. \quad (5)$$

In the dispersive regime where $|\omega_p - \omega_r|$ is the largest frequency, the denominator can be approximated by a constant and Eq. (5) reduces to a constant times $\text{Im}\{\chi\}$. Scanning the probe frequency ω_p around the resonance $\omega_p = \omega_q$, one observes a dip in the circuit steady-state response⁴, and the width of the dip gives $2\Gamma_2$. The articles give the dip width as either the full or half width at half maximum (FWHM or HWHM) in frequency (and not angular frequency) units, or, in more

general scenarios, Γ_2 as one of the fit parameters in fitting the data to Eq. (5) or its analogs. In these cases, we evaluate the inhomogeneous dephasing time using

$$T_2^* = (\Gamma_2)^{-1} = (2\pi\Delta f_{\text{HWHM}})^{-1}. \quad (6)$$

Coming back to the possibility of discriminating between the decay envelopes, we now consider the Fourier transforms $\chi(\omega)$ for the above two examples. Whereas the Fourier transform of a Gaussian is a Gaussian, the exponential transforms into a complex function with the imaginary part a Lorentzian,

$$\text{Gaussian } f(t) \xrightarrow{\text{F.T.}} \chi(\omega) = -i \exp(-\omega^2 T^2/4), \quad (7a)$$

$$\text{Exponential } f(t) \xrightarrow{\text{F.T.}} \chi(\omega) = \frac{-\omega T - i}{\omega^2 T^2 + 1}, \quad (7b)$$

In these equations, we Fourier transformed (F.T.) Eqs. (1) and (2) multiplied by $-i$, normalized the results to the same value at zero frequency, and dropped the time-scale subscripts. To discriminate the two cases given in Eq. (7) in the frequency domain is even more difficult than in the time domain, since both Gaussian and Lorentzian are quadratic at small frequencies. Compared to the time domain, now the two functions differ more strongly at their tails (that is, for large ω), with algebraic and exponential decay, respectively. However, as already stated, these tails are seldom accessible with the required precision. The three envelope functions discussed so far are plotted in Fig. 1(c) for comparison.

The reason for discussing the discrimination between different functional forms of the decay envelopes is that it hints to the origin of the noise causing the decay. A minimal description of noise is to give its autocorrelation function, either in the time or frequency domain. If it is the latter, the function is called the noise spectrum. The form of the noise spectrum decides what will be the decay envelope. Noises with different physical origins, for example nuclear spins versus charge impurities, will have different spectra. The functional form of the decay envelope then can serve as an alternative to obtaining the noise spectrum, in hinting on the possible origin of the dominant noise affecting the qubit. Finally, we note that the above three possibilities, Gaussian, exponential, and Lorentzian, are not the only ones. For example, going to the next order in the calculation reveals that algebraic tails in the decay exist [118]. Algebraic tails were also obtained in calculations considering the backaction of the qubit on its environment giving rise to non-Markovian behavior [77].

To sum up the discussion, the coherence times are typically extracted from fits to simple functional forms. Some are given above, and there are more, such as the ‘stretched exponential’ used to fit data from dynamical-decoupling sequences.⁵ The true decay envelope is a complicated function, which can

³ We copy Eq. (A15) from Ref. [74]. Ref. [53] gives an analogous result in its Eq. (57).

⁴ Since normally $D > 0$. However, the population inversion, $D < 0$, is also possible, see Ref. [104]. It would give a peak in $|r(\omega_p)|$, instead of a dip.

⁵ The standard result is Ref. [59], which derived $\log f(t) \sim (t/T_2)^{1+\alpha}$ as

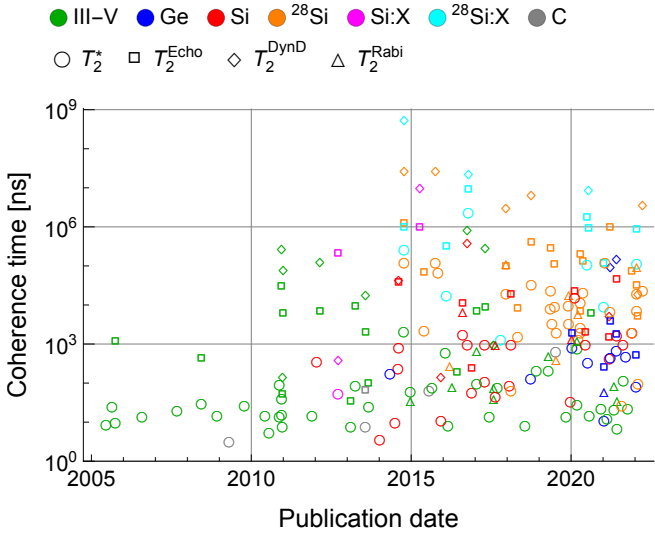


FIG. 2. Spin coherence times according to the publication date. The color shows the device material and the symbol indicates the coherence type as given in the legend. The plotted data are values from Table I excluding the data on the relaxation time T_1 .

hardly be parameterized by a single number. A typical fit returns the time scale over which the envelope decays to a fraction of its initial value, for example, $1/e$. This operational definition should be the first guess on the meaning of a coherence time in the tables we give. Not much is implied about the functional form itself, let alone the decay long-time tails.

The data on coherence times are listed in Table I. We additionally present it here in figures, discussing them shortly. We split the figures to two groups, separating the charge qubits, the states of which do not rely on the spin degree of freedom in any way, from qubits which rely on spin at least to some degree. We start with the latter group.

B. Measured coherence times of spin qubits

The coherence times of spin qubits are given in Fig. 2. The values had started at around 10 ns inhomogeneous dephasing time in early experiments with qubits in GaAs. Echo techniques can extend the coherence by orders of magnitudes, as can a different material choice. The coherence times published during the year 2021 span six orders of magnitude, depending on the qubit type, material, and protection measures.

To examine the influence of some of these factors, we plotted separately each type of coherence in Fig. 3. The separation allows us to group additionally the values according to the qubit type, being the discrete category on the horizontal

the envelope for decay under a generic dynamical-decoupling sequence assuming noise spectrum $1/f^\alpha$. In fitting the experimental data in GaAs, Ref. [186] found that a more robust way is to fit the observed decay time to $T_2 \propto n^\gamma$, where n is the number of echos and, for the CPMG sequence, the noise-spectrum exponent is related to the fit parameter γ by $\alpha = \gamma/(1-\gamma)$.

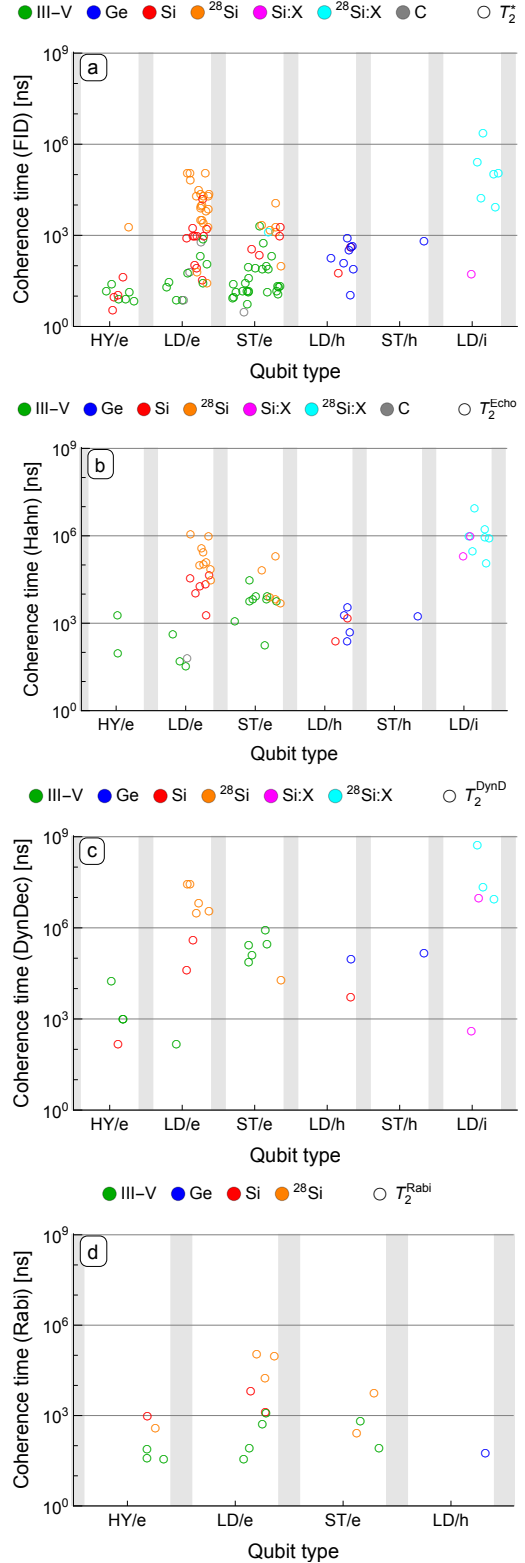


FIG. 3. Spin coherence times. The panels display the data from Fig. 2 split to the four panels according to the coherence type, denoted in the legend, from the set: inhomogeneous dephasing T_2^* , Hahn echo T_2^{Echo} , dynamical decoupling T_2^{DynD} , and Rabi decay T_2^{Rabi} . In each panel, the horizontal axis uses the qubit type as a discrete category, displacing the points according to their publication date: more recent data are shifted to the right within the non-shaded area which is normalized to the year span 2003-2021. All vertical-axes ranges are the same and the point colors show the material.

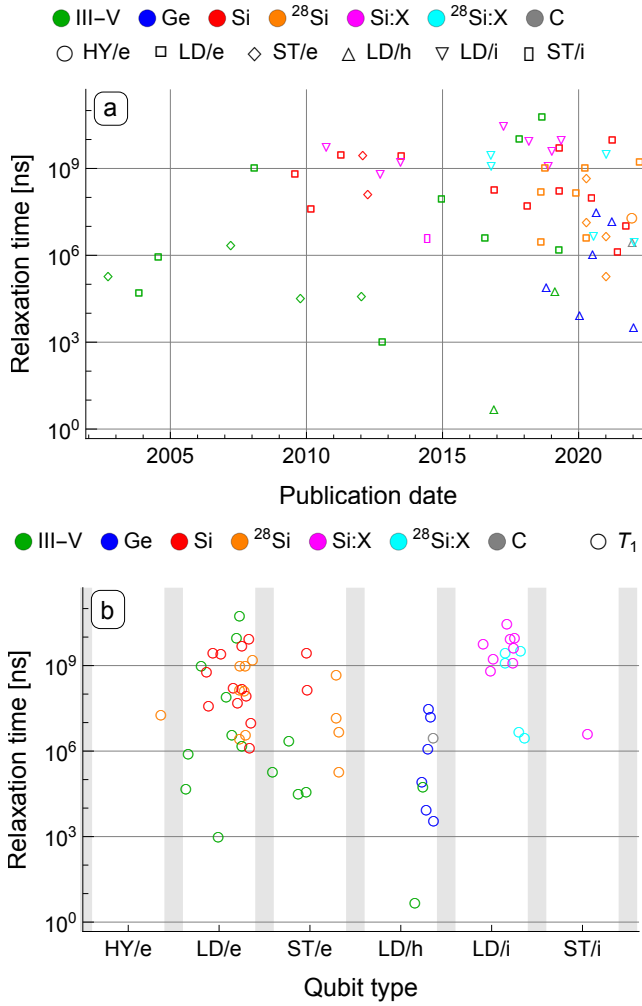


FIG. 4. Relaxation times of spin qubits. Both panels show the same data, the relaxation times from Table I. The datapoint color shows the material. In (a), the horizontal axis shows the publication date and the datapoint symbol shows the qubit type. In (b), the qubit type is on the horizontal axis as a discrete category, whereas the publication date is reflected by shifting the points horizontally, similarly as in Fig. 3.

axis. To reflect the publication date for an easier comparison, we displace the data within each category horizontally. For example, Fig. 3(a) shows that the most recent electron spin-1/2 qubits implemented in purified silicon reach longer coherence times than singlet-triplet qubits, in turn longer than hole qubits. Impurity spins hold record coherence times in each category where data for them exist.

We next turn to the energy relaxation time. For a spin qubit, this time can be made very long by: isolating the qubit from reservoirs, so that the electron does not escape the dot; minimizing its dipole moment, so that the qubit couples weakly to phonons; and decreasing the transition energy, typically using a lower magnetic field, so that the available phase space for the process is reduced [138, 260]. Under these conditions, relaxation times have reached seconds and can be considered not of concern for quantum computing. However, the relaxation

times remain of concern if these conditions are not met: for example, a finite relaxation time of two-electron singlet and triplet states is the main limitation for the spin measurement fidelities [9, 30, 206]. Because of this crucial role, there are numerous values on the relaxation time for (mostly the triplet states of) singlet-triplet qubits, either explicitly reported or implicitly implied in many experiments using Pauli spin blockade for the spin measurement. As the relaxation time in this setting is a by-product of the maximization of the measurement fidelity, rather than a figure of merit maximized itself, we normally do not include singlet-triplet relaxation rates in this Technical Review. We do include a few values, from either early experiments, or when they are the article's main topic.

The reported relaxation times are shown in Fig. 4, plotting the same set of data in two different ways. Figure 4(a) gives them according to the publication date. One can see how the longest-reached times developed: in the first decade, electron one-half spin-qubits were in the lead. Since 2010, impurities took over. Currently, the record is back with a single electron in GaAs, with the relaxation time of one minute [37]. As already noted, while reaching such long times is not directly improving other figures of merit of the qubit, the increase of the record time illustrates the experimental progress with the given qubit platform. Figure 4(b) groups the times according to qubit types, making it easier to judge the progress over the years within each group.

C. Measured coherence times of charge qubits

We end the overview of the coherence times by looking at charge qubits. As already mentioned, we include them even though they implement qubits which do not rely on spin. The reason is a close relation of the devices where the two type of experiments are typically done and of used techniques: for example, the measurement of spin is done indirectly, converting different spin states to different charge states, which are then detected.

All types of coherence times of charge qubits, including the relaxation time, are gathered in Fig. 5. In the three panels of the figure, the same data are shown according to the publication date, the device material, and the coherence type, respectively. One can see several differences compared to spin qubits. First, the relaxation times are often comparable to coherence times, unlike for most spin-qubits where they can be pushed to be by far the longest scale. Therefore, the relaxation is a bigger issue for charge qubits even in single-qubit experiments. Second, unlike for spin qubits, the echo techniques do not prolong coherence substantially. Third, there is much less variation among the data: Despite an upward trend in T_2^* over time, the increase is not dramatic. Since the charge-qubit dephasing time T_2^* is related to charge noise directly, a clear trend would indicate an overall improvement of the available samples and devices concerning the level of charge noise. Finally, as one would expect based on the nuclear-spin noise being irrelevant for charge qubits, there is no apparent difference between devices made in Si and III-V materials concerning charge-qubit coherence.

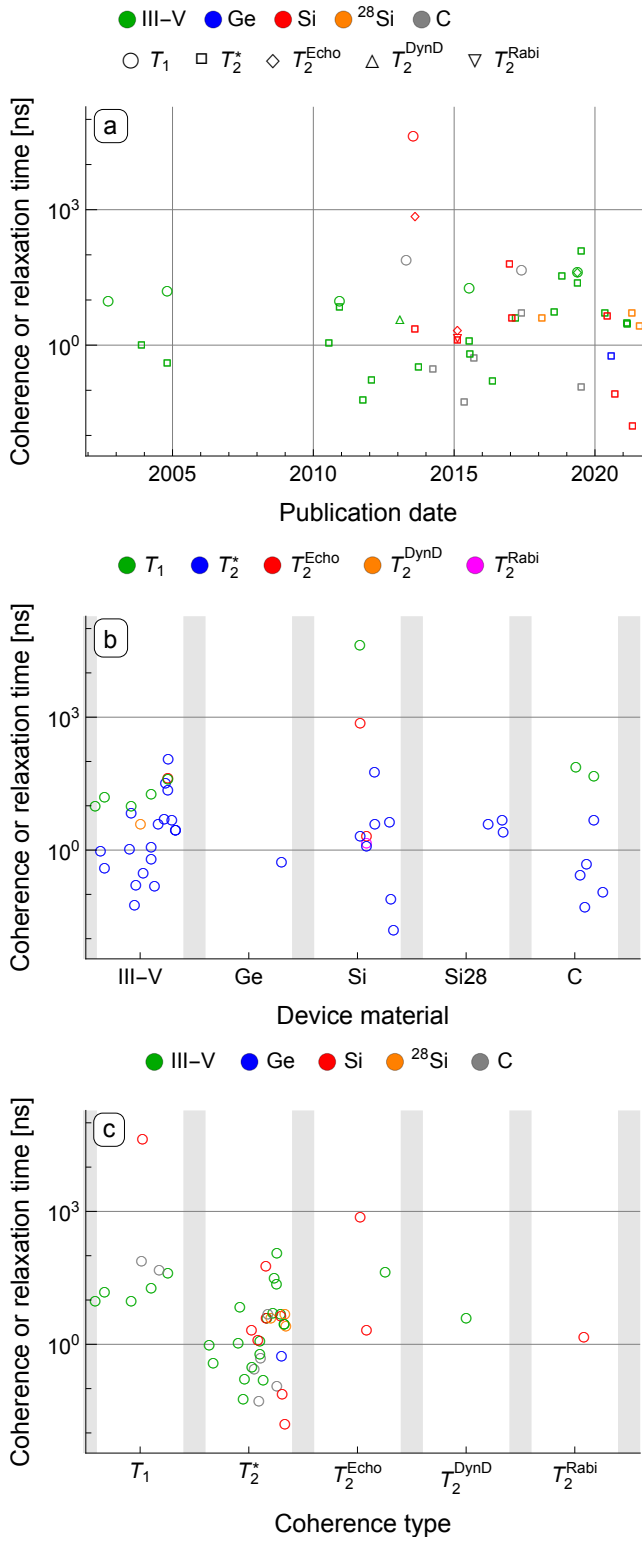


FIG. 5. Charge coherence. Every panel plots the same data, the values from Table II. The panels differ by their horizontal axis, plotting the data according to the quantity given as the horizontal-axis label. Concerning the datapoint symbols and colors, (a) is analogous to Fig. 2. In (b) and (c), the role of the datapoint colors and the horizontal axis is swapped.

III. OPERATION TIMES

The second most abundant data exist on characteristics of spin-qubit operations. We consider the qubit gates, measurements, and initializations as three operation types, treated on equal footing. We are motivated by their actual physical realizations which are similar: all three types of operations are typically implemented by pulsing the system to a specific configuration, or driving it resonantly, for a fixed time. Another reason is that whereas the algorithms considering logical qubits might assign initializations to the beginning and measurements to the end of the algorithm only, physical qubits will need error correction. In this case, the initializations and measurements are used heavily, interspersing the application of gates.

There is an additional attribute introduced in this section, the number of qubits that a given operation involves, '#Qubits'. The typical cases are one-qubit (1Q) and two-qubit (2Q) gates, even though the first three-qubit gate has been already used in an error-correction demonstration [278].

Finally, let us list the operation characteristics. In the next three sections, we discuss, respectively, operation times, a quantitative measure, and operation fidelities and quality factors, two related qualitative measures.

A. The definition of experimentally extracted gate times

The advantage of looking at gate times is that they reveal the natural time-scale for a given qubit and that they can be compared to the coherence times. However, they also have a shortcoming which arises if they are not compared to any coherence time: a fast qubit does not automatically mean a good qubit, since the judgement largely depends also on the coherence time. Conversely, a qubit with extremely long coherence becomes less appealing if the corresponding gates are also extremely slow. This shortcoming, namely a dimensionful quantity having a limited meaning without comparison to other dimensionful quantities, also applies to the coherence times presented in the previous section.

Let us specify the normalization for the operation times. For the measurements and initialization, the definition is straightforward, even though one should also count the preparation if it is a necessary part of the measurement or initialization sequence. More ambiguity exists for gates, since gates are realized as unitary evolutions induced by certain Hamiltonians. A typical signal which is interpreted as a gate being applied looks as in Fig. 1(a). Neglecting for now the decay and taking a single-qubit case, the oscillating signal is due to a unitary evolution such as

$$U(t) = \exp(-i\omega t s_z) \equiv \exp(-i2\pi f t s_z). \quad (8)$$

Here, we used $f = \omega/2\pi$ for the signal frequency and $s_z = \sigma_z/2$ for the rotation generator, with σ_z being the Pauli matrix. At various times, various gates are carried out on the qubit: for $ft = 1/2$, one gets a Z gate, for $ft = 1$ an identity, whereas $ft = 1/4$ gives a $\pi/2$ rotation, often used to prepare coherent superpositions such as $|0\rangle + |1\rangle$. If such a continuous signal

is presented, we define the operation time to be one half of the signal period,

$$T_{\text{op}} \equiv \frac{1}{2f}. \quad (9)$$

In the case of Eq. (8), the value $t = 1/2f$ would be taken as the operation time, and it would correspond to the Z gate, that is a spin rotation by π . Note that this definition is different to the one adopted for the quality factor (see below).

B. Measured values of gate times

Let us now look at the reported values plotted in Fig. 6(a). Since the set of operations is diverse, we present the data with the qubit type as the primary category on the horizontal axis. The data are additionally tagged according to the device material and the number of qubits. The shortest in the set are the times of single-qubit gates on charge qubits, being below 0.1 ns. One can deduce more instances of such short times in the literature than those shown on the figure. The reason is that these values are perhaps not claimed explicitly in the experiments: for charge qubits, the gate speed is limited by the experiment electronics, rather than the qubit itself⁶. The hybrid qubits can reach similar speeds, since they can be tuned into a configuration where they resemble a charge qubit. Arguably, this tunability is their biggest advantage. When they are tuned into a spin-like configuration, their gate (and coherence) times go up. Similarly, a strong direct coupling to the electric field can be exploited also for holes, with gate speeds in hundreds of megahertz seen. Such electric-dipole spin resonance (EDSR) driving is less efficient for electron spin-1/2 qubits, for which the highest speeds were reached using design-optimized micromagnets providing large magnetic-field gradients, or materials with strong spin-orbit interaction (for example, InAs). As seen from the times in the singlet-triplet column of the figure, the singlet-triplet oscillations can reach gigahertz frequencies. Fast exchange-based gates were demonstrated for both one and two-qubit operations of spin-1/2 qubits and singlet-triplet qubits, and for two-qubit operations of hole and impurity qubits. Finally, we would like to note that the exchange-based gate for, first, a pair of one-half spins and, second, the singlet and triplet two-electron states, is an identical process. Whether such a process should be interpreted as a one-qubit gate or two-qubit gate depends on additional functionalities implemented, or implementable, in the given experiment. The boundary between the two cases is blurry.

C. The definition and values of measurement times

We do not review the measurement times of charge qubits because the task of measuring a charge qubit is the task of de-

⁶ Instead of quoting the gate speed, the qubits are often judged by how strongly they couple to a microwave cavity field, using the charge-photon coupling strength. At the moment that figure of merit is not included in this Technical Review.

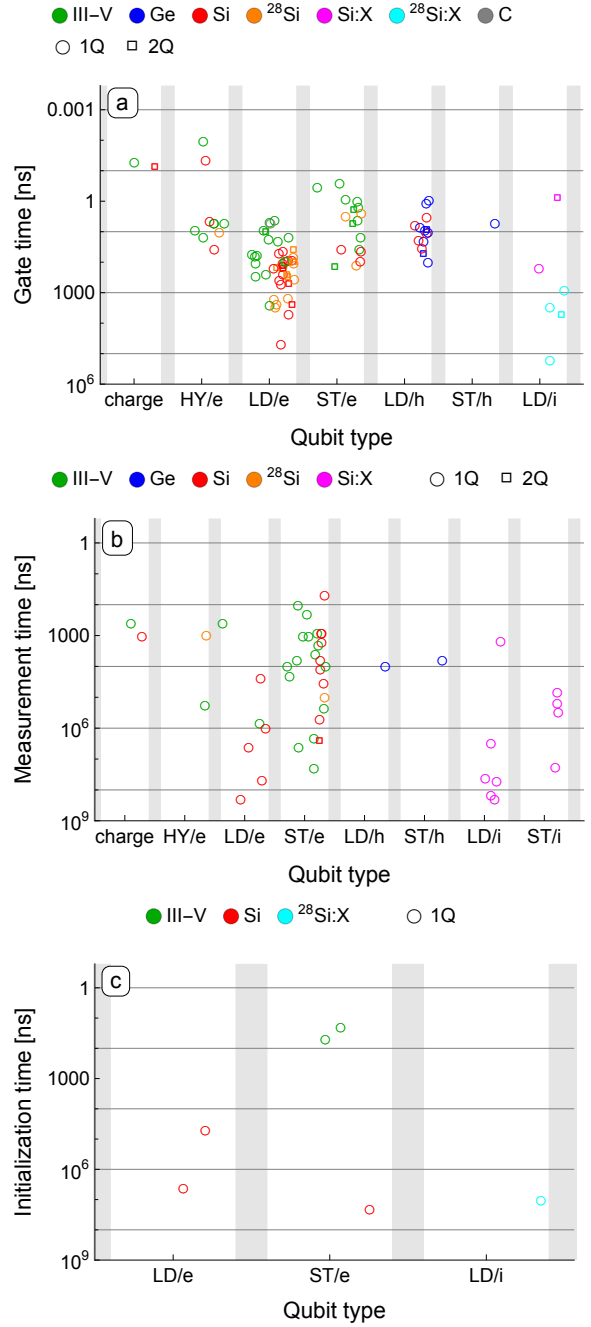


FIG. 6. Operation times: (a) gates, (b) measurements, (c) initializations. In all panels the horizontal axis shows the qubit type, restricting to those for which values exist. Within each type, the publication date is reflected by shifting the points horizontally, similarly as in Fig. 3. The vertical axis shows the operation time in nanoseconds. The data-point color indicates the material and its symbol the number of qubits involved in the operation, according to the panel legend.

tecting a charge—typically an elementary charge—in a nanodevice. First, this task is separable from, and not exclusive to, spin qubits, and thus not our focus. Second, the analysis of methods and results of this task is a topic rich enough for a review in its own right. For our purposes, it will be enough to

give the following minimum. The charge detection is typically characterized through the detection sensitivity s with a typical number being⁷

$$s = \text{a few} \times 10^{-4} e / \sqrt{\text{Hz}}. \quad (10)$$

This parameter quantifies the reliability of the output of a charge-meter signal if integrated for time T_M , through the variance

$$\text{var}[q] = s^2 / T_M. \quad (11)$$

Assuming that one aims to distinguish a signal of one elementary charge, $q_1 = e$, from the signal of zero charge, $q_2 = 0$, where ‘to distinguish’ means to make the signal error, $\sqrt{\text{var}[q]}$, as small as the signal magnitude, $|q_1 - q_2| = e$, would give the required time

$$T_M = s^2 / e^2 \sim 100 \text{ ns}. \quad (12)$$

Although higher sensitivity[251] and shorter times[136] for elementary charge detection were reported, let us take this value for the measurement time T_M as a lower limit realistic for many experimental configurations.

With 100 ns for the time required to detect an event involving elementary charge, we now look at the spin qubit measurements times shown in Fig. 6(b). We see that whereas the times start at about the elementary charge-detection limit of Eq. (12), they might become orders of magnitude longer. The variance reflects the fact that the spin is detected indirectly, by first converting it to a charge event, which is in turn resolved by a charge sensor. The time required for the spin-to-charge conversion can vary a lot, depending on the process details. One example for a spin-to-charge conversion is spin-dependent tunneling: an electron with spin down can tunnel out a quantum dot, whereas the one with spin up can not, the difference originating in their Zeeman energies [97]. Since the quantum dot has to be well isolated for the qubit to keep its coherence, the tunneling out of the dot is slow. As a second example, the spin singlet and triplet can be discriminated according to being allowed or not allowed to traverse a double dot (the Pauli Spin Blockade invented by Ono et al., see Ref. [218]). Although in this case the charge reconfiguration can be very fast, following the gate-voltage pulses on a nanosecond scale, the two charge configurations being discriminated differ only by a dot-size shift of an elementary charge. The discrimination of such states requires a longer time compared to those differing by the presence, rather than the displacement, of an elementary charge. A different class of measurements, called rf-based detection, relies on probing the above described spin-dependent charge reconfigurations by an oscillatory (radio-frequency) electric field. The shortest measurement times seen on Fig. 6(b) were obtained using rf-sensors.

⁷ Here are a few numbers that one can find in the literature: 10 in Ref. [240], 10 in Ref. [307], 30 in Ref. [82], 63 in Ref. [50], 0.8 in Ref. [268], 0.37 in Ref. [92], 8.2 in Ref. [330], 4.1 in Ref. [334], 21 in Ref. [45], 0.60 in Ref. [254]; all in $10^{-4} \times e / \sqrt{\text{Hz}}$.

D. The values of initialization times

The initialization times are shown in Fig. 6(c). Only a few values are present. The reason might be that the most typical experimental scenario is to repeat a cycle: initialization – operation – measurement, where the measurement part plays the role of the initialization, and, therefore, the latter is not reported separately and explicitly. There are more values published on the initialization fidelities, see below.

IV. OPERATION FIDELITY

The operation fidelity is a dimensionless figure of merit allowing the comparison of diverse qubits. Using randomized benchmarking [72], one can extract the gate errors independently of the measurement errors, even if the former are orders of magnitude smaller than the latter. Although it is not strictly correct, the fidelity is used to judge the progress towards error-correction thresholds required for fault-tolerant quantum computing.⁸ For all these reasons, evaluating the gate fidelities is popular and impressive values have been reached.

A. The definition and meaning of experimentally extracted fidelities

The fidelity characterizes how close the actual operation is to the desired one. Although the fidelity of 1 means that the two operations are the same, the quantification of a measure when they are not the same is less straightforward. The usual definitions derive from the fidelity \mathcal{F} , in the sense of the distance between two quantum states described by their respective density matrices ρ and ρ' ,

$$\mathcal{F} = \left(\text{tr} \sqrt{\sqrt{\rho} \rho' \sqrt{\rho}} \right)^2. \quad (13)$$

If one of the two states is pure, say $\rho' = |\Psi\rangle\langle\Psi|$, the formula simplifies to

$$\mathcal{F} = \text{tr} (\rho |\Psi\rangle\langle\Psi|). \quad (14)$$

If the second state ρ is also pure, $\mathcal{F}^{1/2}$ is closely related to an unambiguous discrimination of the two pure states [108], whereas $\arccos \mathcal{F}^{1/2}$ is a measure of their statistical distinguishability [316].⁹

We use the definition of Eq. (13) leading to Eq. (14) because of its connection to the randomized benchmarking. Namely,

⁸ The problem is that the fidelity, as defined below, is not the error parameter entering the threshold theorem. The two parameters can differ by orders of magnitude, in the unfavorable way: whereas the fidelity extracted by the randomized benchmarking can be low, the error rate can remain much larger [19, 245].

⁹ What is the best measure to quantify distance of two operations is discussed at length in Ref. [91]. We thank Andrea Morello for pointing this reference to us.

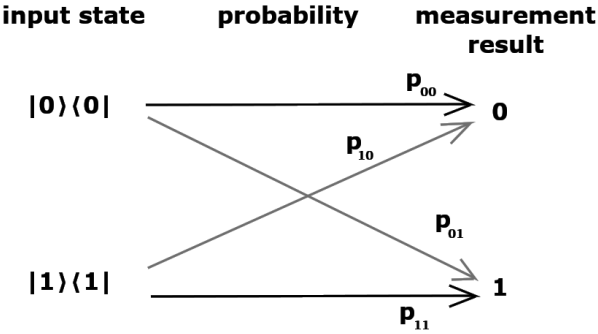


FIG. 7. Probabilities describing a two-outcome qubit measurement. The two mutually orthogonal pure states are on the left, the two measurement outcomes on the right. A perfect measurement would have unit probabilities p_{ii} with $i = 0, 1$ denoted by horizontal lines. Owing to imperfections, diagonal lines appear with non-zero probabilities. The infidelity defined by Eq. (19) gives for this diagram $1 - \mathcal{F} = \frac{1}{2}(p_{01} + p_{10})$.

the essence of the latter is to prepare a pure state $|\Psi\rangle\langle\Psi|$, apply to it a sequence of gates, and then evaluate the overlap of the resulting density matrix ρ with the original state $|\Psi\rangle$ using Eq. 14. In the sequence, the gates are randomly chosen from a discrete set, the Clifford group [94], except for the last gate which is such that the whole sequence reduces to the identity if all gates are perfect. The resulting fidelity, called also the probability of the survival of the initial state, falls off exponentially with the sequence length m ,

$$\mathcal{F}(m) \approx Ap^m + B. \quad (15)$$

Experimentally, the three coefficients A , B , and p are fitted.¹⁰ The first two parameters absorb the errors of the state preparation and measurement, so that the infidelity $1 - \mathcal{F}$ can be found from the parameter p using the formula^{11 12}

$$1 - \mathcal{F} = (1 - p)\frac{d - 1}{d}. \quad (16)$$

Here, $d = 2^n$ with n the number qubits; $d = 2$ for a single-qubit gate benchmarking. Although the exponential decay

¹⁰ Even though Ref. [177] stresses that one should always use a more refined decay model, adding a term proportional to $(m - 1)p^m$ to the right hand side of Eq. (15), this piece of advice does not seem to be followed in practice.

¹¹ Some comments are in order: The exponential decay reflected by Eq. (15) happens under broad conditions investigated in detail in Refs. [72, 177]. The fidelity extracted in this way is the average of \mathcal{F} in Eq. (14) over all pure input states $|\Psi\rangle\langle\Psi|$ and over the gates in the Clifford group. There is an extension procedure called interleaved randomized benchmarking [178] which can assign a fidelity—still averaged over all pure states—to a single specific gate from the Clifford group.

¹² Ref. [91] presents further arguments against using the average fidelity \mathcal{F} , as extracted from randomized benchmarking, Eq. (16), and advocates entanglement fidelity \mathcal{F}_e instead. The two measures are related by $(d + 1)\mathcal{F} = d\mathcal{F}_e + 1$. Since the majority of the spin-qubit publications give \mathcal{F} , we stick to \mathcal{F} as the reported figure of merit.

form displayed by Eq. (15) relies on the discrete set being the Clifford group, many articles convert \mathcal{F} to fidelities of experiment-specific ‘elementary’ or ‘primitive’ gates, such as $\pi/2$ and π rotations around various axes. Even though such a conversion is questionable [177], we follow the prevailing practice and in figures and tables we give the infidelity for the elementary-gate set (and not for the Clifford-gate set). For one-qubit or two-qubit gates, one Clifford gate requires typically a few elementary gates. Therefore, the infidelity of a Clifford gate would be around a factor of 2–3 larger than the infidelity of an elementary gate¹³, the value quoted in this Topical Review.

The fidelities of initialization and measurement are less ambiguous to define as they can be based on Eq. (14) which is more intuitive than Eq. (13). Let us start with the measurement. The probability to get an outcome p in measuring the state described by a density matrix ρ is given by Eq. (14) upon replacing the pure state $|\Psi\rangle\langle\Psi|$ by a positive semi-definite operator A . The most general measurement with possible outcomes labeled by index i is specified by a set $\{A_i\}_i$ of such operators summing to identity, $\sum_i A_i = 1$. In experiments, these operators are approximations of a set of mutually orthogonal projectors spanning the qubit basis $A_i \approx |\Psi_i\rangle\langle\Psi_i|$. Owing to experimental imperfections, these approximations are not exact. The probability of the measurement outcome j upon measuring the pure state $\rho = |\Psi_i\rangle\langle\Psi_i|$ follows as

$$p_{ij} = \text{tr}(|\Psi_i\rangle\langle\Psi_i|A_j). \quad (17)$$

Owing to the normalization of A_i , the probabilities fulfill

$$\sum_j p_{ij} = 1. \quad (18)$$

Were the measurement perfect, all non-diagonal probabilities would be zero. The infidelity of the measurement can be quantified through the off-diagonal probabilities. For example,

$$1 - \mathcal{F} = 1 - \frac{1}{d} \sum_i p_{ii} = \frac{1}{d} \sum_i \sum_{j \neq i} p_{ij}. \quad (19)$$

Here, the first equality sign is a definition, the second one follows from the sum rule, Eq. (18). Also, the number of outcomes is assumed to be equal to the size of the Hilbert space d : For example, $d = 2$ for a two-outcome measurement of a two-level system (a qubit). In this most common case, the measurement probabilities are quantified by two error probabilities, p_{01} and p_{10} , as depicted in Fig. 7. The resulting measurement infidelity according to the definition in Eq. (19) is $(p_{01} + p_{10})/2$.

Finally, let us consider the fidelity of the initialization. Typically, one is interested in an initialization into a single pure state $|\Psi\rangle$. In this case, we can use Eq. (14) to define the initialization fidelity with ρ the actual, perhaps imperfectly prepared, state.

¹³ Ref. [72] gives one list of elementary gates for a single-qubit case, resulting in the ratio of 1.875. For the two-qubit case, Refs. [116, 229] used elementary-gate sets with the ratio of 2.57. However, larger ratios also appear: for example, 9.75 in Ref. [320].

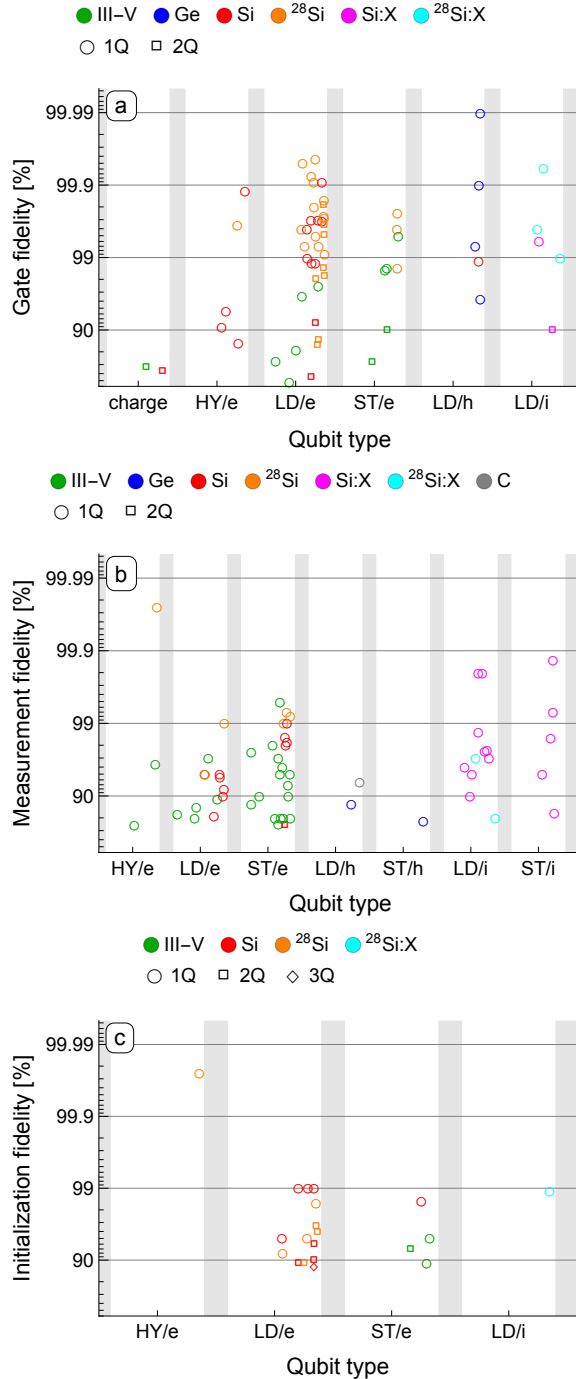


FIG. 8. Operation fidelities: (a) gates, (b) measurements, (c) initializations. In all panels the horizontal axis shows the qubit type, restricting to those for which infidelity values exist. Within each type, the publication date is reflected by shifting the points horizontally, similarly as in Fig. 3. The vertical axis shows the fidelity F in percent. The datapoint color indicates the material and its symbol the number of qubits involved in the operation, according to the individual panel legend.

B. Measured values of fidelities

The three panels of Fig. 8 show the published fidelities of the gates, measurements, and initializations, respectively. For the gates, Fig. 8(a), the electron spin-1/2 qubits previously reached the highest fidelities, well above 99.9 %. Using silicon, both natural and isotopically purified, was crucial for this achievement. Recently, these values were overcome and a new record at 99.99 % has been set by a hole in germanium [166]. There is notable progress in almost every qubit category and increasing the fidelity of single-qubit gates is one of the most impressive achievements within the whole spin-qubit field.

Figure 8(b) shows the fidelities of measurements. Until recently, the infidelities remained above few percent. Relying on a ‘latched’ readout in the Pauli spin blockade [30, 206], the fidelities above 99 % were achieved with singlet-triplet qubits. Comparable high-fidelity results for impurity spins rely on their exceedingly long lifetimes.

We conclude with a remark on two-qubit fidelities. In all categories, meaning gates, measurements, and initializations, their infidelities remain one to two orders of magnitude above the single-qubit ones. There is less data published for the two-qubit versions. Concerning initializations, the more-qubit infidelities that we list are initializations into a nontrivial state achieved through some simple quantum algorithm. For example, initializing all individual qubits into single-qubit fiducial states, and then entangling them with gates into the desired entangled multi-qubit state, such as one of the two-qubit Bell states or the three-qubit Greenberger–Horne–Zeilinger (GHZ) state.

V. QUALITY FACTOR Q

The quality factor is another dimensionless measure allowing for the comparison of diverse qubits, similar to the gate fidelity. The quality factor is a product of a gate frequency and a characteristic time scale. We denote the former by f_R , with the subscript suggesting the most typical case where the gate is implemented by Rabi oscillations. There are two usual choices for the characteristic time, resulting in two groups of quality factors reported in the literature.

The first choice is using the inhomogeneous dephasing time. We call the resulting metric the qubit quality-factor,

$$Q = f_R T_2^*. \quad (20)$$

This Q counts the number of operations which can be performed on a given qubit before other qubits, waiting idly, lose their coherence. With the possibility of applying dynamical decoupling, one might consider using other coherence times instead of T_2^* , as the time for which the other qubits can wait before losing coherence. However, we know only a single case where a different choice was made for this type of the quality factor, T_2^{Echo} in Ref. [67], and therefore stick to Eq. (20).

The second choice is using the gate-signal decay time. Though it is not exclusive to Rabi-induced gates, we denote it using the symbol T_2^{Rabi} introduced in Sec. II, again as the

most typical scenario. We call the resulting quantity the gate quality-factor,

$$Q = f_R T_2^{\text{Rabi}}. \quad (21)$$

In this form, Q gives the number of oscillations at frequency f_R during the decay time T_2^{Rabi} . Loosely speaking, it gives the number of discernible oscillations on a plot showing the Rabi oscillation signal.¹⁴ We note that many references reporting the gate quality-factors use Eq. (21) with the right-hand side multiplied by a factor of two. Whereas such a factor is understandable looking at Eq.(9), we adopt Eq. (21) to make it more directly comparable to Eq. 20. As a consequence, we have to divide several of the reported values for the gate quality-factors by two. Finally, we note that the gate quality-factor is related to the gate fidelity, both being a qualitative measure of the gate imperfections. In Appendix B we derive $1 - \mathcal{F} \approx 1/4Q$ valid for a large Q in a toy model with exponential dephasing.

Figure 9(a) shows the published data on quality factors, both gate and qubit ones. The majority of the values is within the range of few to about a hundred. There are some exceptions which crawl toward a thousand. Figure 9(b) makes it easier to compare different qubit types and discriminate the gate and qubit quality-factors. Of the two dephasing times, T_2^* is typically smaller than T_2^{Rabi} , so one expects that the gate quality-factors reach higher values than qubit quality-factors. There is some evidence in favor of this expectation, but more data is needed to decide on its generality.

VI. SIZE OF QUBIT ARRAYS

Scaling up devices to many qubits is the biggest current challenge of the field. The statement applies to all qubit platforms, not only to semiconducting qubits. For serious applications, being able to build large two-dimensional arrays seems necessary since the fault-tolerant thresholds for error-correction in one-dimensional arrays remain too low (see Table VIII in Ref. [66]).

A. The definition of qubit-array functionality levels

Although it is possible to fabricate relatively large gated arrays with semiconductors, making them functional is a different story. Therefore, we discriminate several functionality levels. We note that the assignment of the levels as defined below to a specific experiment is often difficult. This assignment is perhaps the most subjective of all made in this Technical Review. The reader is advised to consult the original work to judge the details of the achievements.

We define the following values, in ascending order according to the device functionality:

¹⁴ Indeed, Ref. [295] calls Q defined in Eq. (21) a ‘number of gate oscillations’, which might have been a better name than a ‘quality factor’.

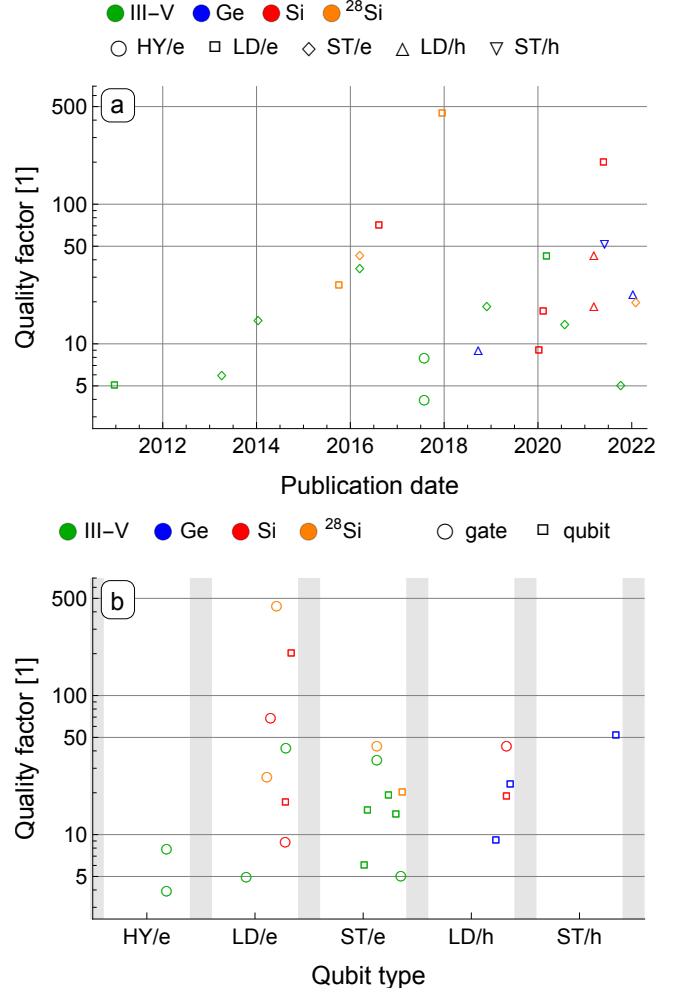


FIG. 9. Quality factors. The two panels show the same data. In (a), according to the publication date, with the color indicating the material and the symbol the qubit type, according to the panel legend. In (b), the qubit type is on the horizontal axis, the publication date is reflected by shifting the points horizontally, similarly as in Fig. 3. The datapoint color indicates the material and its symbol discriminates the qubit and the gate quality-factor as defined in Eq. (20) and Eq. (21), respectively.

N-qubit device. A structure capable of hosting N qubits has been fabricated. The gating and charge sensing work, so that all qubit hosts can be brought into the required charge configuration. On top of this minimal requirement, the articles assigned to this category report a large variation of additional features: single EDSR gates, tunable interdot tunneling or coupling, controllable charge shuffling, spin detection based on Pauli spin blockade, estimations of qubit-qubit interaction strength, and so on.

N-qubit simulator. First of all, the device is stable and tunable enough to search large regions in the high-dimensional charge diagram. For example, aiming at single-electron LD qubits, the structure can be brought into the 1–1–1–⋯–1 charge state, or the (11)–(11)–⋯–(11) state for ST qubits. In such a configuration, qubits can interact pair-wisely and all

N qubits are connected by an interaction path. The interactions are tunable. Either one qubit can be measured and manipulated at the single-qubit level, or at least qubit-qubit (being spin-spin) correlations can be measured.

N -qubit processor. Every qubit (or most of them) has a two-axis control and can be measured. Qubits can interact pair-wisely through tunable interactions. The structure can perform N -qubit algorithms.

To cast more light on the ambiguities that we met and decisions we made to deal with them, let us make a few additional comments.

First, we do not include many-qubit structures which were fabricated, but no functionality was demonstrated, no matter what their size was. We do not include experiments where multiple-dot structure was involved without any intention towards using it for qubits (for example, it was used in a transport experiment).

Second, the vast majority of the experiments within the spin-qubit field until now was done with a single dot implementing spin-1/2 qubit or a double dot implementing a singlet-triplet qubit. Therefore, we normally do not include these two cases into our tables and figures. One exception is if the experiment is somewhat outstanding, perhaps pioneering a spin qubit in a new material or platform. We included some of these.

Third, the number of qubits is not the same as the number of dots. For example, a double-dot with two-electrons can be viewed both as one singlet-triplet qubit as well as two qubits of spin-1/2 with a limited functionality. In these cases, we follow the primary intention of the experiment as we understood it from the reference. For example, a triple dot implementing a resonant-exchange qubit is counted as a single-qubit structure implementing a fully functional resonant-exchange qubit (that is, a hybrid qubit in our nomenclature), and not as a structure implementing three spin-1/2 qubits with a limited functionality.

Finally, in Refs. [60, 287] there is no single-qubit gate nor measurement available. Still, we assign it to the quantum-simulator category, as in these experiments a simulation was the primary target and controllable spin-spin interactions played a critical role.

B. Sizes of qubit arrays achieved experimentally

The sizes of qubit arrays appearing in publications on experiments are displayed in Fig. 10. The panel (a) shows the progress over time. A lot of effort goes into scaling up the spin-qubit structures, with slow, but nevertheless steady progress. It took about ten to fifteen years to bring the most basic structure of the spin-qubit field, the double dot, up to the functionality of a quantum processor, as defined in the above list: With the experiments starting [231] around 2005, Refs. [295, 310, 331] could be acknowledged to have reached the ‘processor’ level, and only in the most recent one the fidelities were high enough to run the most elementary quantum circuits. We assign the accomplishment of the first fully-functional ‘processor’ beyond the double dot to the year 2021, with Ref. [277] using electrons in silicon and Ref. [111] using holes in ger-

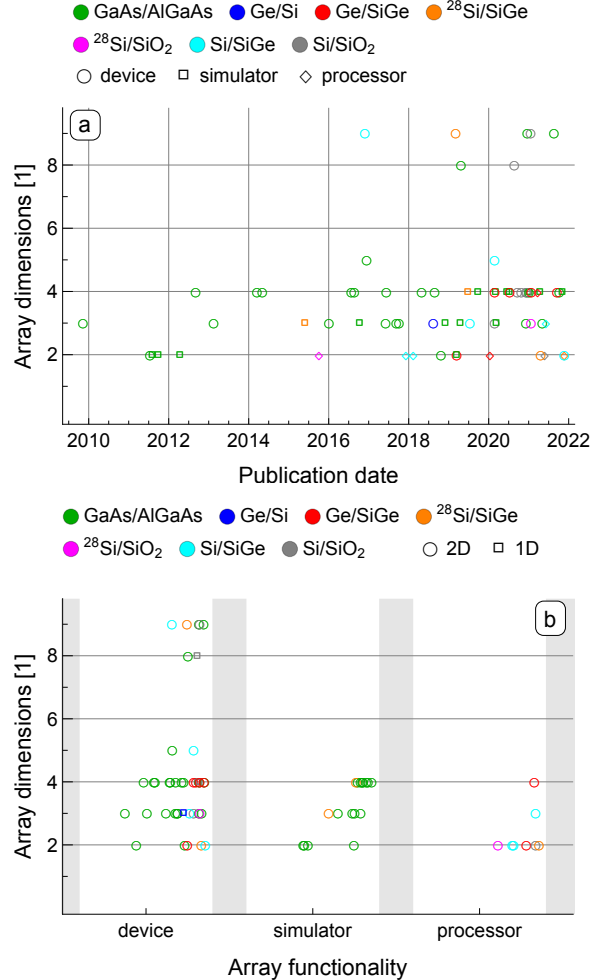


FIG. 10. Size of qubit arrays. The two panels show the same data: in (a) according to the publication date, with the color indicating the material and the symbol the array functionality (see the text for the definitions), according to the panel legend. In (b), the array functionality is on the horizontal axis, the publication date is reflected by shifting the points horizontally, similarly as in Fig. 3. The datapoint color indicates the material and its symbol the host geometry, according to the panel legend.

anium. In Fig. 10(b) one can see that the recent couple of years have brought a surge of results demonstrating progress in building spin-qubit arrays with advanced functionality. The fact that these recent breakthroughs come from many groups and happen in diverse materials and geometries gives excellent reasons for optimism on the scaling-up finally taking off.

VII. ACKNOWLEDGMENTS

We thank Takashi Nakajima, Akito Noiri, Kenta Takeda, and other members of Seigo Tarucha laboratory in RIKEN, for numerous discussions that were invaluable for preparing this review. We thank Leon Camenzind, Matthieu Delbecq, Georgios Katsaros, Benedikt Kratochwil, Ferdinand Kuem-

meth, Tristan Meunier, Andrea Morello, Takashi Nakajima, Akito Noiri, Matthew Reed, and Menno Veldhorst for providing feedback on early versions of the review. We also thank the anonymous and non-anonymous referees for many useful suggestions. Finally, we would like to acknowledge the financial support from CREST JST (JPMJCR1675) and Swiss National Science Foundation (SNSF) and NCCR SPIN.

Appendix A: Relaxation time notations

To define the notation and give an example of the simplest dephasing form, we state here the result of Markovian (or exponential) decay displayed by the Bloch equations. Let us consider the following two parametrizations of the density matrix of a spin-1/2

$$\rho = \begin{pmatrix} \rho_{\uparrow\uparrow} & \rho_{\uparrow\downarrow} \\ \rho_{\downarrow\uparrow} & \rho_{\downarrow\downarrow} \end{pmatrix} = \frac{1}{2} \begin{pmatrix} 1 + s_z & s_x - i s_y \\ s_x + i s_y & 1 - s_z \end{pmatrix} \equiv \frac{1}{2} (1 + \mathbf{s} \cdot \boldsymbol{\sigma}). \quad (\text{A1})$$

The defining and normalization conditions of a density matrix (trace one, Hermiticity, and positive semi-definiteness), require that the vector \mathbf{s} is real and its length is not larger than one.

The Bloch equations [15], describing the exponential decay of the density-matrix components, read

$$\partial_t s_x = -\frac{s_x}{T_2}, \quad (\text{A2a})$$

$$\partial_t s_y = -\frac{s_y}{T_2}, \quad (\text{A2b})$$

$$\partial_t s_z = -\frac{s_z - s_{0z}}{T_1}, \quad (\text{A2c})$$

with s_{0z} being the equilibrium spin polarization. The spin decay is described by two parameters, T_1 and T_2 , called, respectively, the longitudinal and transverse relaxation time in the original work of Bloch. We denote the inverse of these times as rates, $\Gamma_1 = 1/T_1$ and $\Gamma_2 = 1/T_2$, that is, with the indexes corresponding.

We now use the alternative parameterization of the density matrix, where the exponential decay reads

$$\partial_t \rho_{\uparrow\uparrow} = -\Gamma_{ex} \rho_{\uparrow\uparrow} + \Gamma_{rel} \rho_{\downarrow\downarrow}, \quad (\text{A3a})$$

$$\partial_t \rho_{\uparrow\downarrow} = -\left(\frac{\Gamma_{ex} + \Gamma_{rel}}{2} + \Gamma_\varphi\right) \rho_{\uparrow\downarrow}, \quad (\text{A3b})$$

and the remaining matrix elements evolution is fixed by the requirements $\rho_{\uparrow\uparrow} + \rho_{\downarrow\downarrow} = 1$ and $\rho_{\uparrow\downarrow} = \rho_{\downarrow\uparrow}^*$. Here, we use the notation of Ref. [118], which originates in the assumption that the spin-up state is the energy ground state and the equations contain Γ_{ex} , the rate of excitations from the ground state, Γ_{rel} the rate of relaxation into the ground state, and Γ_φ , the “pure-

dephasing” rate. With the following relations,

$$\frac{1}{T_1} = \Gamma_{ex} + \Gamma_{rel}, \quad (\text{A4a})$$

$$\frac{1}{T_2} = \frac{\Gamma_{ex} + \Gamma_{rel}}{2} + \Gamma_\varphi, \quad (\text{A4b})$$

$$s_{0z} = \frac{\Gamma_{rel} - \Gamma_{ex}}{\Gamma_{rel} + \Gamma_{ex}}, \quad (\text{A4c})$$

the two sets of equations, (A2) and (A3), correspond to each other.

In the above equations for the density matrix evolution, we dropped the coherent part, which would read $\partial_t \mathbf{s} = (g\mu_B/\hbar)\mathbf{s} \times \mathbf{B}$, with g being the electron g -factor and \mathbf{B} the magnetic field. Equations (A2) are derived in Ref. [75] in a simple model on p. 707-712. The same reference derives also Eq. (A3) on p. 759-765, considering a spin qubit coupled to phonons as the decay source, following the standard methods of Ref. [18].

Appendix B: Relation of the gate fidelity and the gate quality factor

The gate quality-factor is closely related to the gate fidelity, as we now illustrate. Let us consider a Rabi-oscillations experiment with a qubit. In the rotating frame, we describe it using a density matrix parameterized by vector \mathbf{s} . The Rabi oscillations induced by a resonant drive result in a time dependence of this vector. In an ideal scenario without errors or decoherence, the qubit rotates at a fixed frequency f around certain axis, set by the driving pulse phase. The time evolution is

$$\rho_{ideal}(t) = \frac{1}{2} (1 + \mathbf{s}(t) \cdot \boldsymbol{\sigma}). \quad (\text{B1})$$

The ideal state at certain specific times corresponds to $|\Psi(t)\rangle\langle\Psi(t)|$. For example, with the initial state along z , $\mathbf{s}(0) = (0, 0, 1)$ and a rotation axis x , at time $t = 1/2f$ an ideal π rotation is performed.

Let us now consider the coherence decay given by Eq. (A2). Assuming, for simplicity, that either the rotation is in the plane of the Bloch sphere perpendicular to the energy-quantization axis, or taking $T_2 = T_1$ and $s_{0z} = 0$, the actual density matrix is described by $\mathbf{s}(t) \exp(-t/T_2)$. The amplitude of the oscillating polarization measured as a function of time will decay exponentially, as $\exp(-t/T_2)$. The fitted time-scale of the decay is called the “gate decay time” T_2^{Rabi} entering Eq. (21). Evaluating the fidelity with Eq. (14) gives

$$\mathcal{F} = \frac{1}{2} (1 + \exp(-t/T_2)). \quad (\text{B2})$$

For a π -rotation gate, implemented imperfectly at time $t = 1/2f$, it finally gives

$$\mathcal{F} = \frac{1}{2} (1 + \exp(-1/2Q)) \approx 1 - \frac{1}{4Q}, \quad (\text{B3})$$

where the approximation is valid for small infidelity or large quality factor.

In this toy model, the gate infidelity and the gate quality-factor are in a simple one-to-one correspondence. In reality, the relation is complicated by two facts. First, the dephasing might be more complicated than the Markovian decay described by the Bloch equations. More importantly, the signal decay and the fidelity are influenced differently by unitary gate-errors. The latter are deviations from the desired gate which do not originate in dephasing: for example, if the rotation axis is not exactly along x or the rotation angle is below the target value π . By definition of the name, the unitary errors

are systematic, that is they do not change in time. If known, they could be corrected by additional unitary rotations. Nevertheless, if they are not known, for example due to insufficient calibration, or they could not be corrected, they do diminish the gate fidelity. On the other hand, they do not lead to the gate-signal decay T_2^{Rabi} as extracted experimentally. At most, they diminish the overall signal magnitude, called the visibility. To conclude, because of the unitary errors diminishing the fidelity but not the gate quality-factor, the right hand side in Eq. (B3) becomes only the upper limit for the left hand side.

Appendix C: List of tables

Content	Table	Page
Spin coherence	Table I	16-19
Charge coherence	Table II	22
Operation times	Table III	23-24
Operation fidelities	Table IV	26-27
Quality factors	Table V	29
Qubit arrays	Table VI	30-31

Time	Coherence	Qubit	Material	Host	Date	Reference	Source	
57 s	T_1	LD/e	GaAs/AlGaAs	2D	2018-08	37	p3 and Fig. 4a	0
30 s	T_1	LD/i	Si:P	imp	2017-03	311	Fig. 2b the lowest point	1
10 s	T_1	LD/e	GaAs/AlGaAs	2D	2017-10	114	Fig. 2 the lowest green point	2
9.8 s	T_1	LD/i	Si:P	imp	2019-05	280	Fig. 2c	3
9.3 s	T_1	LD/i	Si:P	imp	2018-03	31	p3 and Fig. 1f	4
9 s	T_1	LD/e	Si/SiO ₂	1D	2021-03	49	p3 and Fig. 3a the leftmost blue point	5
6 s	T_1	LD/i	Si:P	imp	2010-09	199	p2	6
5 s ^a	T_1	LD/e	Si/SiGe	2D	2019-04	25	p4	7
4.2 s	T_1	LD/i	Si:P	imp	2019-01	146	p3	8
3.4 s	T_1	LD/i	²⁸ Si:P	imp	2021-01	175	p6 and SFig. 3c	9
3 s	T_1	LD/i	²⁸ Si:P	imp	2016-10	62	p3	10
3 s	T_1	ST/e	Si/SiGe	2D	2012-01	233	p4	11
2.8 s	T_1	LD/e	Si/SiGe	2D	2011-04	265	p3 and Fig. 3	12
2.6 s	T_1	LD/e	Si/SiO ₂	2D	2013-06	324	p3	13
1.8 s	T_1	LD/i	Si:P	imp	2013-06	33	Fig. 3	14
1.6 s	T_1	LD/e	²⁸ Si/SiO ₂	2D	2022-03	335	p4 and Fig. 3c	15
1.3 s	T_1	LD/i ^b	²⁸ Si:P	imp	2016-10	163	p4	16
1.3 s	T_1	LD/i	Si:P	imp	2018-11	314	p3 and Fig. 2b	17
1 s	T_1	LD/e	GaAs/AlGaAs	2D	2008-01	3	p4 and Fig. 3c the leftmost blue point	18
1 s	T_1	LD/e	²⁸ Si/SiO ₂	2D	2018-10	43	p2	19
1 s	T_1	LD/e	²⁸ Si/SiGe	2D	2020-03	115	p6 and Fig. 4a	20
0.7 s	T_1	LD/i	Si:P	imp	2012-09	232	p3	21
0.6 s ^c	T_1	LD/e	Si/SiGe	2D	2009-08	106	Fig. 5	22
0.5 s ^d	T_1	ST/e	²⁸ Si/SiO ₂	2D	2020-04	326	Fig. 4 the leftmost black point	23
0.17 s	T_1	LD/e	Si/SiGe	2D	2016-11	330	Fig. 6	24
0.16 s ^e	T_1	LD/e	Si/SiGe	2D	2019-04	25	Fig. 2	25
0.15 s ^f	T_1	LD/e	²⁸ Si/SiO ₂	2D	2018-08	228	p2 and p4	26
0.14 s	T_1	ST/e	Si/SiGe	2D	2012-04	257	Fig. 2d	27
0.13 s	T_1	LD/e	²⁸ Si/SiGe	2D	2019-11	263	p4	28
90 ms	T_1	LD/e	Si/SiO ₂	2D	2020-06	332	Fig. 1c	29
85 ms	T_1	LD/e	GaAs/AlGaAs	2D	2014-12	247	p2 and Fig. 3	30
50 ms	T_1	LD/e	Si/SiGe	2D	2018-02	310	p1 and ED Fig. 3b	31
40 ms	T_1	LD/e	Si/SiO ₂	2D	2010-03	318	p4 and Fig. 4 the leftmost red point	32
32 ms	T_1	LD/h	Ge/SiGe	2D	2020-08	165	p3	33
20 ms	T_1	HY/eg	²⁸ Si/SiGe	2D	2021-12	20	p4	34
16 ms	T_1	LD/h	Ge/SiGe	2D	2021-03	111	Fig. S5 dot 3	35
15 ms ^h	T_1	ST/e	²⁸ Si/SiO ₂	2D	2020-04	326	Fig. 4 the rightmost black point	36
10 ms	T_1	LD/e	Si/SiO ₂	1D	2021-09	267	p2 and Fig. 2a	37
5 ms	T_1	LD/i	²⁸ Si:B	imp	2020-07	145	p3 and Fig. 3b	38
5 ms ⁱ	T_1	ST/e	²⁸ Si/SiO ₂	2D	2021-01	255	p4 and Fig. 1d	39
4.1 ms	T_1	ST/i	Si:P	imp	2014-06	61		40
3.7 ms	T_1	LD/e	GaAs/AlGaAs	2D	2016-07	6	p3 and Fig. 2	41
3.7 ms	T_1	LD/e ^j	²⁸ Si/SiO ₂	2D	2020-04	229	p2	42
3.1 ms	T_1	LD/i	²⁸ Si:P	imp	2022-01	176	ED Fig. 3 first column	43
3 ms	T_1	LD/h	BLG	2D	2021-12	87	p5	44
2.8 ms ^k	T_1	LD/e	²⁸ Si/SiO ₂	2D	2018-08	228	p4 and Fig. 3a	45
2.3 ms ^m	T_1	ST/e	GaAs/AlGaAs	2D	2007-03	193	p2	46
1.5 ms	T_1	LD/e	GaAs/AlGaAs	2D	2019-04	207	Fig. 2	47
1.3 ms	T_1	LD/e	Si/SiGe	2D	2021-06	277	p1 for Q3	48
1.2 ms	T_1	LD/h	Ge/SiGe	2D	2020-07	110	p4 and Fig. 3a	49

TABLE I-1. Spin coherence times (part 1). Superscripts stand for the following. ^a: No micromagnet. ^b: Qubit defined in the rotating frame. ^c: (estimated) Fig. 5 the lowest point. ^d: At 0.04 kelvin. ^e: With micromagnet. ^f: At 0.1 kelvin. ^g: EO qubit. ^h: At 1.5 kelvin. ⁱ: Lifetime of T_- state. ^j: At 1 kelvin. ^k: The reference states ‘...the relaxation time is on the order of milliseconds’. We use 3 ms as a representative value, as it corresponds to the ‘load phase’ in the measurement cycle. ^l: At 1.1 kelvin. ^m: Triplet-singlet relaxation in a single dot.

Time	Coherence	Qubit	Material	Host	Date	Reference	Source	
0.85 ms	T_1	LD/e	GaAs/AlGaAs	2D	2004-07	70	p4	1
0.20 ms ^a	T_1	ST/e	$^{28}\text{Si}/\text{SiO}_2$	2D	2021-01	255	p4 and Fig. 1d	2
0.20 ms	T_1	ST/e	InGaAs/AlGaAs	2D	2002-09	85	p3 and Fig. 3e	3
86 μs	T_1	LD/h	Ge/Si	1D	2018-10	302	p3 and Fig. 3c the leftmost point	4
60 μs	T_1	LD/h	GaAs/AlGaAs	2D	2019-02	22	abstract and Fig. 4	5
50 μs	T_1	LD/e	GaAs/AlGaAs	2D	2003-11	97	abstract	6
40 μs^b	T_1	ST/e	GaAs/AlGaAs	2D	2012-01	12	p5	7
34 μs	T_1	ST/e	GaAs/AlGaAs	2D	2009-10	9	p3	8
9 μs	T_1	LD/h	Ge/SiGe	2D	2020-01	109	p3 and Fig. 2f	9
3.7 μs	T_1	LD/h	Ge/Si	1D	2022-01	306	SM p13 and SFig. 7.1d	10
1 μs	T_1	LD/e	InAs	1D	2012-10	227	Fig. 4d	11
5 ns	T_1	LD/h	GaAs/AlGaAs	1D	2016-11	304	p4 and SM pS5	12
2.4 ms	T_2^*	LD/i ^c	$^{28}\text{Si}/\text{P}$	imp	2016-10	163	p4	13
0.27 ms	T_2^*	LD/i	$^{28}\text{Si}/\text{P}$	imp	2014-10	203	p1 and Fig. 2b	14
0.12 ms	T_2^*	LD/e	$^{28}\text{Si}/\text{SiO}_2$	2D	2015-10	295	p1	15
0.12 ms	T_2^*	LD/e	$^{28}\text{Si}/\text{SiO}_2$	2D	2014-10	293	p2 and Fig. 3a	16
0.12 ms	T_2^*	LD/e	$^{28}\text{Si}/\text{SiO}_2$	2D	2021-01	44	p13 and Fig. 4a	17
0.12 ms	T_2^*	LD/i	$^{28}\text{Si}/\text{P}$	imp	2022-01	176	ED Fig. 3 first column	18
0.11 ms	T_2^*	LD/i	$^{28}\text{Si}/\text{P}$	imp	2020-07	174	Fig. 2b and i	19
70 μs	T_2^*	LD/e ^d	$^{28}\text{Si}/\text{SiO}_2$	2D	2015-11	294	p2 and Fig. 2b	20
33 μs	T_2^*	LD/e	$^{28}\text{Si}/\text{SiO}_2$	2D	2018-10	43	p2	21
24 μs	T_2^*	LD/e	$^{28}\text{Si}/\text{SiO}_2$	2D	2019-05	116	p3 and ExtData Fig. 1a	22
24 μs	T_2^*	LD/e	$^{28}\text{Si}/\text{SiO}_2$	2D	2022-03	335	p5 and SM Fig. 14	23
21 μs	T_2^*	LD/e	Ge/SiGe	2D	2020-05	271	Fig. 3b	24
20 μs	T_2^*	LD/e	Ge/SiGe	2D	2017-12	329	p3 and Fig. 3a	25
20 μs	T_2^*	LD/e	Ge/SiGe	2D	2022-01	323	Fig. 3c	26
18 μs	T_2^*	LD/i	$^{28}\text{Si}/\text{P}$	imp	2016-02	283	Fig. 4c	27
16 μs	T_2^*	LD/e ^e	Si/SiO_2	2D	2020-02	167	SM Tab. I	28
12 μs^f	T_2^*	ST/e	$^{28}\text{Si}/\text{SiO}_2$	2D	2020-04	326	Fig. 3c	29
10 μs	T_2^*	LD/e	Ge/SiGe	2D	2019-11	263	p4	30
9.4 μs	T_2^*	LD/e	Ge/SiGe	2D	2019-06	264	Tab.1	31
9 μs	T_2^*	LD/i	$^{28}\text{Si}/\text{P}$	imp	2021-01	175	p7 and SFig. 3a	32
8.2 μs	T_2^*	LD/e	$^{28}\text{Si}/\text{SiO}_2$	2D	2019-05	279	p5 and Fig. 3b	33
7.4 μs	T_2^*	LD/e	Ge/SiGe	2D	2022-01	214	ED Fig.2f the topmost trace	34
6.8 μs	T_2^*	LD/e	Ge/SiGe	2D	2021-03	137	Fig. 6 the blue point	35
3.4 μs	T_2^*	LD/e	$^{28}\text{Si}/\text{SiO}_2$	2D	2019-05	102	p2	36
3.3 μs	T_2^*	LD/e	$^{28}\text{Si}/\text{SiO}_2$	2D	2019-12	333	Tab. 1	37
2.7 μs	T_2^*	LD/e ^g	$^{28}\text{Si}/\text{SiO}_2$	2D	2020-04	229	p2 and Fig. 2e	38
2.3 μs	T_2^*	ST/e	Ge/SiGe	2D	2015-05	71	p3	39
2.1 μs^h	T_2^*	ST/e	GaAs/AlGaAs	2D	2014-10	262	p4 and Fig. 3b	40
2.0 μs	T_2^*	ST/e ⁱ	Ge/SiGe	2D	2021-11	36	Fig. 6b	41
2 μs^j	T_2^*	HY/e ^k	$^{28}\text{Si}/\text{SiGe}$	2D	2019-07	4	Fig. S2a	42
2 μs^l	T_2^*	ST/e	$^{28}\text{Si}/\text{SiO}_2$	2D	2020-04	326	Fig. 3g	43
2 μs^m	T_2^*	LD/e	Ge/SiGe	2D	2021-11	198	p1	44
1.8 μs	T_2^*	LD/e	Ge/SiGe	2D	2016-08	274	p3 and Fig. 2c	45
1.7 μs	T_2^*	LD/e	Ge/SiGe	2D	2021-06	277	p1 for Q3	46
1.6 μs	T_2^*	ST/e	$^{28}\text{Si}/\text{SiO}_2$	2D	2018-05	126	p6	47
1.3 μs	T_2^*	ST/e ⁿ	$^{28}\text{Si}/\text{P}$	imp	2017-10	100	p4	48
1.3 μs	T_2^*	ST/e	Ge/SiGe	2D	2020-03	276	Fig. 3c	49
1 μs^o	T_2^*	LD/e	Ge/SiGe	2D	2016-10	135	p3	50

TABLE I-2. Spin coherence times (part 2). Superscripts stand for the following. ^a: Lifetime of T_0 state. ^b: From several relaxation times defined, we take the inverse of the "bare triplet relaxation rate" $1/\Gamma_T = 40 \mu\text{s}$. ^c: Qubit defined in the rotating frame. ^d: A three-electron qubit. ^e: In a five-electron dot configuration. ^f: At 0.04 kelvin. ^g: At 1 kelvin. ^h: With feedback. ⁱ: $S-T_-$ qubit. ^j: (estimated) from Fig. S2a as the signal decay by factor $1/e$. ^k: EO qubit. ^l: At 1.5 kelvin. ^m: The average of the figure of merit for the two qubits measured. ⁿ: Impurity-gated dot hybrid qubit. ^o: From EDSR linewidth.

Time	Coherence	Qubit	Material	Host	Date	Reference	Source	
1 μs^{a}	T_2^*	LD/e	Si/SiGe	2D	2017-04	248	p2	1
1 μs	T_2^*	LD/e	Si/SiGe	2D	2018-02	310	p1 and ED Fig. 3d	2
1 μs	T_2^*	ST/e	Si/SiGe	2D	2021-08	171	p3	3
0.97 μs	T_2^*	LD/e	Si/SiGe	2D	2020-06	29	p3	4
0.84 μs^{a}	T_2^*	LD/e	Si/SiGe	2D	2014-08	134	p2	5
0.83 μs	T_2^*	LD/h	Ge/SiGe	2D	2020-01	109	p2 and Fig. 2f	6
0.77 μs^{b}	T_2^*	LD/e	GaAs/AlGaAs	2D	2020-03	208	p3 and Fig. 3b	7
0.70 μs	T_2^*	ST/h	Ge/SiGe	2D	2021-06	125	Fig. 3f 1.0 mT trace	8
0.64 μs^{c}	T_2^*	LD/e	CNT	1D	2019-07	58	p2 and Fig. 3d	9
0.60 μs^{d}	T_2^*	ST/e	GaAs/AlGaAs	2D	2016-01	64	p3	10
0.47 μs^{e}	T_2^*	LD/h	Ge/SiGe	2D	2021-09	166	Fig. 1 caption	11
0.45 μs	T_2^*	LD/h	Ge/SiGe	2D	2021-03	111	Fig. S6 dot 3	12
0.44 μs	T_2^*	LD/h ^f	Si/SiO ₂	1D	2021-03	38	p8 and SM Sec. 9	13
0.36 μs	T_2^*	ST/e	Si/SiGe	2D	2012-01	184	p3	14
0.33 μs	T_2^*	LD/h	Ge/SiGe	2D	2020-07	110	p4 and Fig. 4b	15
0.24 μs	T_2^*	ST/e	Si/SiGe	2D	2014-08	317	Fig. 2d the blue trace	16
0.21 μs	T_2^*	LD/e	GaAs/AlGaAs	2D	2019-04	207	Fig. 2	17
0.21 μs	T_2^*	ST/e	GaAs/AlGaAs	2D	2018-11	211	p4	18
0.18 μs	T_2^*	LD/h	Ge/Si	1D	2014-05	113	p3	19
0.13 μs	T_2^*	LD/h	Ge/Si	1D	2018-09	313	p4 and Fig. 6d	20
0.12 μs^{g}	T_2^*	LD/e	GaAs/AlGaAs	2D	2021-08	201	Fig. 5f the topmost point	21
0.11 $\mu\text{s}^{\text{a,h}}$	T_2^*	LD/e	Si/SiGe	2D	2017-04	248	Fig. 3a	22
100 ns^{i}	T_2^*	ST/e	2D	2022-02	127	p4 and Fig. 2e-g	23	
0.10 μs^{b}	T_2^*	ST/e	GaAs/AlGaAs	2D	2017-01	209	p2	24
94 ns^{b}	T_2^*	ST/e	GaAs/AlGaAs	2D	2010-11	16	Fig. 3b	25
90 ns	T_2^*	ST/e	GaAs/AlGaAs	2D	2013-04	67	p2	26
88 ns^{j}	T_2^*	LD/e	Si/SiGe	2D	2018-01	244	p1	27
82 ns	T_2^*	LD/h	Ge/Si	1D	2022-01	306	p3 and Fig. 3d	28
80 ns^{k}	T_2^*	ST/e	GaAs/AlGaAs	2D	2015-08	14	Fig. 4d	29
80 ns^{l}	T_2^*	ST/e	GaAs/AlGaAs	2D	2017-09	78	p3	30
66 ns^{m}	T_2^*	LD/e	2D	2018-02	196	p3 and Fig. 3b	31	
64 ns^{n}	T_2^*	LD/e	CNT	1D	2015-07	297	p4	32
61 ns^{a}	T_2^*	LD/e	GaAs/AlGaAs	2D	2014-12	327	p3	33
59 ns	T_2^*	LD/h	Si/SiO ₂	1D	2016-11	185	p4 and Fig. 3a	34
55 ns	T_2^*	LD/i	Si:P	imp	2012-09	232	p2	35
45 ns	T_2^*	HY/e ^o	Si/SiGe	2D	2017-08	282	Fig. 2i the blue trace	36
40 ns^{b}	T_2^*	ST/e	GaAs/AlGaAs	2D	2010-12	17	SM SFig. 1	37
34 ns^{p}	T_2^*	LD/e	Si/SiGe	2D	2019-12	24	p1	38
30 ns	T_2^*	LD/e	GaAs/AlGaAs	2D	2008-06	151	p2	39
28 ns	T_2^*	LD/e	GaAs/AlGaAs	2D	2020-03	208	p2 and Fig. 2c	40
27 ns^{q}	T_2^*	LD/e	2D	2021-08	103	p3	41	
27 ns	T_2^*	ST/e	GaAs/AlGaAs	2D	2009-10	9	p4	42
25 ns	T_2^*	ST/e	GaAs/AlGaAs	2D	2005-08	148	p5	43
25 ns	T_2^*	HY/e ^r	GaAs/AlGaAs	2D	2013-09	187	p3	44
22 ns	T_2^*	ST/e	GaAs/AlGaAs	2D	2021-10	76	Fig. 2c Qubit 2	45
22 ns	T_2^*	ST/e	GaAs/AlGaAs	2D	2020-12	122	Fig. 2a the green trace	46
21 ns	T_2^*	ST/e	GaAs/AlGaAs	2D	2021-05	147	p5	47
20 ns	T_2^*	LD/e	GaAs/AlGaAs	2D	2007-09	150	p1	48
16 ns	T_2^*	ST/e	GaAs/AlGaAs	2D	2010-12	17	SM SFig. 1	49
15 ns	T_2^*	ST/e	GaAs/AlGaAs	2D	2010-06	242	p2 and Fig. 1	50

TABLE I-3. Spin coherence times (part 3). Superscripts stand for the following. ^a: From EDSR linewidth. ^b: With feedback. ^c: From $f_{\text{FWHM}} = 498 \text{ kHz}$. ^d: In non-ergodic regime. ^e: We take the value for qubit 3 at 0.6 tesla. ^f: At 1.5 kelvin. ^g: The value of the point, 118 ns, is from T. Meunier, private communication. ^h: Valley and spin flip. ⁱ: (derived) from $T_2^* = Q/f$ with $f = 200 \text{ MHz}$ and $Q = 20$. ^j: From $\Gamma_2/2\pi = 1.8 \text{ MHz}$. ^k: (estimated) from Fig. 4d. ^l: Dephasing of transported spin. ^m: From $\Gamma_2/2\pi = 2.4 \text{ MHz}$. ⁿ: From $\Gamma_2/2\pi = 2.5 \text{ MHz}$. ^o: Tunable between spin- and charge- qubit. ^p: From $\Gamma_2/2\pi = 4.7 \text{ MHz}$. ^q: From $f_{\text{FWHM}} = 11.7 \text{ MHz}$. ^r: EO qubit.

Time	Coherence	Qubit	Material	Host	Date	Reference	Source	
15 ns	T_2^*	ST/e	GaAs/AlGaAs	2D	2008-12	241	p2 and Fig. 1e	0
15 ns	T_2^*	ST/e	GaAs/AlGaAs	2D	2020-07	123	p4	1
15 ns ^a	T_2^*	HY/e ^b	GaAs/AlGaAs	2D	2011-11	89	p2 and Fig. 3d	2
14 ns ^c	T_2^*	HY/e ^d	GaAs/AlGaAs	2D	2019-11	160	p3	3
14 ns ^e	T_2^*	ST/e	GaAs/AlGaAs	2D	2010-11	16	p2 and Fig. 3a	4
14 ns	T_2^*	ST/e	GaAs/AlGaAs	2D	2006-07	155	p1	5
14 ns	T_2^*	ST/e	GaAs/AlGaAs	2D	2017-06	86	p2	6
12 ns	T_2^*	ST/e	GaAs/AlGaAs	2D	2021-02	121	p1 and Fig. 2b	7
11 ns	T_2^*	LD/h	Ge/Si	1D	2021-01	84	Fig. 2e	8
11 ns	T_2^*	HY/e	Si/SiGe	2D	2015-12	142	Fig. 2c	9
10 ns	T_2^*	ST/e	GaAs/AlGaAs	2D	2005-09	231	p3 and Fig. 3b	10
10 ns	T_2^*	HY/e ^f	Si/SiGe	2D	2014-07	140	p1	11
9 ns	T_2^*	ST/e	GaAs/AlGaAs	2D	2005-06	128	p3	12
8.1 ns ^g	T_2^*	HY/e ^d	GaAs/AlGaAs	2D	2018-07	159	p2	13
8.1 ns	T_2^*	HY/e	GaAs/AlGaAs	2D	2016-02	40	p4 and Fig. 4d	14
8 ns	T_2^*	LD/e	InSb	1D	2013-02	285	p3	15
8 ns	T_2^*	LD/e	InAs	1D	2010-12	205	p3	16
8 ns	T_2^*	LD/e	CNT	1D	2013-07	158	p4 and Fig. 4	17
7 ns	T_2^*	HY/e	GaAs/AlGaAs	2D	2021-06	124	p4 and Fig. 3c	18
5.6 ns	T_2^*	ST/e	GaAs/AlGaAs	2D	2010-07	226	p4	19
3.7 ns	T_2^*	HY/e	Si/SiGe	2D	2014-01	259	p2	20
3.2 ns ^h	T_2^*	ST/e	CNT	1D	2009-04	48	p3	21
0.45 ns ⁱ	T_2^*	ST/e	GaAs/AlGaAs	2D	2019-05	161	p2	22
0.12 ns ^j	T_2^*	LD/h	GaAs/AlGaAs	2D	2018-05	21	p4	23
9.2 ms	T_2^{Echo}	LD/i ^k	²⁸ Si:P	imp	2016-10	163	p4	24
1.7 ms	T_2^{Echo}	LD/i	²⁸ Si:P	imp	2020-07	174	Fig. 3	25
1.2 ms	T_2^{Echo}	LD/e	²⁸ Si/SiO ₂	2D	2014-10	293	p2 and Fig. 3b	26
1 ms	T_2^{Echo}	LD/i	²⁸ Si:P	imp	2014-10	203	p2 and Fig. 2d	27
1 ms	T_2^{Echo}	LD/e	²⁸ Si/SiGe	2D	2021-03	137	p6 and Fig. 5	28
0.97 ms	T_2^{Echo}	LD/i	Si:P	imp	2015-04	162	p4 and Fig. 3h	29
0.92 ms	T_2^{Echo}	LD/i	²⁸ Si:B	imp	2020-07	145	p3 and Fig. 3a	30
0.85 ms	T_2^{Echo}	LD/i	²⁸ Si:P	imp	2022-01	176	ED Fig. 3 first column	31
0.40 ms	T_2^{Echo}	LD/e	²⁸ Si/SiO ₂	2D	2018-10	43	p2	32
0.31 ms	T_2^{Echo}	LD/i	²⁸ Si:P	imp	2016-02	283	Fig. 4d	33
0.29 ms	T_2^{Echo}	LD/e	²⁸ Si/SiO ₂	2D	2019-05	116	p3 and ExtData Fig. 1b	34
0.21 ms	T_2^{Echo}	LD/i	Si:P	imp	2012-09	232	p3	35
0.2 ms ^l	T_2^{Echo}	ST/e	²⁸ Si/SiO ₂	2D	2020-04	326	Fig. 4 the leftmost blue point	36
0.13 ms	T_2^{Echo}	LD/e	²⁸ Si/SiGe	2D	2020-05	271	Fig. 2d	37
0.12 ms	T_2^{Echo}	LD/i	²⁸ Si:P	imp	2021-01	175	SFig. 3b	38
0.11 ms	T_2^{Echo}	LD/e	²⁸ Si/SiGe	2D	2019-06	264	Tab. 1	39
99 μ s	T_2^{Echo}	LD/e	²⁸ Si/SiGe	2D	2017-12	329	p3 and Fig. 3c	40
73 μ s ^m	T_2^{Echo}	LD/e	²⁸ Si/SiGe	2D	2021-11	198	p1	41
70 μ s	T_2^{Echo}	ST/e	²⁸ Si/SiGe	2D	2015-05	71	Fig. S2 the topmost red point	42
46 μ s	T_2^{Echo}	LD/e	Si/SiGe	2D	2021-06	277	p1 for Q3	43
37 μ s	T_2^{Echo}	LD/e	Si/SiGe	2D	2014-08	134	p4 and Fig. 4a	44
32 μ s	T_2^{Echo}	LD/e	²⁸ Si/SiGe	2D	2022-01	214	ED Fig. 2i the topmost trace	45
30 μ s	T_2^{Echo}	ST/e	GaAs/AlGaAs	2D	2010-12	17	abstract and SM p9	46
22 μ s	T_2^{Echo}	LD/e ⁿ	²⁸ Si/O ₂	2D	2020-02	167	SM Tab. I	47
19 μ s	T_2^{Echo}	LD/e	Si/SiGe	2D	2018-02	310	p1 and ED Fig. 3e	48
11 μ s ^o	T_2^{Echo}	LD/e	Si/SiGe	2D	2016-08	274	p3 and Fig. 2c	49

TABLE I-4. Spin coherence times (part 4). Superscripts stand for the following. ^a: From interference of Landau-Zener transitions. ^b: EO qubit. ^c: From $\Gamma_2/2\pi = 11$ MHz. ^d: RX qubit. ^e: Without feedback. ^f: Hybrid qubit with three electrons in two dots. ^g: From $\Gamma_2/2\pi = 19.6$ MHz. ^h: Carbon nanotube made from ¹³C isotope. ⁱ: From $\Gamma_2/2\pi = 357$ MHz. ^j: From Landau-Zener interference. ^k: Qubit defined in the rotating frame. ^l: At 0.04 kelvin. ^m: The average of the figure of merit for the two qubits measured. ⁿ: In a five-electron dot configuration. ^o: Measured in Ref. [275].

Time	Coherence	Qubit	Material	Host	Date	Reference	Source	0
9 μs	T_2^{Echo}	ST/e	GaAs/AlGaAs	2D	2013-04	67	p3	1
8.5 μs	T_2^{Echo}	ST/e	GaAs/AlGaAs	2D	2017-04	180	Fig. 4c the point n=1	2
8.4 μs	T_2^{Echo}	ST/e	$^{28}\text{Si}/\text{SiO}_2$	2D	2018-05	126	p6 and Fig. 4f	3
7 μs^a	T_2^{Echo}	ST/e	GaAs/AlGaAs	2D	2012-02	186	Fig. 4	4
7 μs^b	T_2^{Echo}	ST/e	$^{28}\text{Si}/\text{SiO}_2$	2D	2020-04	326	Fig. 4 the rightmost blue point	5
7.0 μs	T_2^{Echo}	ST/e	GaAs/AlGaAs	2D	2017-01	209	Fig. 2b	6
6.1 μs	T_2^{Echo}	ST/e	GaAs/AlGaAs	2D	2020-08	42	p4	7
6 μs	T_2^{Echo}	ST/e	GaAs/AlGaAs	2D	2010-12	11	p3	8
5 μs^c	T_2^{Echo}	ST/e	$^{28}\text{Si}/\text{SiO}_2$	2D	2022-02	127	Fig. 4c	9
3.8 μs	T_2^{Echo}	LD/h	Ge/SiGe	2D	2021-03	111	Fig. S6 dot 3	10
2 μs^d	T_2^{Echo}	HY/e ^e	GaAs/AlGaAs	2D	2013-07	188	Fig. 5	11
2 μs	T_2^{Echo}	LD/e	Si/SiGe	2D	2020-06	29	Fig. 4	12
1.9 μs	T_2^{Echo}	LD/h	Ge/SiGe	2D	2020-01	109	p2 and Fig. 2f	13
1.8 μs^f	T_2^{Echo}	ST/h	Ge/SiGe	2D	2021-06	125	Fig. 5 of arXiv-v3	14
1.5 μs^g	T_2^{Echo}	LD/h ^b	Si/SiO_2	1D	2021-03	38	Fig. 4a	15
1.2 μs	T_2^{Echo}	ST/e	GaAs/AlGaAs	2D	2005-09	231	p4 and Fig. 5c	16
0.52 μs	T_2^{Echo}	LD/h	Ge/Si	1D	2022-01	306	p3 and Fig. 3f	17
0.44 μs	T_2^{Echo}	LD/e	GaAs/AlGaAs	2D	2008-06	151	p4 and Fig. 4b	18
0.25 μs	T_2^{Echo}	LD/h	Ge/Si	1D	2021-01	84	Fig. 2e	19
0.25 μs	T_2^{Echo}	LD/h	Si/SiO_2	1D	2016-11	185	p5 and Fig. 4b	20
0.18 μs	T_2^{Echo}	ST/e	GaAs/AlGaAs	2D	2016-06	41	p4	21
0.10 μs	T_2^{Echo}	HY/e ^h	GaAs/AlGaAs	2D	2013-09	187	p3	22
65 ns	T_2^{Echo}	LD/e	CNT	1D	2013-07	158	p4 and Fig. 4	23
50 ns	T_2^{Echo}	LD/e	InAs	1D	2010-12	205	p3	24
34 ns	T_2^{Echo}	LD/e	InSb	1D	2013-02	285	p3	25
0.56 s	T_2^{DynD}	LD/i	$^{28}\text{Si}:P$	imp	2014-10	203	p2 and Fig. 2e	26
28 ms	T_2^{DynD}	LD/e	$^{28}\text{Si}/\text{SiO}_2$	2D	2015-10	295	p1	27
28 ms	T_2^{DynD}	LD/e	$^{28}\text{Si}/\text{SiO}_2$	2D	2014-10	293	p2 and Fig. 3c	28
23 ms	T_2^{DynD}	LD/i ⁱ	$^{28}\text{Si}:P$	imp	2016-10	163	p4	29
10 ms	T_2^{DynD}	LD/i	Si:P	imp	2015-04	162	p4 and Fig. 3j	30
9.2 ms	T_2^{DynD}	LD/i	$^{28}\text{Si}:B$	imp	2020-07	145	p3 and Fig. 4	31
6.7 ms	T_2^{DynD}	LD/e	$^{28}\text{Si}/\text{SiO}_2$	2D	2018-10	43	p2	32
3.7 ms	T_2^{DynD}	LD/e	$^{28}\text{Si}/\text{SiO}_2$	2D	2022-03	335	Fig. 4d	33
3.1 ms	T_2^{DynD}	LD/e	$^{28}\text{Si}/\text{SiGe}$	2D	2017-12	329	Fig. 4a	34
0.87 ms	T_2^{DynD}	ST/e	GaAs/AlGaAs	2D	2016-10	179	Fig. 5	35
0.40 ms	T_2^{DynD}	LD/e	Si/SiGe	2D	2016-10	135	p3	36
0.30 ms	T_2^{DynD}	ST/e	GaAs/AlGaAs	2D	2017-04	180	Fig. 4c the point n=256	37
0.28 ms	T_2^{DynD}	ST/e	GaAs/AlGaAs	2D	2010-12	17	Fig. 3	38
0.16 ms	T_2^{DynD}	ST/h	Ge/SiGe	2D	2021-06	125	p6 and Fig. 5	39
0.13 ms ^j	T_2^{DynD}	ST/e	GaAs/AlGaAs	2D	2012-02	186	Fig. 3b	40
0.10 ms	T_2^{DynD}	LD/h	Ge/SiGe	2D	2021-03	111	Fig. S6 dot 3	41
80 μs	T_2^{DynD}	ST/e	GaAs/AlGaAs	2D	2010-12	11	p3	42
44 μs	T_2^{DynD}	LD/e	Si/SiGe	2D	2014-08	134	Fig. 4b	43
20 μs^k	T_2^{DynD}	ST/e	$^{28}\text{Si}/\text{SiO}_2$	2D	2022-02	127	Fig. 4c the rightmost blue point	44
19 μs	T_2^{DynD}	HY/e ^e	GaAs/AlGaAs	2D	2013-07	188	p3 and Fig. 5 the rightmost point	45
5.4 μs	T_2^{DynD}	LD/h ^b	Si/SiO_2	1D	2021-03	38	p7 and Fig. 4a	46
1 μs	T_2^{DynD}	HY/e ^{l,m}	GaAs/AlGaAs	2D	2017-07	181	Fig. 5b	47
1 μs	T_2^{DynD}	HY/e ^{n,m}	GaAs/AlGaAs	2D	2017-07	181	Fig. 5b	48
0.41 μs	T_2^{DynD}	LD/i	Si:P	imp	2012-09	232	p3	49
0.15 μs	T_2^{DynD}	LD/e	InAs	1D	2010-12	205	Fig. 4a inset the highest point	50

TABLE I-5. Spin coherence times (part 5). Superscripts stand for the following. ^a: (estimated) Fig. 4 the leftmost point. ^b: At 1.5 kelvin. ^c: (estimated) from Fig. 4c the blue points extrapolation to $N_\pi = 1$. ^d: (estimated) Fig. 5 the leftmost point. ^e: RX qubit. ^f: arXiv:2011.13755v3. ^g: (estimated) we take the value for $n = 2$ CPMG sequence, which seems comparable to the Hahn echo data according to Fig. S12. ^h: EO qubit. ⁱ: Qubit defined in the rotating frame. ^j: (estimated) Fig. 3b the rightmost point. ^k: (estimated) from Fig. 4c. ^l: At a partial sweet spot. ^m: Resonant exchange qubit. ⁿ: At a full sweet spot.

Time	Coherence	Qubit	Material	Host	Date	Reference	Source	
0.15 μs	T_2^{DynD}	HY/e	Si/SiGe	2D	2015-12	142	abstract and Fig. 3d	1
0.11 ms	T_2^{Rabi}	LD/e	$^{28}\text{Si}/\text{SiGe}$	2D	2017-12	329	p2	2
0.10 ms ^a	T_2^{Rabi}	LD/e	$^{28}\text{Si}/\text{SiGe}$	2D	2022-01	214	ED Fig. 2l the topmost trace	3
19 μs	T_2^{Rabi}	LD/e	$^{28}\text{Si}/\text{SiO}_2$	2D	2019-12	333	p3 and Fig. 2d	4
7 μs ^b	T_2^{Rabi}	LD/e	Si/SiGe	2D	2016-08	274	p3	5
6 μs	T_2^{Rabi}	ST/e	$^{28}\text{Si}/\text{SiGe}$	2D	2020-03	276	p3	6
1.4 μs	T_2^{Rabi}	LD/e	Si/SiGe	2D	2020-01	56	p4	7
1.3 μs	T_2^{Rabi}	LD/e	GaAs/AlGaAs	2D	2020-03	208	Fig. 6	8
1 μs	T_2^{Rabi}	HY/e ^c	Si/SiGe	2D	2017-08	282	Fig. 3g	9
0.70 μs	T_2^{Rabi}	ST/e	GaAs/AlGaAs	2D	2017-01	209	p3 and Fig. 2b	10
0.53 μs	T_2^{Rabi}	LD/e	GaAs/AlGaAs	2D	2019-04	207	Fig. 2	11
0.40 μs ^d	T_2^{Rabi}	HY/e ^e	$^{28}\text{Si}/\text{SiGe}$	2D	2019-07	4	Fig. S2c	12
0.28 μs ^f	T_2^{Rabi}	ST/e	$^{28}\text{Si}/\text{SiGe}$	2D	2016-03	239	p3, Fig. 4a and b	13
86 ns	T_2^{Rabi}	ST/e	GaAs/AlGaAs	2D	2021-05	147	p3	14
84 ns	T_2^{Rabi}	LD/e	GaAs/AlGaAs	2D	2016-04	212	Fig. 3	15
80 ns ^g	T_2^{Rabi}	HY/e ^{h,i}	GaAs/AlGaAs	2D	2017-07	181	Fig. 4c	16
60 ns	T_2^{Rabi}	LD/h	Ge/Si	1D	2021-01	84	Fig. 3d	17
40 ns ^g	T_2^{Rabi}	HY/e ^{j,i}	GaAs/AlGaAs	2D	2017-07	181	Fig. 4c	18
37 ns	T_2^{Rabi}	HY/e	GaAs/AlGaAs	2D	2021-06	124	Fig. 3b	19
37 ns ^k	T_2^{Rabi}	LD/e	GaAs/AlGaAs	2D	2014-12	327	p3	20

TABLE I-6. Spin coherence times (part 6). Superscripts stand for the following. ^a: The Rabi decay time $T_2^{\text{Rabi}} = 100 \mu\text{s}$ is obtained by fitting the Rabi decay data to a function with two parameters, T_2^{Rabi} and T_2^* . ^b: From $Q = 140$ and $f_R = 10 \text{ MHz}$. ^c: Tunable between spin- and charge-qubit. ^d: (estimated) from Fig. S2c as the signal decay by factor $1/e$. ^e: EO qubit. ^f: (derived) from $T = hN_R/J$ with $J/h = 160 \text{ MHz}$ and $N_R = 44$. ^g: Approximate value at $f_R = 100 \text{ MHz}$. ^h: At a full sweet spot. ⁱ: Resonant exchange qubit. ^j: At a partial sweet spot. ^k: At Rabi frequency $f_R = 85.9 \text{ MHz}$.

Time	Coherence	Qubit	Material	Host	Date	Reference	Source	
45 μ s	T_1	charge	Si/SiGe	2D	2013-07	305	p3 and Fig. 3c	1
78 ns	T_1	charge	SLG	2D	2013-04	300	Fig. 4b	2
48 ns	T_1	charge	CNT	1D	2017-05	223	p4 and Fig. 3c	3
42 ns	T_1	charge	GaAs/AlGaAs	2D	2019-05	250	p4 and Fig. 5d	4
19 ns	T_1	charge	GaAs/AlGaAs	2D	2015-07	170	p4	5
16 ns	T_1	charge	GaAs/AlGaAs	2D	2004-10	230	p3 and Fig. 4	6
10 ns	T_1	charge	GaAs/AlGaAs	2D	2010-12	225	p2	7
10 ns	T_1	charge	InGaAs/AlGaAs	2D	2002-09	85	p1 and Fig. 2d	8
0.12 μ s ^a	T_2^*	charge	GaAs/AlGaAs	2D	2019-07	249	p2	9
61 ns ^b	T_2^*	charge	Si/SiGe	2D	2016-12	194	p2	10
33 ns ^c	T_2^*	charge	GaAs/AlGaAs	2D	2018-10	291	p2	11
23 ns	T_2^*	charge	GaAs/AlGaAs	2D	2019-05	250	p4 and Fig. 5c	12
7 ns	T_2^*	charge	GaAs/AlGaAs	2D	2010-12	225	p4	13
5.3 ns ^d	T_2^*	charge	GaAs/AlGaAs	2D	2018-07	159	p4	14
5 ns	T_2^*	charge	CNT	1D	2017-05	223	p4 and Fig. 3b	15
5.0 ns ^e	T_2^*	charge	GaAs/AlGaAs	2D	2020-05	152	p3	16
5.0 ns ^e	T_2^*	charge	²⁸ Si/SiGe	2D	2021-04	28	p6	17
4.4 ns ^f	T_2^*	charge	Si/SiGe	2D	2020-06	26	Fig. 3b	18
4.0 ns ^g	T_2^*	charge	GaAs/AlGaAs	2D	2017-03	270	p5	19
4.0 ns ^h	T_2^*	charge	Si/SiGe	2D	2017-01	195	p5	20
4.0 ns ^h	T_2^*	charge	²⁸ Si/SiGe	2D	2018-02	196	p2 and Fig. 1d	21
3.0 ns ⁱ	T_2^*	charge	GaAs/AlGaAs	2D	2021-02	153	p5 and Fig. 4a	22
2.9 ns ^j	T_2^*	charge	GaAs/AlGaAs	2D	2021-02	303	p4	23
2.7 ns ^k	T_2^*	charge	²⁸ Si/SiGe	2D	2021-08	103	p5	24
2.2 ns	T_2^*	charge	Si/SiGe	2D	2013-08	258	abstract and Fig. 1	25
1.3 ns	T_2^*	charge	Si/SiGe	2D	2015-02	141	Fig. 2c	26
1.2 ns	T_2^*	charge	GaAs/AlGaAs	2D	2015-07	170	p4	27
1.1 ns	T_2^*	charge	GaAs/AlGaAs	2D	2010-07	226	p3	28
1 ns	T_2^*	charge	GaAs/AlGaAs	2D	2003-11	105	p3	29
0.64 ns ^l	T_2^*	charge	GaAs/AlGaAs	2D	2015-07	269	Fig. 2b	30
0.57 ns ^m	T_2^*	charge	Ge/SiGe	1D	2020-08	319	p5 and Fig. 3	31
0.51 ns ⁿ	T_2^*	charge	SLG	2D	2015-09	65	p3	32
0.40 ns	T_2^*	charge	GaAs/AlGaAs	2D	2004-10	230	p4 and Fig. 4	33
0.3 ns ^o	T_2^*	charge	GaAs/AlGaAs	2D	2013-09	13	Fig. 3b	34
0.29 ns ^p	T_2^*	charge	CNT	1D	2014-04	296	p2	35
0.17 ns ^q	T_2^*	charge	GaAs/AlGaAs	2D	2012-01	81	p4	36
0.2 ns ^r	T_2^*	charge	InSb	1D	2016-05	308	p4	37
0.12 ns ^s	T_2^*	charge	CNT	1D	2019-07	58	p2	38
80 ps	T_2^*	charge	Si/SiGe	2D	2020-09	173	p3	39
60 ps	T_2^*	charge	GaAs/AlGaAs	2D	2011-10	68	p2	40
50 ps ^t	T_2^*	charge	CNT	1D	2015-05	237	Fig. 4f the lowest black point	41
16 ps ^u	T_2^*	charge	Si/SiO ₂	1D	2021-05	117	p4	42
0.76 μ s	T_2^{Echo}	charge	Si/SiGe	2D	2013-08	258	Fg. 2	43
43 ns	T_2^{Echo}	charge	GaAs/AlGaAs	2D	2019-05	250	p4 and Fig. 5e	44
2.2 ns	T_2^{Echo}	charge	Si/SiGe	2D	2015-02	141	p3	45
4 ns ^v	T_2^{DynD}	charge	GaAs/AlGaAs	2D	2013-01	39	p5	46
1.5 ns	T_2^{Rabi}	charge	Si/SiGe	2D	2015-02	141	Fig. 1e	47

TABLE II. Charge coherence times. Superscripts stand for the following. ^a: From $f_{\text{FWHM}}/2\pi = 2.7$ MHz. ^b: From $\Gamma_2/2\pi = 2.6$ MHz. ^c: From $\Gamma_2/2\pi = 4.8$ MHz. ^d: From $\Gamma_2/2\pi = 30$ MHz. ^e: From $\Gamma_2/2\pi = 32$ MHz. ^f: From $\Gamma_2/2\pi = 36$ MHz. ^g: From $f_{\text{FWHM}}/2\pi = 80$ MHz. ^h: From $\Gamma_2/2\pi = 40$ MHz. ⁱ: From $\Gamma_2/2\pi = 53$ MHz. ^j: From $\Gamma_2/2\pi = 55$ MHz. ^k: From $\Gamma_2/2\pi = 60$ MHz. ^l: From $\Gamma_2/2\pi = 250$ MHz. ^m: From $\Gamma_2/2\pi = 0.28$ GHz. ⁿ: From $\Gamma_p/\text{hi}/2\pi = 0.31$ GHz. ^o: From $\Gamma_\phi/2pi = 0.5$ GHz. ^p: From $\Gamma_2/2\pi = 550$ MHz. ^q: From $\Gamma_\phi/2\pi = 0.9$ GHz and $\Gamma_1 = 100$ MHz. ^r: From $\Gamma_\phi/2\pi$; we take the lower limit from the range 1-4 GHz given in the reference. ^s: From $\Gamma_2/2\pi = 1.35$ GHz. ^t: From $\Gamma_2/2\pi \approx 3$ GHz (estimated) from Fig. 4f. ^u: From $\Gamma_2/2\pi = 9.95$ GHz. ^v: From Landau-Zener interference.

Time	Operation	#Qubits	Qubit	Material	Host	Date	Reference	Source	
50 ps	gate	1Q	charge	GaAs/AlGaAs	2D	2013-01	39	p4	0
11 ps	gate	1Q	HY/e ^a	GaAs/AlGaAs	2D	2013-09	187	p2	1
45 ps ^b	gate	1Q	HY/e ^c	Si/SiGe	2D	2014-07	140	Fig. 2b	2
4.6 ns	gate	1Q	HY/e	Si/SiGe	2D	2015-12	142	Fig. 1g	3
5.0 ns	gate	1Q	HY/e ^{d,e}	GaAs/AlGaAs	2D	2017-07	181	Fig. 4c	4
5.0 ns	gate	1Q	HY/e ^{f,e}	GaAs/AlGaAs	2D	2017-07	181	Fig. 4c	5
5.0 ns	gate	1Q	HY/e	GaAs/AlGaAs	2D	2021-06	124	p3 and Fig. 3a	6
9 ns ^g	gate	1Q	HY/e ^a	GaAs/AlGaAs	2D	2010-08	157	Fig. 4	7
10 ns	gate	1Q	HY/e ^a	²⁸ Si/SiGe	2D	2019-07	4	Fig. 4c caption	8
15 ns	gate	1Q	HY/e ^h	GaAs/AlGaAs	2D	2013-07	188	Fig. 4 the blue set	9
36 ns	gate	1Q	HY/e ⁱ	Si/SiGe	2D	2017-08	282	Fig. 3g	10
4.1 ns	gate	1Q	LD/e	GaAs/AlGaAs	2D	2014-12	327	p2	11
4.8 ns	gate	1Q	LD/e	InSb	1D	2013-02	285	Fig. 2c	12
5.0 ns ^j	gate	1Q	LD/e	CNT	1D	2013-07	158	Fig. 3b	13
8.6 ns	gate	1Q	LD/e	InAs	1D	2010-12	205	p2	14
15 ns	gate	1Q	LD/e	GaAs/AlGaAs	2D	2020-03	208	Fig. 6	15
17 ns ^k	gate	1Q	LD/e	InAs	1D	2012-10	227	p3 and Fig. 4f	16
20 ns	gate	1Q	LD/e	GaAs/AlGaAs	2D	2016-04	212	p4 and Fig. 3	17
42 ns	gate	1Q	LD/e	Si/SiO ₂	1D	2018-02	52	Fig. 4b	18
50 ns	gate	1Q	LD/e	Si/SiGe	2D	2016-08	274	p3	19
54 ns	gate	1Q	LD/e	GaAs/AlGaAs	2D	2006-08	149	p4	20
60 ns	gate	1Q	LD/e	GaAs/AlGaAs	2D	2008-06	151	Fig. 2b the blue trace	21
60 ns ^l	gate	1Q	LD/e	GaAs/AlGaAs	2D	2007-09	150	p3	22
70 ns	gate	1Q	LD/e	²⁸ Si/SiGe	2D	2021-11	198	p1	23
80 ns	gate	1Q	LD/e	Si/SiGe	2D	2020-01	56	p4	24
80 ns	gate	1Q	LD/e	Si/SiGe	2D	2021-06	277	p1	25
92 ns	gate	1Q	LD/e	GaAs/AlGaAs	2D	2019-04	207	Fig. 2	26
94 ns	gate	1Q	LD/e	GaAs/AlGaAs	2D	2018-08	120	p3 and Fig. 3b	27
0.10 μs	gate	1Q	LD/e	²⁸ Si/SiGe	2D	2022-01	214	p4	28
0.10 μs	gate	1Q	LD/e	Si/SiGe	2D	2017-12	331	p2	29
0.11 μs	gate	1Q	LD/e	GaAs/AlGaAs	2D	2007-11	215	p3	30
0.13 μs	gate	1Q	LD/e	²⁸ Si/SiGe	2D	2017-12	329	p2	31
0.15 μs ^m	gate	1Q	LD/e	Si/SiGe	2D	2014-08	134	Fig. 3b	32
0.2 μs ⁿ	gate	1Q	LD/e	GaAs/AlGaAs	2D	2011-09	32	Fig 2b	33
0.2 μs	gate	1Q	LD/e	Si/SiGe	2D	2018-02	310	p1	34
0.28 μs ^o	gate	1Q	LD/e	GaAs/AlGaAs	2D	2007-12	156	p3 and Fig. 3b	35
0.36 μs	gate	1Q	LD/e	²⁸ Si/SiO ₂	2D	2022-03	335	ED Fig. 7a	36
0.37 μs	gate	1Q	LD/e	Si/SiGe	2D	2016-10	135	p3	37
0.5 μs	gate	1Q	LD/e	Si/SiGe	2D	2017-04	248	p2	38
1.5 μs	gate	1Q	LD/e	²⁸ Si/SiO ₂	2D	2019-12	333	Tab. 1	39
1.6 μs ^p	gate	1Q	LD/e	²⁸ Si/SiO ₂	2D	2014-10	293	Fig. 4 and Fig. 2d	40
2.4 μs	gate	1Q	LD/e	²⁸ Si/SiO ₂	2D	2015-10	295	p5	41
3 μs ^q	gate	1Q	LD/e	GaAs/AlGaAs	2D	2013-03	256	p3	42
3 μs	gate	1Q	LD/e	²⁸ Si/SiO ₂	imp	2015-03	202	Fig. 3c the topmost point	43
5 μs	gate	1Q	LD/e ^r	Si/SiO ₂	2D	2020-02	167	SM Fig. 4a at around 50 nV	44
50 μs ^s	gate	1Q	LD/e	Si/SiGe	2D	2017-04	248	p7	45
0.2 ns	gate	1Q	ST/e	GaAs/AlGaAs	2D	2014-01	112	Fig. 4a and Fig. 3d	46
0.35 ns	gate	1Q	ST/e	GaAs/AlGaAs	2D	2005-09	231	p3 and Fig. 5d	47
0.83 ns ^t	gate	1Q	ST/e	GaAs/AlGaAs	2D	2016-03	183	Fig. 4d	48
1.0 ns	gate	1Q	ST/e	GaAs/AlGaAs	2D	2020-07	123	p4	49

TABLE III-1. Operation times (part 1). Superscripts stand for the following. ^a: EO qubit. ^b: (estimated) 3 oscillations in 270 ps. ^c: Hybrid qubit with three electrons in two dots. ^d: At a partial sweet spot. ^e: Resonant exchange qubit. ^f: At a full sweet spot. ^g: (estimated) from the uppermost trace in Fig. 4. ^h: RX qubit. ⁱ: Tunable between spin- and charge- qubit. ^j: (estimated) from Fig. 3b the rightmost point. ^k: Driving through the cavity. ^l: Using $T_R = 4\pi\hbar/g\mu_B B_{ac}$ with $B_{ac} = 2.5$ mT and $g = 0.44$. ^m: 2 × 75 ns. ⁿ: (estimated) from Fig. 2b. ^o: Nuclear-driven EDSR. ^p: (estimated) from Fig. 2d: 9 oscillations in 30 μs at resonance. ^q: EDSR without a micromagnet. ^r: In a five-electron dot configuration. ^s: Valley and spin flip. ^t: (estimated) from Fig. 4d the rightmost red point.

Time	Operation	#Qubits	Qubit	Material	Host	Date	Reference	Source	
1.6 ns	gate	1Q	ST/e	GaAs/AlGaAs	2D	2020-12	122	Fig. 2a the green trace	1
2.5 ns	gate	1Q	ST/e	²⁸ Si/SiO ₂	2D	2022-02	127	p4 and Fig. 2e the rightmost point	2
3.1 ns	gate	1Q	ST/e	²⁸ Si/SiGe	2D	2016-03	239	Fig. 4a	3
4.2 ns	gate	1Q	ST/e	GaAs/AlGaAs	2D	2020-08	42	p4	4
15 ns	gate	1Q	ST/e	GaAs/AlGaAs	2D	2021-10	76	p3	5
36 ns	gate	1Q	ST/e	Si/SiGe	2D	2014-08	317	p3	6
38 ns	gate	1Q	ST/e	GaAs/AlGaAs	2D	2021-05	147	p3	7
44 ns ^a	gate	1Q	ST/e ^b	Si/SiGe	2D	2021-11	36	p4	8
91 ns	gate	1Q	ST/e	Si/SiGe	2D	2021-08	171	p3	9
0.1 μs	gate	1Q	ST/e	²⁸ Si/SiGe	2D	2020-03	276	p3	10
0.92 ns	gate	1Q	LD/h	Ge/Si	1D	2022-01	306	p3	11
1.2 ns	gate	1Q	LD/h	Ge/Si	1D	2021-01	84	Fig. 4	12
3.4 ns	gate	1Q	LD/h ^c	Si/SiO ₂	1D	2021-03	38	p4	13
5.9 ns	gate	1Q	LD/h	Si/SiO ₂	1D	2016-11	185	p4	14
7.1 ns	gate	1Q	LD/h	Ge/Si	1D	2018-09	313	Fig. 5d the point at 11 Db	15
8.8 ns	gate	1Q	LD/h	Ge/SiGe	2D	2020-07	110	p4 and Fig. 3b	16
10 ns ^d	gate	1Q	LD/h	Ge/SiGe	2D	2021-09	166	Fig. 2g	17
11 ns ^e	gate	1Q	LD/h ^c	Si/SiO ₂	1D	2021-03	38	p7 and Fig. 3e	18
18 ns ^f	gate	1Q	LD/h	Si/SiO ₂	1D	2018-03	55	Fig. 1d	19
20 ns	gate	1Q	LD/h	Ge/SiGe	2D	2020-01	109	p2	20
33 ns	gate	1Q	LD/h	Si/SiO ₂	1D	2019-07	54	p5 and Fig. 4d	21
96 ns	gate	1Q	LD/h	Ge/SiGe	2D	2021-09	166	p3	22
5.0 ns	gate	1Q	ST/h	Ge/SiGe	2D	2021-06	125	p2 and Fig. 3e	23
0.15 μs	gate	1Q	LD/i	Si:P	imp	2012-09	232	p2 and Fig. 2	24
0.83 μs	gate	1Q	LD/i	²⁸ Si:P	imp	2022-01	176	ED Fig. 3 first column	25
3 μs	gate	1Q	LD/i	²⁸ Si:P	imp	2016-10	62	p3	26
0.16 ms	gate	1Q	LD/ig ^g	²⁸ Si:P	imp	2016-10	163	p3 and Fig. 3d	27
74 ps	gate	2Q	charge	Si/SiGe	2D	2020-09	173	p4	28
10 ns ^h	gate	2Q	LD/e	GaAs/AlGaAs	2D	2011-09	32	p4	29
40 ns	gate	2Q	LD/e	²⁸ Si/SiGe	2D	2021-11	198	Fig. 2B caption	30
0.10 μs	gate	2Q	LD/e	²⁸ Si/SiGe	2D	2022-01	323	p6	31
0.13 μs	gate	2Q	LD/e	Si/SiGe	2D	2017-12	331	p2	32
0.16 μs	gate	2Q	LD/e	²⁸ Si/SiO ₂	2D	2015-10	295	p4	33
0.2 μs ⁱ	gate	2Q	LD/e	Si/SiGe	2D	2018-02	310	ED Fig. 9	34
0.27 μs	gate	2Q	LD/e	²⁸ Si/SiGe	2D	2019-06	264	Fig. 4d	35
0.30 μs	gate	2Q	LD/e	²⁸ Si/SiGe	2D	2019-11	263	p5	36
0.53 μs	gate	2Q	LD/e	Si/SiGe	2D	2020-03	328	p3	37
3 μs	gate	2Q	LD/e	Si/SiO ₂	2D	2021-05	168	Fig. 2j the rightmost point	38
2 ns	gate	2Q	ST/e	GaAs/AlGaAs	2D	2019-03	182	Fig. 2c	39
5.5 ns ^j	gate	2Q	ST/e	GaAs/AlGaAs	2D	2018-11	211	p4 and Fig. 3	40
0.14 μs	gate	2Q	ST/e	GaAs/AlGaAs	2D	2012-04	261	p3	41
9 ns	gate	2Q	LD/h	Ge/SiGe	2D	2021-03	111	Tab. S2	42
55 ns	gate	2Q	LD/h	Ge/SiGe	2D	2020-01	109	p4	43
0.80 ns	gate	2Q	LD/i	Si:P	imp	2019-07	107	Fig. 3 and abstract	44
5.6 μs ^k	gate	2Q	LD/i	²⁸ Si:P	imp	2021-01	175	Fig. 5c	45
0.40 μs ^l	measure	1Q	charge	InAs	1D	2015-07	268	p5	46
1 μs ^m	measure	1Q	charge	Si/SiO ₂	2D	2020-02	251	p5 and Fig. 4c the leftmost green point	47
0.98 μs ⁿ	measure	1Q	HY/e ^o	²⁸ Si/SiGe	2D	2021-12	20	p4	48
0.17 ms ^p	measure	1Q	HY/e	GaAs/AlGaAs	2D	2021-06	124	p3	49
0.4 μs	measure	1Q	LD/e	GaAs/AlGaAs	2D	2003-11	97	Fig. 3	50

TABLE III-2. Operation times (part 2). Superscripts stand for the following. ^a: The reference calls the observed signal ‘Rabi oscillations’ even though there is no ac field; these oscillations arise as a coherent precession upon pulsing the dot detuning. ^b: S-T_z qubit. ^c: At 1.5 kelvin. ^d: (estimated) Fig. 2g the leftmost point. ^e: Z-gate. ^f: (derived) from Fig. 1d showing 11 oscillations in 400 ns. ^g: Qubit defined in the rotating frame. ^h: SWAP time. ⁱ: The reference gives also the ‘decay time of the CZ operation’ of 1.6 μs in ED Fig. 9, which would correspond to a gate quality factor of 4.8. ^j: Gate between a single-spin and a singlet-triplet qubit. ^k: Fidelity not measured; signal visibility was 50 %. ^l: The value is for detecting an interdot charge transition with SNR 76. ^m: Dot-donor transition; SNR ≈ 5. ⁿ: SNR = 6.5. ^o: EO qubit. ^p: 32 μs+140 μs.

Time	Operation	#Qubits	Qubit	Material	Host	Date	Reference	Source	
24 μs^{a}	measure	1Q	LD/e	Si/SiGe	2D	2019-08	301	p7	1
0.70 ms	measure	1Q	LD/e	GaAs/AlGaAs	2D	2019-04	207	Fig. 1f	2
1 ms	measure	1Q	LD/e	Si/SiO ₂	1D	2021-09	267	p2	3
4 ms	measure	1Q	LD/e	Si/SiGe	2D	2014-08	134	p1	4
49 μs^{b}	measure	1Q	LD/e	Si/SiGe	2D	2020-04	321	p3	5
0.20 s	measure	1Q	LD/e	Si/SiGe	2D	2011-04	265	Fig. 2 caption	6
50 ns^{c}	measure	1Q	ST/e	Si/SiO ₂	1D	2021-05	117	p5 and Fig. 3	7
0.10 μs^{d}	measure	1Q	ST/e	GaAs/AlGaAs	2D	2010-04	10	p3 and Fig. 3	8
0.20 μs^{e}	measure	1Q	ST/e	GaAs/AlGaAs	2D	2014-01	112	SM Fig. S1d	9
0.80 μs	measure	1Q	ST/e	Si/SiGe	2D	2020-02	51	Fig. 5b	10
0.8 μs	measure	1Q	ST/e	GaAs/AlGaAs	2D	2018-04	204	p4	11
0.8 μs^{f}	measure	1Q	ST/e	Si/SiGe	2D	2020-01	213	Fig. 3c	12
1 μs	measure	1Q	ST/e	GaAs/AlGaAs	2D	2012-04	261	p1	13
1 μs	measure	1Q	ST/e	GaAs/AlGaAs	2D	2014-10	262	p2	14
1.7 μs	measure	1Q	ST/e	Si/SiGe	2D	2020-02	51	p6	15
2 μs	measure	1Q	ST/e	GaAs/AlGaAs	2D	2018-09	220	Fig. 4b the rightmost point	16
4 μs	measure	1Q	ST/e	GaAs/AlGaAs	2D	2017-07	206	p2 and SM p1	17
6 μs	measure	1Q	ST/e	GaAs/AlGaAs	2D	2009-10	9	p3	18
6 μs	measure	1Q	ST/e	Si/SiGe	2D	2019-08	334	p3 and Fig. 3f	19
10 μs	measure	1Q	ST/e	GaAs/AlGaAs	2D	2005-09	231	p2	20
10 μs^{g}	measure	1Q	ST/e	GaAs/AlGaAs	2D	2021-10	76	p3	21
13 μs^{h}	measure	1Q	ST/e	Si/SiGe	2D	2019-07	130	p3 and p6	22
20 μs	measure	1Q	ST/e	GaAs/AlGaAs	2D	2006-11	192	p2	23
33 μs^{i}	measure	1Q	ST/e	Si/SiO ₂	1D	2020-12	23	p6 and Fig. 7e	24
0.10 ms	measure	1Q	ST/e	2D	2021-04	27	p5	25	
0.22 ms	measure	1Q	ST/e	GaAs/AlGaAs	2D	2021-02	121	Fig. 2a caption	26
0.5 ms	measure	1Q	ST/e	Si/SiO ₂	1D	2019-05	284	abstract	27
2 ms	measure	1Q	ST/e	GaAs/AlGaAs	2D	2016-11	143	p3	28
4 μs^{j}	measure	1Q	ST/e	GaAs/AlGaAs	2D	2010-07	226	p4	29
20 ms	measure	1Q	ST/e	GaAs/AlGaAs	2D	2016-11	143	p3	30
10 μs	measure	1Q	LD/h	Ge/SiGe	2D	2021-09	166	p1	31
6 μs	measure	1Q	ST/h	Ge/SiGe	2D	2020-07	110	p4	32
1.5 μs	measure	1Q	LD/i	Si:P	imp	2019-10	136	p4	33
3 ms	measure	1Q	LD/i	Si:P	imp	2015-10	309	p4	34
40 ms	measure	1Q	LD/i	Si:P	imp	2013-06	33	Fig. 2b caption	35
50 μs^{k}	measure	1Q	LD/i	Si:P	imp	2018-03	31	SFig. 2d	36
0.15 s ^l	measure	1Q	LD/i	Si:P	imp	2015-10	309	Fig. 2b-c	37
0.20 s	measure	1Q	LD/i	Si:P	imp	2017-03	311	p3	38
65 μs^{m}	measure	1Q	ST/i ⁿ	Si:P	imp	2018-05	101	Tab. II	39
0.15 ms	measure	1Q	ST/i ⁿ	Si:P	imp	2018-05	101	Tab. II	40
0.3 ms	measure	1Q	ST/i	Si:P	imp	2018-11	222	p2	41
18 μs^{o}	measure	1Q	ST/i	Si:P	imp	2017-07	30	p3	42
2.6 ms	measure	2Q	ST/e	Si/SiO ₂	2D	2019-03	315	p3	43
50 μs^{p}	initialize	1Q	LD/e	Si/SiGe	2D	2018-02	310	ED Fig. 2	44
4 ms	initialize	1Q	LD/e	Si/SiGe	2D	2014-08	134	p1	45
20 μs^{q}	initialize	1Q	ST/e	GaAs/AlGaAs	2D	2014-10	262	p2	46
50 ns	initialize	1Q	ST/e	GaAs/AlGaAs	2D	2012-04	261	p1	47
20 μs^{r}	initialize	1Q	ST/e	Si/SiO ₂	1D	2019-05	284	Fig. 3	48
10 ms	initialize	1Q	LD/i	imp	2021-10	129	p5	49	

TABLE III-3. Operation times (part 3). Superscripts stand for the following. ^a: SNR = 3.4. ^b: 15 QND measurements, each taking 3.263 ms. ^c: SNR = 3.3 for an interdot charge transition ‘mimicking the singlet-triplet readout scheme’. ^d: SNR ~3. ^e: SNR = 4.1. ^f: SNR = 6. ^g: SNR = 5. ^h: SNR = 6.5. ⁱ: Detecting single electron transfer between neighboring dots. ^j: The reference estimates this time as required for SNR = 1. ^k: (estimated) as the duration of phase 3 in SFig. 2d. ^l: (estimated) from Fig. 2b-c. ^m: Latched readout. ⁿ: Hybrid ST qubit: impurity – gated dot. ^o: Latched readout; SNR = 6.4. ^p: Using spin hot-spot. ^q: Into singlet. ^r: Into triplet.

Fidelity	Operation	#Qubits	Qubit	Material	Host	Date	Reference	Source	
99.88 % ^a	gate	1Q	HY/e	Si/SiGe	2D	2021-11	95	p4	1
99.65 %	gate	1Q	HY/e ^b	²⁸ Si/SiGe	2D	2019-07	4	abstract	2
94.5 % ^c	gate	1Q	HY/e	Si/SiGe	2D	2015-12	142	p5 and Fig. 4e and g	3
91 % ^d	gate	1Q	HY/e ^e	Si/SiGe	2D	2014-07	140	p3	4
85 %	gate	1Q	HY/e ^f	Si/SiGe	2D	2019-11	224	p4	5
99.957 %	gate	1Q	LD/e	²⁸ Si/SiO ₂	2D	2019-04	325	abstract	6
99.95 %	gate	1Q	LD/e	²⁸ Si/SiO ₂	imp	2015-03	202	p6	7
99.926 %	gate	1Q	LD/e	²⁸ Si/SiGe	2D	2017-12	329	p4 and Fig. 5	8
99.91 %	gate	1Q	LD/e	²⁸ Si/SiO ₂	2D	2018-10	43	p3	9
99.91 %	gate	1Q	LD/e	Si/SiGe	2D	2021-06	277	p1 for Q3	10
99.84 %	gate	1Q	LD/e	²⁸ Si/SiGe	2D	2022-01	214	p4 and Fig. 2c	11
99.8 %	gate	1Q	LD/e	²⁸ Si/SiGe	2D	2018-10	275	p5	12
99.73 % ^g	gate	1Q	LD/e	²⁸ Si/SiGe	2D	2021-11	198	p1 and Fig. 1C	13
99.72 %	gate	1Q	LD/e	²⁸ Si/SiGe	2D	2022-01	323	p2	14
99.7 %	gate	1Q	LD/e	Si/SiGe	2D	2017-12	331	p2	15
99.7 %	gate	1Q	LD/e ^h	Si/SiO ₂	2D	2020-02	167	SM Fig. 3	16
99.69 %	gate	1Q	LD/e ⁱ	Si/SiGe	2D	2021-05	322	p4	17
99.6 %	gate	1Q	LD/e	Si/SiGe	2D	2016-08	274	p4	18
99.6 %	gate	1Q	LD/e	²⁸ Si/SiO ₂	2D	2014-10	293	p2 and Fig. 4	19
99.5 %	gate	1Q	LD/e	²⁸ Si/SiO ₂	2D	2019-05	116	ED Tab. 2	20
99.3 %	gate	1Q	LD/e ^j	²⁸ Si/SiO ₂	2D	2015-11	294	p4 and Fig. 4c	21
99.3 %	gate	1Q	LD/e ^k	²⁸ Si/SiO ₂	2D	2020-04	229	p3 and Fig. 2g	22
99.1 %	gate	1Q	LD/e	²⁸ Si/SiO ₂	2D	2022-03	335	p5 and S Fig. 15f	23
99 %	gate	1Q	LD/e	Si/SiGe	2D	2016-10	135	p5	24
98.8 %	gate	1Q	LD/e	Si/SiGe	2D	2018-02	310	p1 and ED Fig. 4	25
98.8 %	gate	1Q	LD/e	Si/SiGe	2D	2019-04	320	p7	26
97.5 %	gate	1Q	LD/e	GaAs/AlGaAs	2D	2020-03	208	p3 and Fig. 4e	27
96.6 %	gate	1Q	LD/e	GaAs/AlGaAs	2D	2014-12	327	p2	28
81 %	gate	1Q	LD/e	InSb	1D	2013-02	285	p3	29
73 %	gate	1Q	LD/e	GaAs/AlGaAs	2D	2006-08	149	p5	30
48 %	gate	1Q	LD/e	InAs	1D	2010-12	205	p2	31
99.76 % ^l	gate	1Q	ST/e	²⁸ Si/SiO ₂	2D	2020-04	326	Fig. 3d	32
99.6 %	gate	1Q	ST/e	²⁸ Si/SiGe	2D	2020-03	276	p4	33
99.5 %	gate	1Q	ST/e	GaAs/AlGaAs	2D	2020-08	42	Fig. 3	34
98.6 %	gate	1Q	ST/e	GaAs/AlGaAs	2D	2017-01	209	p3 and Fig. 2c	35
98.6 % ^m	gate	1Q	ST/e	²⁸ Si/SiO ₂	2D	2020-04	326	Fig. 3h	36
98.5 %	gate	1Q	ST/e	GaAs/AlGaAs	2D	2016-06	41	p4	37
99.9899%	gate	1Q	LD/h	Ge/SiGe	2D	2021-09	166	p2 and Fig. 2k	38
99.9 %	gate	1Q	LD/h	Ge/SiGe	2D	2021-03	111	Fig. S4 dot 3	39
99.3 %	gate	1Q	LD/h	Ge/SiGe	2D	2020-01	109	p2 and Fig. 2d	40
98.9 %	gate	1Q	LD/h ^m	Si/SiO ₂	1D	2021-03	38	p6 and Fig. 3b	41
96.3 % ⁿ	gate	1Q	LD/h	Ge/SiGe	2D	2021-09	166	Fig. 2g	42
99.942 %	gate	1Q	LD/i	²⁸ Si:P	imp	2016-10	62	p6 and Fig. 3	43
99.6 %	gate	1Q	LD/i	²⁸ Si:P	imp	2014-10	203	p2	44
99.4 %	gate	1Q	LD/i	Si:P	imp	2015-04	162	p4 and Fig. 4a	45
99 % ^o	gate	1Q	LD/i	²⁸ Si:P	imp	2022-01	176	p3	46
68 %	gate	2Q	charge	GaAs/AlGaAs	2D	2015-07	170	p4	47
63 %	gate	2Q	charge	Si/SiGe	2D	2020-09	173	p4	48
99.81 % ^p	gate	2Q	LD/e	²⁸ Si/SiGe	2D	2021-11	198	p3	49
99.65 % ^q	gate	2Q	LD/e	²⁸ Si/SiGe	2D	2022-01	323	p3 and ED Fig. 5	50

TABLE IV-1. Operation infidelities (part 1). Superscripts stand for the following. ^a: Per Clifford gate. ^b: EO qubit. ^c: Average of $\mathcal{F}[X_\pi] = 93\%$ and $\mathcal{F}[Z_\pi] = 96\%$. ^d: The average of the six fidelity values given. ^e: Hybrid qubit with three electrons in two dots. ^f: Electron-valley qubit. ^g: The average of the six values given in Fig. 1C. ^h: In a five-electron dot configuration. ⁱ: With the control chip inside the fridge. ^j: A three-electron qubit. ^k: At 1 kelvin. ^l: At 0.04 kelvin. ^m: At 1.5 kelvin. ⁿ: (estimated) Fig. 2g the leftmost point. ^o: Lower limit. ^p: CZ gate. ^q: CZ.

Fidelity	Operation	#Qubits	Qubit	Material	Host	Date	Reference	Source	
99.51	% ^a	gate	2Q	LD/e	²⁸ Si/SiGe	2D	2022-01	214	p4 and Fig. 2g
98.62	% ^b	gate	2Q	LD/e	²⁸ Si/SiGe	2D	2021-11	198	p3
98.2	%	gate	2Q	LD/e	²⁸ Si/SiO ₂	2D	2022-02	73	p4 and Fig. 3a
98	%	gate	2Q	LD/e	²⁸ Si/SiO ₂	2D	2019-05	116	p4 and Fig. 4
92	%	gate	2Q	LD/e	Si/SiGe	2D	2019-04	320	p7
86.1	%	gate	2Q	LD/e ^c	²⁸ Si/SiO ₂	2D	2020-04	229	p3 and Fig. 3d
84	% ^d	gate	2Q	LD/e	²⁸ Si/SiGe	2D	2019-11	263	p6
56	% ^e	gate	2Q	LD/e	Si/SiGe	2D	2017-12	331	p3
90	%	gate	2Q	ST/e	GaAs/AlGaAs	2D	2017-01	209	p4 and Fig. 4e
72	% ^f	gate	2Q	ST/e	GaAs/AlGaAs	2D	2012-04	261	p3
90	%	gate	2Q	LD/i	Si:P	imp	2019-07	107	p3
99.975	% ^{g,h}	measure	1Q	HY/e ⁱ	²⁸ Si/SiGe	2D	2021-12	20	p8 and Fig. 7
96.4	%	measure	1Q	HY/e	GaAs/AlGaAs	2D	2021-06	124	p4 and Fig. 2d
75	%	measure	1Q	HY/e ⁱ	GaAs/AlGaAs	2D	2013-09	187	p4
99	% ^j	measure	1Q	LD/e	²⁸ Si/SiGe	2D	2021-11	198	p1
97	%	measure	1Q	LD/e	GaAs/AlGaAs	2D	2016-01	7	abstract
95	%	measure	1Q	LD/e	Si/SiGe	2D	2014-08	134	p1
95	%	measure	1Q	LD/e	²⁸ Si/SiO ₂	2D	2014-10	293	p2
95	%	measure	1Q	LD/e	Si/SiGe	2D	2020-03	328	p5
94.5	%	measure	1Q	LD/e	Si/SiGe	2D	2020-04	321	abstract and p3
92	%	measure	1Q	LD/e	Si/SiO ₂	1D	2021-09	267	p2
89.9	%	measure	1Q	LD/e	Si/SiGe	2D	2021-06	277	p1 for Q3
89	%	measure	1Q	LD/e	GaAs/AlGaAs	2D	2019-04	207	p3
86	%	measure	1Q	LD/e	GaAs/AlGaAs	2D	2011-08	216	p4
82.5	% ^k	measure	1Q	LD/e	GaAs/AlGaAs	2D	2004-07	70	p4
81	%	measure	1Q	LD/e	Si/SiGe	2D	2018-02	310	p1
80	%	measure	1Q	LD/e	InAs	1D	2010-12	205	p1
99.5	% ^l	measure	1Q	ST/e	GaAs/AlGaAs	2D	2017-07	206	p4
99.3	%	measure	1Q	ST/e	²⁸ Si/SiO ₂	2D	2019-12	333	p2
99.2	%	measure	1Q	ST/e	²⁸ Si/SiGe	2D	2021-04	27	p5
99	%	measure	1Q	ST/e	²⁸ Si/SiO ₂	2D	2018-10	80	p2
99	%	measure	1Q	ST/e	Si/SiGe	2D	2020-02	51	p6
98.45	% ^m	measure	1Q	ST/e	Si/SiO ₂	1D	2019-05	284	abstract and p2
98.2	%	measure	1Q	ST/e	Si/SiGe	2D	2020-02	51	Fig. 5b
98	%	measure	1Q	ST/e	GaAs/AlGaAs	2D	2014-10	262	p2
98	%	measure	1Q	ST/e	Si/SiGe	2D	2019-08	334	p3 and Fig. 3f
97.5	%	measure	1Q	ST/e	GaAs/AlGaAs	2D	2006-11	191	p3
97	% ⁿ	measure	1Q	ST/e	GaAs/AlGaAs	2D	2016-11	143	p4
96	%	measure	1Q	ST/e	GaAs/AlGaAs	2D	2018-04	204	p4
95	%	measure	1Q	ST/e	GaAs/AlGaAs	2D	2017-06	86	p2
95	%	measure	1Q	ST/e	GaAs/AlGaAs	2D	2021-02	121	p1
93	%	measure	1Q	ST/e	GaAs/AlGaAs	2D	2020-06	235	p5 and SM Fig. 11
90	%	measure	1Q	ST/e	GaAs/AlGaAs	2D	2009-10	9	p3
90	%	measure	1Q	ST/e	GaAs/AlGaAs	2D	2020-07	123	p4
87	%	measure	1Q	ST/e	GaAs/AlGaAs	2D	2006-11	192	p2
80	%	measure	1Q	ST/e	GaAs/AlGaAs	2D	2015-08	14	p3
80	%	measure	1Q	ST/e	GaAs/AlGaAs	2D	2017-09	78	p2
80	%	measure	1Q	ST/e	GaAs/AlGaAs	2D	2018-09	220	p4
80	%	measure	1Q	ST/e	GaAs/AlGaAs	2D	2021-05	147	p2 and p3
76	% ^o	measure	1Q	ST/e	GaAs/AlGaAs	2D	2016-11	143	p4

TABLE IV-2. Operation infidelities (part 2). Superscripts stand for the following. ^a: CNOT. ^b: CNOT gate synthetized using the CZ gate. ^c: At 1 kelvin. ^d: SWAP. ^e: Resonantly induced CNOT. ^f: Fidelity of a Bell state produced using CPHASE. ^g: The corresponding infidelity includes both preparation and measurement errors. ^h: Reference reports F_{BC} , standing for ‘benchmark contrast fidelity’ and advocates using it instead of ‘assignment fidelity’ F_A which corresponds to our Eq. (19). ⁱ: EO qubit. ^j: The average of the figure of merit for the two qubits measured. ^k: The average of 93 % and 72 %. ^l: Latched readout. ^m: The average of 99.6 % and 97.3 %; latched readout. ⁿ: S/T binary result. ^o: $S/T_0/T_+$ ternary result.

Fidelity	Operation	#Qubits	Qubit	Material	Host	Date	Reference	Source	
93.55	% ^a	measure	1Q	LD/h	BLG	2D	2021-12	87	p5 and Fig. 4
87	% ^b	measure	1Q	LD/h	Ge/Si	1D	2018-10	302	p3
78	% ^c	measure	1Q	ST/h	Ge/SiGe	2D	2020-07	110	p4
99.8	%	measure	1Q	LD/i	Si:P	imp	2017-03	311	p3 and p4
99.8	%	measure	1Q	LD/i	Si:P	imp	2015-10	309	p3 and Fig. 4a
98.7	%	measure	1Q	LD/i	Si:P	imp	2015-10	309	p3 and Fig. 4b
97.7	%	measure	1Q	LD/i	Si:P	imp	2019-01	146	p3
97.6	%	measure	1Q	LD/i	Si:P	imp	2018-03	31	p2 and STable 1 line F_M qubit R
97	%	measure	1Q	LD/i	²⁸ Si:P	imp	2014-10	203	p2
97	%	measure	1Q	LD/i	Si:P	imp	2019-10	136	p4
96	%	measure	1Q	LD/i	Si:P	imp	2010-09	199	p4 and Fig. 4c
95	% ^d	measure	1Q	LD/i	Si:P	imp	2013-06	33	p3 and Fig. S2
90	%	measure	1Q	LD/i	Si:P	imp	2012-09	232	p3
80	%	measure	1Q	LD/i	²⁸ Si:P	imp	2022-01	176	p9
99.864	% ^e	measure	1Q	ST/i ^f	Si:P	imp	2018-05	101	Tab. II
99.3	%	measure	1Q	ST/i ^f	Si:P	imp	2018-05	101	Tab. II
98.4	% ^e	measure	1Q	ST/i	Si:P	imp	2017-07	30	p3 and abstract
95	%	measure	1Q	ST/i	Si:P	imp	2014-06	61	p3
82.9	%	measure	1Q	ST/i	Si:P	imp	2018-11	222	p4
75	%	measure	2Q	ST/e	Si/SiO ₂	2D	2019-03	315	p3
99.975	% ^{g,h}	initialize	1Q	HY/e ⁱ	²⁸ Si/SiGe	2D	2021-12	20	p8 and Fig. 7
99	% ^j	initialize	1Q	LD/e	Si/SiGe	2D	2018-02	310	p1
99	%	initialize	1Q	LD/e	Si/SiGe	2D	2020-03	328	p5
99	%	initialize	1Q	LD/e	Si/SiGe	2D	2021-06	277	p1
98.4	% ^k	initialize	1Q	LD/e	²⁸ Si/SiGe	2D	2021-11	198	p1
95	%	initialize	1Q	LD/e	Si/SiGe	2D	2014-08	134	p1
95	%	initialize	1Q	LD/e	²⁸ Si/SiGe	2D	2019-11	263	p1
92	%	initialize	1Q	LD/e	²⁸ Si/SiO ₂	2D	2014-10	293	p2
98.5	% ^l	initialize	1Q	ST/e	Si/SiO ₂	1D	2019-05	284	p3
95	%	initialize	1Q	ST/e	GaAs/AlGaAs	2D	2021-02	121	p1
89	%	initialize	1Q	ST/e	GaAs/AlGaAs	2D	2020-06	235	p5
98.9	%	initialize	1Q	LD/i	²⁸ Si:P	imp	2021-10	129	p5 and Fig. 3
96.6	% ^{k,n}	initialize	2Q	LD/e	²⁸ Si/SiGe	2D	2021-11	198	p2
96	% ⁿ	initialize	2Q	LD/e	²⁸ Si/SiO ₂	2D	2022-02	73	p6 and Fig. 3b
94.1	% ^o	initialize	2Q	LD/e	Si/SiGe	2D	2021-06	277	p2
90	% ^o	initialize	2Q	LD/e	Si/SiO ₂	2D	2021-05	168	Fig. 3 caption
89	% ^o	initialize	2Q	LD/e	Si/SiGe	2D	2018-02	310	p3
89	% ^o	initialize	2Q	LD/e	²⁸ Si/SiO ₂	2D	2019-05	116	p3
93	% ^o	initialize	2Q	ST/e	GaAs/AlGaAs	2D	2017-01	209	p4
88	% ^p	initialize	3Q	LD/e	Si/SiGe	2D	2021-06	277	p4

TABLE IV-3. Operation infidelities (part 3). Superscripts stand for the following. ^a: The average of 97 % and 90.1 %, the measurement fidelities for the two spin states. ^b: The average of 90.7 % and 83.3 %. ^c: (*derived*) from visibility, $1 - F = [1 - v]/2$ with $v = 0.56$. ^d: (*derived*) from visibility $V = 93.4 \%$. ^e: Latched readout. ^f: Hybrid ST qubit: impurity – gated dot. ^g: The corresponding infidelity includes both preparation and measurement errors. ^h: Reference reports F_{BC} , standing for ‘benchmark contrast fidelity’ and advocates using it instead of ‘assignment fidelity’ F_A which corresponds to our Eq. (19). ⁱ: EO qubit. ^j: Using spin hot-spot. ^k: The average of the figure of merit for the two qubits measured. ^l: Into triplet. ^m: The average fidelity of the four Bell-states; there was no correction for SPAM. ⁿ: Fidelity of a Bell state; the article gives a range 94.6–98.3 %. The value 96 % was (*estimated*) from Fig. 3b. ^o: Into a Bell state using a two-qubit algorithm. ^p: Initialization into the GHZ state through a quantum algorithm.

Quality factor	#Qubits	Qubit	Material	Host	Date	Reference	Source	0
200 ^a	2Q	LD/e	Si/SiO ₂	2D	2021-05	168	Fig. 2j the rightmost point	1
52	1Q	ST/h	Ge/SiGe	2D	2021-06	125	p4 and SM Fig. 15c	2
22.8 ^b	1Q	LD/h	Ge/Si	1D	2022-01	306	p4	3
20	1Q	ST/e	²⁸ Si/SiO ₂	2D	2022-02	127	p4 and Fig. 2g the rightmost point	4
19 ^c	2Q	ST/e	GaAs/AlGaAs	2D	2018-11	211	p4	5
18.8 ^d	1Q	LD/h ^e	Si/SiO ₂	1D	2021-03	38	SM Fig. S11	6
17 ^f	1Q	LD/eg	Si/SiO ₂	2D	2020-02	167	SM Fig. 4c	7
15 ^h	1Q	ST/e	GaAs/AlGaAs	2D	2014-01	112	abstract and Fig. 4a	8
14 ^f	1Q	ST/e	GaAs/AlGaAs	2D	2020-07	123	p4	9
9.1 ⁱ	1Q	LD/h	Ge/Si	1D	2018-09	313	p4	10
6 ^j	1Q	ST/e	GaAs/AlGaAs	2D	2013-04	67	p3	11

TABLE V-1. Quality factors (qubit). Superscripts stand for the following. ^a: The reference defines $Q = JT_2^{\text{CZ}}$, with T_2^{CZ} the decay time of the controlled-Z two-qubit gate. ^b: (derived) the reference defines $Q = 2f_R T_2^*$. To convert to our definition, we divide by 2 and use $f_R = 542$ MHz and $T_2^* = 42$ ns. ^c: The reference defines $Q = 2JT_2^*/\hbar$. To convert to our definition, we divide by 2. ^d: The reference defines $Q^* = 2f_R T_2^*$ and reports up to $Q^* = 37.6$ (*estimated*) as the rightmost blue point in Fig. S11. To convert to our definition, we divide by 2. ^e: At 1.5 kelvin. ^f: The reference defines $Q = T_2^*/T_{\text{op}}$. To convert to our definition, we divide by 2. ^g: In a five-electron dot configuration. ^h: The reference defines $Q = [J/2\pi\hbar]/\Gamma_\Sigma$ with $J/2\pi\hbar \approx 1.5$ GHz and $\Gamma_\Sigma \approx 100$ MHz from Fig. 3d. ⁱ: The reference defines "the ratio T_2^*/T_{op} ", without using the term "quality factor" explicitly. To convert to our definition, we divide by 2 and use $f_R = 70$ MHz and $T_2^* = 130$ ns. ^j: The reference defines $Q = T_2^{\text{Echo}} J/2\pi\hbar$, giving the maximal value $Q = 600$ for $T_2^{\text{Echo}} = 9$ μ s. Converting to our definition results in the quality factor at least hundred times smaller, since the maximal T_2^* was 90 ns, see Fig. 4b.

Quality factor	#Qubits	Qubit	Material	Host	Date	Reference	Source	0
444 ^a	1Q	LD/e	²⁸ Si/SiGe	2D	2017-12	329	p2	1
70 ^b	1Q	LD/e	Si/SiGe	2D	2016-08	274	p3	2
44	1Q	ST/e	²⁸ Si/SiGe	2D	2016-03	239	Fig. 4b the topmost red point	3
43.5 ^c	1Q	LD/h ^d	Si/SiO ₂	1D	2021-03	38	p5	4
42.5 ^e	1Q	LD/e	GaAs/AlGaAs	2D	2020-03	208	Fig. 6	5
35 ^f	1Q	ST/e	GaAs/AlGaAs	2D	2016-03	183	p2 and Fig. 4d	6
26 ^g	2Q	LD/e	²⁸ Si/SiO ₂	2D	2015-10	295	p4	7
9 ^h	1Q	LD/e	Si/SiGe	2D	2020-01	56	p4	8
8 ⁱ	1Q	HY/e ^{j,k}	GaAs/AlGaAs	2D	2017-07	181	Fig. 4c	9
5.1	1Q	ST/e	GaAs/AlGaAs	2D	2021-10	76	Fig. 2c Qubit 2	10
5 ^l	1Q	LD/e	InAs	1D	2010-12	205	p2 and Fig. 2d	11
4 ⁱ	1Q	HY/e ^{m,k}	GaAs/AlGaAs	2D	2017-07	181	Fig. 4c	12

TABLE V-2. Quality factors (gate). Superscripts stand for the following. ^a: The reference defines $Q = 2f_R T_2^{\text{Rabi}}$. To convert to our definition, we divide 2, and use $f_R = 3.9$ MHz and $T_2^{\text{Rabi}} = 113$ μ s to get $Q = 444$. ^b: The reference defines $Q = 2f_R T_2^{\text{Rabi}}$. To convert to our definition, we divide by 2. ^c: The reference defines $Q = 2f_R T_2^{\text{Rabi}}$ and finds $Q \gg 87$. To convert to our definition, we divide by 2 and take the stated lower limit. ^d: At 1.5 kelvin. ^e: The reference defines $Q = 2f_R T_2^{\text{Rabi}}$. To convert to our definition, we divide by 2. ^f: The reference defines the quality factor as "the number of [exchange-induced singlet-triplet] oscillations before the [oscillation-signal] amplitude decays to $1/e$ of its initial value", corresponding qualitatively to $f_R T_2^{\text{Rabi}}$. ^g: The reference defines $N_{\text{CZ}} = f_{\text{CZ}} T_2^{\text{CZ}}$ with $T_2^{\text{CZ}} = 8.3$ μ s. ^h: The reference defines $Q = 2T_2^{\text{Rabi}} f_R$. To convert to our definition, we divide by 2. ⁱ: Approximate value at $f_R = 100$ MHz. ^j: At a full sweet spot. ^k: Resonant exchange qubit. ^l: Rough approximation, given as 'number of resolved Rabi oscillation periods'. ^m: At a partial sweet spot.

Dimensions	Functionality	Qubit	Material	Host	Date	Reference	o
9	device	LD/e	Si/SiGe	2D	2016-11	330	1
9	device	LD/e	²⁸ Si/SiGe	2D	2019-03	197	2
3 × 3	device	LD/e	GaAs/AlGaAs	2D	2020-12	200	3
3 × 3	device	LD/e	Si/SiO ₂	2D	2021-01	243	4
3 × 3	device	LD/e	GaAs/AlGaAs	2D	2021-08	201	5
8	device	LD/e	GaAs/AlGaAs	2D	2019-04	299	6
4 × 2	device	LD/e	Si/SiO ₂	1D	2020-08	45	7
5	device	LD/e	GaAs/AlGaAs	2D	2016-12	119	8
5	device	LD/e	Si/SiGe	2D	2020-02	164	9
4	device	LD/e	GaAs/AlGaAs	2D	2014-03	273	10
4	device	LD/e	GaAs/AlGaAs	2D	2014-05	63	11
4	device	LD/e	GaAs/AlGaAs	2D	2016-07	6	12
4	device	LD/e	GaAs/AlGaAs	2D	2016-08	221	13
4	device	LD/e	GaAs/AlGaAs	2D	2017-06	86	14
4	device	LD/e	GaAs/AlGaAs	2D	2018-08	120	15
4	device	LD/e	GaAs/AlGaAs	2D	2021-01	288	16
2 × 2	device	LD/e	GaAs/AlGaAs	2D	2012-09	281	17
2 × 2	device	LD/e	GaAs/AlGaAs	2D	2018-04	204	18
2 × 2	device	LD/e	Si/SiO ₂	1D	2020-09	69	19
2 × 2	device	LD/e	Si/SiO ₂	1D	2020-10	90	20
2 × 2	device	LD/e	Si/SiO ₂	1D	2020-12	23	21
2 × 2	device	LD/e	Si/SiO ₂	1D	2020-12	5	22
2 × 2	device	ST/e	GaAs/AlGaAs	2D	2021-10	76	23
2 × 2	device	LD/h	Ge/SiGe	2D	2020-02	164	24
2 × 2	device	LD/h	Ge/SiGe	2D	2020-07	110	25
2 × 2	device	LD/h	Ge/SiGe	2D	2021-01	289	26
2 × 2	device	LD/h	Ge/SiGe	2D	2021-09	166	27
3	device	LD/e	GaAs/AlGaAs	2D	2009-11	88	28
3	device	LD/e	GaAs/AlGaAs	2D	2013-02	35	29
3	device	LD/e	GaAs/AlGaAs	2D	2016-01	7	30
3	device	LD/e	GaAs/AlGaAs	2D	2017-06	79	31
3	device	LD/e	GaAs/AlGaAs	2D	2017-09	78	32
3	device	LD/e	GaAs/AlGaAs	2D	2017-10	210	33
3	device	LD/e	Si/SiGe	2D	2019-07	130	34
3	device	LD/e	Si/SiO ₂	2D	2020-02	164	35
3	device	LD/e	²⁸ Si/SiO ₂	2D	2021-01	44	36
3	device	LD/e	GaAs/AlGaAs	2D	2021-05	147	37
3	device	ST/e	GaAs/AlGaAs	2D	2020-12	122	38
3	device	LD/h	Ge/Si	1D	2018-08	83	39
2	device	HY/e	²⁸ Si/SiGe	2D	2021-04	47	40

TABLE VI-1. Qubit arrays (part 1).

Dimensions	Functionality	Qubit	Material	Host	Date	Reference	o
2	device	HY/e	Si/SiGe	2D	2021-11	95	1
2	device	ST/e	GaAs/AlGaAs	2D	2011-07	290	2
2	device	ST/e	GaAs/AlGaAs	2D	2018-10	57	3
2	device	LD/h	Ge/SiGe	2D	2019-03	99	4
4	simulator	LD/e	²⁸ Si/SiGe	2D	2019-06	264	5
4	simulator	LD/e	GaAs/AlGaAs	2D	2019-09	131	6
4	simulator	LD/e	GaAs/AlGaAs	2D	2020-06	235	7
4	simulator	LD/e	GaAs/AlGaAs	2D	2020-07	234	8
4	simulator	LD/e	GaAs/AlGaAs	2D	2021-01	236	9
4	simulator	LD/e	GaAs/AlGaAs	2D	2021-04	132	10
4	simulator	LD/e	GaAs/AlGaAs	2D	2021-11	287	11
2 × 2	simulator	LD/e	GaAs/AlGaAs	2D	2020-03	60	12
3	simulator	LD/e	²⁸ Si/SiGe	2D	2015-05	71	13
3	simulator	LD/e	GaAs/AlGaAs	2D	2016-10	8	14
3	simulator	LD/e	GaAs/AlGaAs	2D	2018-11	211	15
3	simulator	LD/e	GaAs/AlGaAs	2D	2019-04	207	16
3	simulator	LD/e	GaAs/AlGaAs	2D	2020-03	208	17
2	simulator	LD/e	GaAs/AlGaAs	2D	2011-08	216	18
2	simulator	LD/e	GaAs/AlGaAs	2D	2011-09	32	19
2	simulator	ST/e	GaAs/AlGaAs	2D	2012-04	261	20
2	simulator	ST/e	GaAs/AlGaAs	2D	2019-03	182	21
2 × 2	processor	LD/h	Ge/SiGe	2D	2021-03	111	22
3	processor	LD/e	Si/SiGe	2D	2021-06	277	23
2	processor	LD/e	²⁸ Si/SiO ₂	2D	2015-10	295	24
2	processor	LD/e	Si/SiGe	2D	2017-12	331	25
2	processor	LD/e	Si/SiGe	2D	2018-02	310	26
2	processor	LD/e	Si/SiO ₂	2D	2021-05	168	27
2	processor	LD/e	²⁸ Si/SiGe	2D	2021-11	198	28
2	processor	LD/h	Ge/SiGe	2D	2020-01	109	29

TABLE VI-2. Qubit arrays (part 2).

Appendix D: Glossary

This section defines keywords with specific meaning used in plots and tables. Some are defined in the text, some are defined only here.

First, we define the following special keywords.

(derived): The value is not stated in the reference. We derived it as described in the ‘note’.

(estimated): The value is not stated in the reference. We estimated it from available information, most often from a figure. The estimate is only rough, with a typical error of order one.

attribute: A generic attribute. Several ‘value’s belong under it.

value: A generic value. It belongs under a unique ‘attribute’.

The list of the ‘attribute’s and ‘value’s, the latter for the case when the allowed values are from a small set of enumerated alternatives.

1D: The quantum dot host is quasi-one-dimensional, such as a nanowire. This is one of the values of ‘Host’.

2D: The quantum dot host is quasi-two-dimensional, such as a two-dimensional electron (or hole) gas of a quantum well, an epilayer, or a similar heterostructure. This is one of the values of ‘Host’.

charge: The qubit basis is represented by two different orbitals of a confined particle. Most often, the orbitals differ in their centers (positions), for example a pair of states localized each in one minimum of a double-well potential of a double dot. Unlike for spin-related qubits, we do not discriminate the carrier, be it electron, hole, or impurity. However, most charge-qubit experiments use electrons. This is one of the values of ‘Qubit’.

Coherence: It describes in what type of experiment the corresponding coherence time has been measured. This attribute can have the following values: T_1 , T_2^* , T_2^{Echo} , T_2^{DynD} , and T_2^{Rabi} .

Date: Publication date. In tables, the year and month are given. In plots, the full date down to a day (if available) is used in sorting and horizontal shifts. If the reference is unpublished (only an arxiv version exists), we use the submission date of the first arxiv version.

device: The array functionality is at the lowest level out of those spanning the range from fabricating a sample to implementing a fully functional quantum processor. See Sec. VI A for details. This is one of the values of ‘Functionality’.

Dimensions: The single dimension of a one-dimensional array, or the two dimensions of a two-dimensional array starting with the larger one.

Fidelity: Operation fidelity. See Sec. IV A for details.

Functionality: What functionality is available for the qubit-array initialization, manipulation, and measurement. See Sec. VI A. This attribute can have the following values: ‘device’, ‘simulator’, and ‘processor’.

gate: The operation is a gate. We use the following acronyms: the “C” in the two-qubit gates CZ, CPHASE, and CNOT stands for “controlled”. SWAP is a two-qubit gate exchanging the two states. See [190] for more on how such gates are used in basic algorithms. Single qubit gates are often induced by ESR (electron spin resonance) or EDSR (electric dipole spin resonance). This is one of the values of ‘Operation’.

Host: Where are the dots defined. This attribute can have the following values: ‘2D’, ‘1D’, and ‘imp’.

HY/e: The qubit basis is represented by electron states having hybrid character, most often differing in both the spin and charge degrees of freedom. This is one of the values of ‘Qubit’.

imp: The quantum dot host is an impurity. In this review we include only experiments on gated impurities accessed electrically. This is one of the values of ‘Host’.

initialize: The operation is an initialization. Concerning three-qubit initializations, “GHZ” stands for Greenberger-Horne-Zeilinger state. This is one of the values of ‘Operation’.

LD/e: The qubit basis is represented by the spin-up and spin-down state of a confined conduction-band electron (or many-electron) state. The acronym stands for the names of Daniel Loss and David DiVincenzo, who established the field of spin qubits by their Ref. [172]. This is one of the values of ‘Qubit’.

LD/h: The same as ‘LD/e’ but using valence-band holes instead of conduction-band electrons. This is one of the values of ‘Qubit’.

LD/i: The same as ‘LD/e’ but using impurity-bound electrons instead of conduction-band electrons confined by gates [133]. This is one of the values of ‘Qubit’.

Material: Material of the device. Most of the structures used in experiments are composites, for example a heterostructure with GaAs and AlGaAs layers is given as

GaAs/AlGaAs. In some plots we merge groups of materials by retaining only the primary material where the qubit host particle is located. For example, under such a contraction both "Si/SiO₂" and "Si/Ge" become "Si". When merging in this way, we further merge binary and ternary alloys of Al, Ga, In, As, and Sb under the key "III-V". For carbon-based materials, we use "SLG" for single-layer graphene (usually etched), "BLG" for bi-layer graphene, and "CNT" for a carbon nanotube. When merging, carbon-based materials become "C". We use "Si:P" and "Si:B" for a phosphorus and a boron impurity in silicon (at the moment, we have no data on other impurities). When merging, they become "Si:X".

'measure': The operation is a measurement. This is one of the values of 'Operation'.

'Note': Additional information concerning the 'value' exists, indicated by a superscript. The corresponding note is given in the table caption.

'Operation': The operation type. This attribute can have the following values: 'gate', 'measure', and 'initialize'.

'processor': The array functionality is at the highest level out of those spanning the range from fabricating a sample to implementing a fully functional quantum processor. See Sec. VI A for details. This is one of the values of 'Functionality'.

'Quality factor': (For a gate). The number of gate-signal oscillations before the signal amplitude drops to 1/e. See Sec. V for details.

'Quality factor': (For a qubit). The number of gate-signal oscillations within the inhomogeneous dephasing time. See Sec. V for details.

'Qubit': Which degree of freedom defines the qubit. It includes the carrier (such as the electron, hole, or impurity) and the subspace representing the qubit states' pair, such as the spin-1/2 (the LD qubit), the singlet and triplet (the ST qubit), orbitals (the charge qubit), and their hybrids, among others the exchange-only (EO) and resonant-exchange (RX) qubits. This attribute can have the following values: 'charge', 'HY/e', 'LD/e', 'ST/e', 'LD/h', 'ST/h', 'LD/i', and 'ST/i'.

'#Qubits': Number of qubits that the operation involves.

'Reference': The number referring to the bibliography at the end of the document. The bibliography is sorted alphabetically in first authors' names.

'simulator': The array functionality is at the second level out of those spanning the range from fabricating a sample to implementing a fully functional quantum processor. See Sec. VI A for details. This is one of the values of 'Functionality'.

'Source': Where in the reference the value can be found. Typical sources are page X, denoted as pX, or figure Y, denoted as Fig. Y. Multiple places might be given, if relevant. An example of the value source is "p3 and Fig. 2a".

'ST/e': The qubit basis is represented by the spin-singlet and spin-triplet state of a confined conduction-band electron pair [169]. This is one of the values of 'Qubit'.

'ST/h': The same as 'ST/e' but using valence-band holes instead of conduction-band electrons. This is one of the values of 'Qubit'.

'ST/i': The same as 'ST/e' but using impurity-bound electrons instead of conduction-band electrons confined by gates. This is one of the values of 'Qubit'.

'T₁: Energy relaxation. The decay of population of the energy basis state(s) was measured. Even though relaxation is physically a different process than decoherence, to simplify the database design we include the relaxation time among the coherence times. This is one of the values of 'Coherence'.

'T₂*': Inhomogeneous dephasing. The experiment measured the decay of phase of an idling qubit without any echos. Most often, it corresponds to a Ramsey sequence: initialization – $\pi/2$ pulse – free precession for time $\tau - \pi/2$ pulse – measurement. This is one of the values of 'Coherence'.

'T₂^{DynD}: Dephasing under a dynamical decoupling protocol. The experiment measured the decay of phase of a qubit applying more than one echo-pulse. While there are several families of pulse sequences, we do not discriminate them. This is one of the values of 'Coherence'.

'T₂^{Echo}: Dephasing under Hahn echo. The experiment measured the decay of phase of a qubit applying a single echo-pulse. A typical sequence is: initialization – $\pi/2$ pulse – free precession for time $\tau/2 - \pi$ pulse – free precession for time $\tau/2 - \pi/2$ pulse – measurement. This is one of the values of 'Coherence'.

'T₂^{Rabi}: Dephasing of a driven qubit. Strictly speaking, this time should describe the decay of the relative phase of the two quasi-energy states in the rotating frame of reference. Usually, it is extracted as the observed decay time of Rabi oscillations. This is one of the values of 'Coherence'.

'Time': (In tables on coherence). The timescale of the coherence decay observed in a certain type of experiment. The type is described by 'Coherence'.

'Time': (In tables on operation times) The duration of the operation. If the reference gives a frequency f for a gate signal, we convert it to time t using $t = 1/2f$, see Eq. 9.

'Value': This keyword wraps the value of Terminal oNode.

-
- [1] URL <https://github.com/PeterStano/ReviewOfSpinQubits>.
- [2] Gonzalo A. Álvarez, Ashok Ajoy, Xinhua Peng, and Dieter Suter. Performance comparison of dynamical decoupling sequences for a qubit in a rapidly fluctuating spin bath. *Physical Review A*, 82(4):042306, October 2010. ISSN 1050-2947, 1094-1622. doi: 10.1103/PhysRevA.82.042306. URL <https://link.aps.org/doi/10.1103/PhysRevA.82.042306>.
- [3] S. Amasha, K. MacLean, Iuliana P. Radu, D. M. Zumbühl, M. A. Kastner, M. P. Hanson, and A. C. Gossard. Electrical Control of Spin Relaxation in a Quantum Dot. *Physical Review Letters*, 100(4):046803, January 2008. ISSN 0031-9007, 1079-7114. doi: 10.1103/PhysRevLett.100.046803. URL <http://link.aps.org/doi/10.1103/PhysRevLett.100.046803>.
- [4] Reed W. Andrews, Cody Jones, Matthew D. Reed, Aaron M. Jones, Sieu D. Ha, Michael P. Jura, Joseph Kerckhoff, Mark Levendorf, Séan Meenehan, Seth T. Merkel, Aaron Smith, Bo Sun, Aaron J. Weinstein, Matthew T. Rakher, Thaddeus D. Ladd, and Matthew G. Borselli. Quantifying error and leakage in an encoded Si/SiGe triple-dot qubit. *Nature Nanotechnology*, 14(8):747–750, July 2019. ISSN 1748-3387, 1748-3395. doi:10.1038/s41565-019-0500-4. URL <http://www.nature.com/articles/s41565-019-0500-4>.
- [5] Fabio Ansalomi, Anasua Chatterjee, Heorhii Bohuslavskyi, Benoit Bertrand, Louis Hutin, Maud Vinet, and Ferdinand Kuemmeth. Single-electron operations in a foundry-fabricated array of quantum dots. *Nature Communications*, 11(1):6399, December 2020. ISSN 2041-1723. doi:10.1038/s41467-020-20280-3. URL <http://www.nature.com/articles/s41467-020-20280-3>.
- [6] T. A. Baart, N. Jovanovic, C. Reichl, W. Wegscheider, and L. M. K. Vandersypen. Nanosecond-timescale spin transfer using individual electrons in a quadruple-quantum-dot device. *Applied Physics Letters*, 109(4):043101, July 2016. ISSN 0003-6951, 1077-3118. doi: 10.1063/1.4959183. URL <http://aip.scitation.org/doi/10.1063/1.4959183>.
- [7] T. A. Baart, M. Shafiei, T. Fujita, C. Reichl, W. Wegscheider, and L. M. K. Vandersypen. Single-spin CCD. *Nature Nanotechnology*, 11 (4):330–334, January 2016. ISSN 1748-3387, 1748-3395. doi:10.1038/nnano.2015.291. URL <http://www.nature.com/doifinder/10.1038/nnano.2015.291>.
- [8] Timothy Alexander Baart, Takafumi Fujita, Christian Reichl, Werner Wegscheider, and Lieven Mark Koenraad Vandersypen. Coherent spin-exchange via a quantum mediator. *Nature Nanotechnology*, 12(1):26–30, October 2016. ISSN 1748-3387, 1748-3395. doi:10.1038/nano.2016.188. URL <http://www.nature.com/doifinder/10.1038/nano.2016.188>.
- [9] C. Barthel, D. J. Reilly, C. M. Marcus, M. P. Hanson, and A. C. Gossard. Rapid Single-Shot Measurement of a Singlet-Triplet Qubit. *Physical Review Letters*, 103(16), October 2009. ISSN 0031-9007, 1079-7114. doi:10.1103/PhysRevLett.103.160503. URL <https://link.aps.org/doi/10.1103/PhysRevLett.103.160503>.
- [10] C. Barthel, M. Kjærgaard, J. Medford, M. Stopa, C. M. Marcus, M. P. Hanson, and A. C. Gossard. Fast sensing of double-dot charge arrangement and spin state with a radio-frequency sensor quantum dot. *Physical Review B*, 81(16):161308, April 2010. ISSN 1098-0121, 1550-235X. doi:10.1103/PhysRevB.81.161308. URL <https://link.aps.org/doi/10.1103/PhysRevB.81.161308>.
- [11] C. Barthel, J. Medford, C. M. Marcus, M. P. Hanson, and A. C. Gossard. Interlaced Dynamical Decoupling and Coherent Operation of a Singlet-Triplet Qubit. *Physical Review Letters*, 105(26):266808, December 2010. ISSN 0031-9007, 1079-7114. doi: 10.1103/PhysRevLett.105.266808. URL <https://link.aps.org/doi/10.1103/PhysRevLett.105.266808>.
- [12] C. Barthel, J. Medford, H. Bluhm, A. Yacoby, C. M. Marcus, M. P. Hanson, and A. C. Gossard. Relaxation and readout visibility of a singlet-triplet qubit in an Overhauser field gradient. *Physical Review B*, 85(3):035306, January 2012. ISSN 1098-0121, 1550-235X. doi:10.1103/PhysRevB.85.035306. URL <https://link.aps.org/doi/10.1103/PhysRevB.85.035306>.
- [13] J. Basset, D.-D. Jarausch, A. Stockklauser, T. Frey, C. Reichl, W. Wegscheider, T. M. Ihn, K. Ensslin, and A. Wallraff. Single-electron double quantum dot dipole-coupled to a single photonic mode. *Physical Review B*, 88(12):125312, September 2013. ISSN 1098-0121, 1550-235X. doi:10.1103/PhysRevB.88.125312. URL <https://link.aps.org/doi/10.1103/PhysRevB.88.125312>.
- [14] Benoit Bertrand, Hanno Flentje, Shintaro Takada, Michihisa Yamamoto, Seigo Tarucha, Arne Ludwig, Andreas D. Wieck, Christopher Bäuerle, and Tristan Meunier. Quantum Manipulation of Two-Electron Spin States in Isolated Double Quantum Dots. *Physical Review Letters*, 115(9):096801, August 2015. ISSN 0031-9007, 1079-7114. doi:10.1103/PhysRevLett.115.096801. URL <https://link.aps.org/doi/10.1103/PhysRevLett.115.096801>.
- [15] F. Bloch. Nuclear Induction. *Physical Review*, 70(7-8):460–474, October 1946. ISSN 0031-899X. doi:10.1103/PhysRev.70.460. URL <https://link.aps.org/doi/10.1103/PhysRev.70.460>.
- [16] Hendrik Bluhm, Sandra Foletti, Diana Mahalu, Vladimir Umansky, and Amir Yacoby. Enhancing the Coherence of a Spin Qubit by Operating it as a Feedback Loop That Controls its Nuclear Spin Bath. *Physical Review Letters*, 105(21):216803, November 2010. ISSN 0031-9007, 1079-7114. doi:10.1103/PhysRevLett.105.216803. URL <http://link.aps.org/doi/10.1103/PhysRevLett.105.216803>.
- [17] Hendrik Bluhm, Sandra Foletti, Izhar Neder, Mark Rudner, Diana Mahalu, Vladimir Umansky, and Amir Yacoby. Dephasing time of GaAs electron-spin qubits coupled to a nuclear bath exceeding 200 μ s. *Nature Physics*, 7(2):109–113, December 2010. ISSN 1745-2473, 1745-2481. doi:10.1038/nphys1856. URL <http://www.nature.com/doifinder/10.1038/nphys1856>.
- [18] Karl Blum. *Density Matrix Theory and Applications*. Springer US, Boston, MA, 1996. ISBN 978-1-4419-3257-0 978-1-4757-4931-1. OCLC: 905455687.
- [19] Robin Blume-Kohout, John King Gamble, Erik Nielsen, Kenneth Rudinger, Jonathan Mizrahi, Kevin Fortier, and Peter Maunz. Demonstration of qubit operations below a rigorous fault tolerance threshold with gate set tomography. *Nature Communications*, 8(1):14485, April 2017. ISSN 2041-1723. doi:10.1038/ncomms14485. URL <http://www.nature.com/articles/ncomms14485>.
- [20] Jacob Z. Blumoff, Andrew S. Pan, Tyler E. Keating, Reed W. Andrews, David W. Barnes, Teresa L. Brecht, Edward T. Croke, Larken E. Cumberland, Jacob A. Fast, Clayton A. C. Jackson, Aaron M. Jones, Joseph Kerckhoff, Robert K. Lanza, Kate Raach, Bryan J. Thomas, Roland Velunta, Aaron J. Weinstein, Thaddeus D. Ladd, Kevin Eng, Matthew G. Borselli, Andrew T. Hunter, and Matthew T. Rakher. Fast and high-fidelity state preparation and measurement in triple-quantum-dot spin qubits. *arXiv:2112.09801 [quant-ph]*, December 2021. URL <http://arxiv.org/abs/2112.09801>. arXiv: 2112.09801.

- [21] Alex Bogan, Sergei Studenikin, Marek Korkusinski, Louis Gaudreau, Piotr Zawadzki, Andy S. Sachrajda, Lisa Tracy, John Reno, and Terry Hargett. Landau-Zener-Stückelberg-Majorana Interferometry of a Single Hole. *Physical Review Letters*, 120(20):207701, May 2018. ISSN 0031-9007, 1079-7114. doi:10.1103/PhysRevLett.120.207701. URL <https://link.aps.org/doi/10.1103/PhysRevLett.120.207701>.
- [22] Alex Bogan, Sergei Studenikin, Marek Korkusinski, Louis Gaudreau, Piotr Zawadzki, Andy Sachrajda, Lisa Tracy, John Reno, and Terry Hargett. Single hole spin relaxation probed by fast single-shot latched charge sensing. *Communications Physics*, 2(1):17, February 2019. ISSN 2399-3650. doi:10.1038/s42005-019-0113-0. URL <http://www.nature.com/articles/s42005-019-0113-0>.
- [23] Heorhii Bohuslavskyi, Fabio Ansaloni, Anasua Chatterjee, Federico Fedele, Torbjørn Rasmussen, Bertram Brovang, Jing Li, Louis Hutin, Benjamin Venitucci, Benoit Bertrand, Maud Vinet, Yann-Michel Niquet, and Ferdinand Kuemmeth. Reflectometry of charge transitions in a silicon quadruple dot. *arXiv:2012.04791 [cond-mat, physics:quant-ph]*, December 2020. URL <http://arxiv.org/abs/2012.04791>. arXiv: 2012.04791.
- [24] F. Borjans, X. G. Croot, X. Mi, M. J. Gullans, and J. R. Petta. Resonant microwave-mediated interactions between distant electron spins. *Nature*, 577(7789):195–198, December 2019. ISSN 0028-0836, 1476-4687. doi:10.1038/s41586-019-1867-y. URL <http://www.nature.com/articles/s41586-019-1867-y>.
- [25] F. Borjans, D.M. Zajac, T.M. Hazard, and J.R. Petta. Single-Spin Relaxation in a Synthetic Spin-Orbit Field. *Physical Review Applied*, 11(4):044063, April 2019. ISSN 2331-7019. doi:10.1103/PhysRevApplied.11.044063. URL <https://link.aps.org/doi/10.1103/PhysRevApplied.11.044063>.
- [26] F. Borjans, X. Croot, S. Putz, X. Mi, S. M. Quinn, A. Pan, J. Kerckhoff, E. J. Pritchett, C. A. Jackson, L. F. Edge, R. S. Ross, T. D. Ladd, M. G. Borselli, M. F. Gyure, and J. R. Petta. Split-gate cavity coupler for silicon circuit quantum electrodynamics. *Applied Physics Letters*, 116(23):234001, June 2020. ISSN 0003-6951, 1077-3118. doi:10.1063/5.0006442. URL <http://aip.scitation.org/doi/10.1063/5.0006442>.
- [27] F. Borjans, X. Mi, and J.R. Petta. Spin Digitizer for High-Fidelity Readout of a Cavity-Coupled Silicon Triple Quantum Dot. *Physical Review Applied*, 15(4):044052, April 2021. ISSN 2331-7019. doi:10.1103/PhysRevApplied.15.044052. URL <https://link.aps.org/doi/10.1103/PhysRevApplied.15.044052>.
- [28] F. Borjans, X. Zhang, X. Mi, G. Cheng, N. Yao, C.A.C. Jackson, L.F. Edge, and J.R. Petta. Probing the Variation of the Intervalle Tunnel Coupling in a Silicon Triple Quantum Dot. *PRX Quantum*, 2(2):020309, April 2021. ISSN 2691-3399. doi:10.1103/PRXQuantum.2.020309. URL <https://link.aps.org/doi/10.1103/PRXQuantum.2.020309>.
- [29] Jelmer M. Boter, Xiao Xue, Tobias Krähenmann, Thomas F. Watson, Vickram N. Premakumar, Daniel R. Ward, Donald E. Savage, Max G. Lagally, Mark Friesen, Susan N. Coppersmith, Mark A. Eriksson, Robert Joynt, and Lieven M. K. Vandersypen. Spatial noise correlations in a Si/SiGe two-qubit device from Bell state coherences. *Physical Review B*, 101(23):235133, June 2020. ISSN 2469-9950, 2469-9969. doi:10.1103/PhysRevB.101.235133. URL <https://link.aps.org/doi/10.1103/PhysRevB.101.235133>.
- [30] M. A. Broome, T. F. Watson, D. Keith, S. K. Gorman, M. G. House, J. G. Keizer, S. J. Hile, W. Baker, and M. Y. Simmons. High-Fidelity Single-Shot Singlet-Triplet Readout of Precision-Placed Donors in Silicon. *Physical Review Letters*, 119(4):046802, July 2017. ISSN 0031-9007, 1079-7114. doi:10.1103/PhysRevLett.119.046802. URL <http://link.aps.org/doi/10.1103/PhysRevLett.119.046802>.
- [31] M. A. Broome, S. K. Gorman, M. G. House, S. J. Hile, J. G. Keizer, D. Keith, C. D. Hill, T. F. Watson, W. J. Baker, L. C. L. Hollenberg, and M. Y. Simmons. Two-electron spin correlations in precision placed donors in silicon. *Nature Communications*, 9(1):980, March 2018. ISSN 2041-1723. doi:10.1038/s41467-018-02982-x. URL <http://www.nature.com/articles/s41467-018-02982-x>.
- [32] R. Brunner, Y.-S. Shin, T. Obata, M. Pioro-Ladrière, T. Kubo, K. Yoshida, T. Taniyama, Y. Tokura, and S. Tarucha. Two-Qubit Gate of Combined Single-Spin Rotation and Interdot Spin Exchange in a Double Quantum Dot. *Physical Review Letters*, 107(14):146801, September 2011. ISSN 0031-9007, 1079-7114. doi:10.1103/PhysRevLett.107.146801. URL <https://link.aps.org/doi/10.1103/PhysRevLett.107.146801>.
- [33] H. Büch, S. Mahapatra, R. Rahman, A. Morello, and M. Y. Simmons. Spin readout and addressability of phosphorus-donor clusters in silicon. *Nature Communications*, 4(1):2017, June 2013. ISSN 2041-1723. doi:10.1038/ncomms3017. URL <http://www.nature.com/articles/ncomms3017>.
- [34] Guido Burkard, Thaddeus D. Ladd, John M. Nichol, Andrew Pan, and Jason R. Petta. Semiconductor Spin Qubits. *arXiv:2112.08863 [cond-mat, physics:physics, physics:quant-ph]*, December 2021. URL <http://arxiv.org/abs/2112.08863>. arXiv: 2112.08863.
- [35] M. Busl, G. Granger, L. Gaudreau, R. Sánchez, A. Kam, M. Pioro-Ladrière, S. A. Studenikin, P. Zawadzki, Z. R. Wasilewski, A. S. Sachrajda, and G. Platero. Bipolar spin blockade and coherent state superpositions in a triple quantum dot. *Nature Nanotechnology*, 8(4):261–265, February 2013. ISSN 1748-3387, 1748-3395. doi:10.1038/nnano.2013.7. URL <http://www.nature.com/articles/nnano.2013.7>.
- [36] Xinxin Cai, Elliot J Connors, and John M Nichol. Coherent spin-valley oscillations in silicon. *arXiv:2111.14847*, page 24, November 2021. URL <http://arxiv.org/abs/2111.14847>. arXiv: 2111.14847.
- [37] Leon C. Camenzind, Liuqi Yu, Peter Stano, Jeramy D. Zimmerman, Arthur C. Gossard, Daniel Loss, and Dominik M. Zumbühl. Hyperfine-phonon spin relaxation in a single-electron GaAs quantum dot. *Nature Communications*, 9(1):3454, August 2018. ISSN 2041-1723. doi:10.1038/s41467-018-05879-x. URL <http://www.nature.com/articles/s41467-018-05879-x>.
- [38] Leon C. Camenzind, Simon Geyer, Andreas Fuhrer, Richard J. Warburton, Dominik M. Zumbühl, and Andreas V. Kuhlmann. A spin qubit in a fin field-effect transistor. *arXiv:2103.07369 [cond-mat, physics:quant-ph]*, March 2021. URL <http://arxiv.org/abs/2103.07369>. arXiv: 2103.07369.
- [39] Gang Cao, Hai-Ou Li, Tao Tu, Li Wang, Cheng Zhou, Ming Xiao, Guang-Can Guo, Hong-Wen Jiang, and Guo-Ping Guo. Ultrafast universal quantum control of a quantum-dot charge qubit using Landau-Zener-Stückelberg interference. *Nature Communications*, 4(1):1401, January 2013. ISSN 2041-1723. doi:10.1038/ncomms2412. URL <http://www.nature.com/articles/ncomms2412>.
- [40] Gang Cao, Hai-Ou Li, Guo-Dong Yu, Bao-Chuan Wang, Bao-Bao Chen, Xiang-Xiang Song, Ming Xiao, Guang-Can Guo, Hong-Wen Jiang, Xuedong Hu, and Guo-Ping Guo. Tunable Hybrid Qubit in a GaAs Double Quantum Dot. *Physical Review Letters*, 116(8):

- 086801, February 2016. ISSN 0031-9007, 1079-7114. doi:10.1103/PhysRevLett.116.086801. URL <https://link.aps.org/doi/10.1103/PhysRevLett.116.086801>.
- [41] Pascal Cerdantaine, Tim Botzem, Simon Sebastian Humpohl, Dieter Schuh, Dominique Bougeard, and Hendrik Bluhm. Feedback-tuned noise-resilient gates for encoded spin qubits. *arXiv preprint arXiv:1606.01897*, June 2016. URL <https://arxiv.org/abs/1606.01897>. arXiv:1606.01897.
- [42] Pascal Cerdantaine, Tim Botzem, Julian Ritzmann, Simon Sebastian Humpohl, Arne Ludwig, Dieter Schuh, Dominique Bougeard, Andreas D. Wieck, and Hendrik Bluhm. Closed-loop control of a GaAs-based singlet-triplet spin qubit with 99.5% gate fidelity and low leakage. *Nature Communications*, 11(1):4144, August 2020. ISSN 2041-1723. doi:10.1038/s41467-020-17865-3. URL <http://www.nature.com/articles/s41467-020-17865-3>.
- [43] K. W. Chan, W. Huang, C. H. Yang, J. C. C. Hwang, B. Hensen, T. Tanttu, F. E. Hudson, K. M. Itoh, A. Laucht, A. Morello, and A. S. Dzurak. Assessment of a Silicon Quantum Dot Spin Qubit Environment via Noise Spectroscopy. *Physical Review Applied*, 10(4):044017, October 2018. ISSN 2331-7019. doi:10.1103/PhysRevApplied.10.044017. URL <https://link.aps.org/doi/10.1103/PhysRevApplied.10.044017>.
- [44] Kok Wai Chan, Harshad Sahasrabudhe, Wister Huang, Yu Wang, Henry C. Yang, Menno Veldhorst, Jason C. C. Hwang, Fahd A. Mohiyaddin, Fay E. Hudson, Kohei M. Itoh, Andre Saraiva, Andrea Morello, Arne Laucht, Rajib Rahman, and Andrew S. Dzurak. Exchange coupling in a linear chain of three quantum-dot spin qubits in silicon. *Nano Letters*, 21(3):1517–1522, January 2021. ISSN 1530-6984, 1530-6992. doi:10.1021/acs.nanolett.0c04771. URL <https://pubs.acs.org/doi/10.1021/acs.nanolett.0c04771>. arXiv: 2004.07666.
- [45] Emmanuel Chanrion, David J. Niegemann, Benoit Bertrand, Cameron Spence, Baptiste Jadot, Jing Li, Pierre-André Mortemousque, Louis Hutin, Romain Maurand, Xavier Jehl, Marc Sanquer, Silvano De Franceschi, Christopher Bäuerle, Franck Balestro, Yann-Michel Niquet, Maud Vinet, Tristan Meunier, and Matias Urdampilleta. Charge Detection in an Array of CMOS Quantum Dots. *Physical Review Applied*, 14(2):024066, August 2020. ISSN 2331-7019. doi:10.1103/PhysRevApplied.14.024066. URL <https://link.aps.org/doi/10.1103/PhysRevApplied.14.024066>.
- [46] Anasua Chatterjee, Paul Stevenson, Silvano De Franceschi, Andrea Morello, Nathalie P. de Leon, and Ferdinand Kuemmeth. Semiconductor qubits in practice. *Nature Reviews Physics*, 3(3):157–177, March 2021. ISSN 2522-5820. doi:10.1038/s42254-021-00283-9. URL <http://www.nature.com/articles/s42254-021-00283-9>.
- [47] Edward H. Chen, Kate Raach, Andrew Pan, Andrey A. Kiselev, Edwin Acuna, Jacob Z. Blumoff, Teresa Brecht, Maxwell D. Choi, Wonill Ha, Daniel R. Hulbert, Michael P. Jura, Tyler E. Keating, Ramsey Noah, Bo Sun, Bryan J. Thomas, Matthew G. Borselli, C.A.C. Jackson, Matthew T. Rakher, and Richard S. Ross. Detuning Axis Pulsed Spectroscopy of Valley-Orbital States in Si / Si - Ge Quantum Dots. *Physical Review Applied*, 15(4):044033, April 2021. ISSN 2331-7019. doi:10.1103/PhysRevApplied.15.044033. URL <https://link.aps.org/doi/10.1103/PhysRevApplied.15.044033>.
- [48] H. O. H. Churchill, F. Kuemmeth, J. W. Harlow, A. J. Bestwick, E. I. Rashba, K. Flensberg, C. H. Stwertka, T. Taychatanapat, S. K. Watson, and C. M. Marcus. Relaxation and Dephasing in a Two-Electron C 13 Nanotube Double Quantum Dot. *Physical Review Letters*, 102(16):166802, April 2009. ISSN 0031-9007, 1079-7114. doi:10.1103/PhysRevLett.102.166802. URL <https://link.aps.org/doi/10.1103/PhysRevLett.102.166802>.
- [49] Virginia N. Ciriano-Tejel, Michael A. Fogarty, Simon Schaal, Louis Hutin, Benoit Bertrand, Lisa Ibberson, M. Fernando Gonzalez-Zalba, Jing Li, Yann-Michel Niquet, Maud Vinet, and John J.L. Morton. Spin Readout of a CMOS Quantum Dot by Gate Reflectometry and Spin-Dependent Tunneling. *PRX Quantum*, 2(1):010353, March 2021. ISSN 2691-3399. doi:10.1103/PRXQuantum.2.010353. URL <https://link.aps.org/doi/10.1103/PRXQuantum.2.010353>.
- [50] J. I. Colless, A. C. Mahoney, J. M. Hornibrook, A. C. Doherty, H. Lu, A. C. Gossard, and D. J. Reilly. Dispersive Readout of a Few-Electron Double Quantum Dot with Fast rf Gate Sensors. *Physical Review Letters*, 110(4), January 2013. ISSN 0031-9007, 1079-7114. doi:10.1103/PhysRevLett.110.046805. URL <https://link.aps.org/doi/10.1103/PhysRevLett.110.046805>.
- [51] Elliot J. Connors, Jj Nelson, and John M. Nichol. Rapid High-Fidelity Spin-State Readout in Si / Si - Ge Quantum Dots via rf Reflectometry. *Physical Review Applied*, 13(2):024019, February 2020. ISSN 2331-7019. doi:10.1103/PhysRevApplied.13.024019. URL <https://link.aps.org/doi/10.1103/PhysRevApplied.13.024019>.
- [52] Andrea Corra, Léo Bourdet, Romain Maurand, Alessandro Crippa, Dharmraj Kotekar-Patil, Heorhii Bohuslavskyi, Romain Laviéville, Louis Hutin, Sylvain Barraud, Xavier Jehl, Maud Vinet, Silvano De Franceschi, Yann-Michel Niquet, and Marc Sanquer. Electrically driven electron spin resonance mediated by spin-valley-orbit coupling in a silicon quantum dot. *npj Quantum Information*, 4(1):6, February 2018. ISSN 2056-6387. doi:10.1038/s41534-018-0059-1. URL <http://www.nature.com/articles/s41534-018-0059-1>.
- [53] Audrey Cottet, Matthieu C Dartailh, Matthieu M Desjardins, Tino Cubaynes, Lauriane C Contamin, Matthieu Delbecq, Jérémie J Viennot, Laure E Bruhat, Benoit Dougot, and Takis Kontos. Cavity QED with hybrid nanocircuits: from atomic-like physics to condensed matter phenomena. *Journal of Physics: Condensed Matter*, 29(43):433002, November 2017. ISSN 0953-8984, 1361-648X. doi:10.1088/1361-648X/aa7b4d. URL <https://doi.org/10.1088/1361-648X/aa7b4d>.
- [54] A. Crippa, R. Ezzouch, A. Aprá, A. Amisse, R. Laviéville, L. Hutin, B. Bertrand, M. Vinet, M. Urdampilleta, T. Meunier, M. Sanquer, X. Jehl, R. Maurand, and S. De Franceschi. Gate-reflectometry dispersive readout and coherent control of a spin qubit in silicon. *Nature Communications*, 10(1):2776, July 2019. ISSN 2041-1723. doi:10.1038/s41467-019-10848-z. URL <http://www.nature.com/articles/s41467-019-10848-z>.
- [55] Alessandro Crippa, Romain Maurand, Léo Bourdet, Dharmraj Kotekar-Patil, Anthony Amisse, Xavier Jehl, Marc Sanquer, Romain Laviéville, Heorhii Bohuslavskyi, Louis Hutin, Sylvain Barraud, Maud Vinet, Yann-Michel Niquet, and Silvano De Franceschi. Electrical Spin Driving by g -Matrix Modulation in Spin-Orbit Qubits. *Physical Review Letters*, 120(13):137702, March 2018. ISSN 0031-9007, 1079-7114. doi:10.1103/PhysRevLett.120.137702. URL <https://link.aps.org/doi/10.1103/PhysRevLett.120.137702>.
- [56] X. Croot, X. Mi, S. Putz, M. Benito, F. Borjans, G. Burkard, and J. R. Petta. Flopping-mode electric dipole spin resonance. *Physical Review Research*, 2(1):012006, January 2020. ISSN 2643-1564. doi:10.1103/PhysRevResearch.2.012006. URL <http://arxiv.org/abs/1905.00346>. arXiv: 1905.00346.

- [57] X.G. Croot, S.J. Pauka, J.D. Watson, G.C. Gardner, S. Fallahi, M.J. Manfra, and D.J. Reilly. Device Architecture for Coupling Spin Qubits via an Intermediate Quantum State. *Physical Review Applied*, 10(4):044058, October 2018. ISSN 2331-7019. doi: 10.1103/PhysRevApplied.10.044058. URL <https://link.aps.org/doi/10.1103/PhysRevApplied.10.044058>.
- [58] T. Cubaynes, M. R. Delbecq, M. C. Dartailh, R. Assouly, M. M. Desjardins, L. C. Contamin, L. E. Bruhat, Z. Leghtas, F. Mallet, A. Cottet, and T. Kontos. Highly coherent spin states in carbon nanotubes coupled to cavity photons. *npj Quantum Information*, 5(1):47, July 2019. ISSN 2056-6387. doi:10.1038/s41534-019-0169-4. URL <http://www.nature.com/articles/s41534-019-0169-4>.
- [59] Łukasz Cywiński, Roman M. Lutchyn, Cody P. Nave, and S. Das Sarma. How to enhance dephasing time in superconducting qubits. *Physical Review B*, 77(17):174509, May 2008. ISSN 1098-0121, 1550-235X. doi:10.1103/PhysRevB.77.174509. URL <https://link.aps.org/doi/10.1103/PhysRevB.77.174509>.
- [60] J. P. Dehollain, U. Mukhopadhyay, V. P. Michal, Y. Wang, B. Wunsch, C. Reichl, W. Wegscheider, M. S. Rudner, E. Demler, and L. M. K. Vandersypen. Nagaoka ferromagnetism observed in a quantum dot plaquette. *Nature*, 579:528–533, March 2020. ISSN 0028-0836, 1476-4687. doi:10.1038/s41586-020-2051-0. URL <http://www.nature.com/articles/s41586-020-2051-0>.
- [61] Juan P. Dehollain, Juha T. Muhonen, Kuan Y. Tan, Andre Saraiva, David N. Jamieson, Andrew S. Dzurak, and Andrea Morello. Single-Shot Readout and Relaxation of Singlet and Triplet States in Exchange-Coupled P 31 Electron Spins in Silicon. *Physical Review Letters*, 112(23):236801, June 2014. ISSN 0031-9007, 1079-7114. doi:10.1103/PhysRevLett.112.236801. URL <https://link.aps.org/doi/10.1103/PhysRevLett.112.236801>.
- [62] Juan P. Dehollain, Juha T. Muhonen, Robin Blume-Kohout, Kenneth M. Rudinger, John King Gamble, Erik Nielsen, Arne Laucht, Stephanie Simmons, Rachpon Kalra, Andrew S. Dzurak, and Andrea Morello. Optimization of a solid-state electron spin qubit using gate set tomography. *New Journal of Physics*, 18(10):103018, October 2016. ISSN 1367-2630. doi:10.1088/1367-2630/18/10/103018. URL <https://doi.org/10.1088/1367-2630/18/10/103018>.
- [63] M. R. Delbecq, T. Nakajima, T. Otsuka, S. Amaha, J. D. Watson, M. J. Manfra, and S. Tarucha. Full control of quadruple quantum dot circuit charge states in the single electron regime. *Applied Physics Letters*, 104(18):183111, May 2014. ISSN 0003-6951, 1077-3118. doi:10.1063/1.4875909. URL <http://aip.scitation.org/doi/10.1063/1.4875909>.
- [64] M. R. Delbecq, T. Nakajima, P. Stano, T. Otsuka, S. Amaha, J. Yoneda, K. Takeda, G. Allison, A. Ludwig, A. D. Wieck, and S. Tarucha. Quantum Dephasing in a Gated GaAs Triple Quantum Dot due to Nonergodic Noise. *Physical Review Letters*, 116(4):046802, January 2016. ISSN 0031-9007, 1079-7114. doi:10.1103/PhysRevLett.116.046802. URL <https://link.aps.org/doi/10.1103/PhysRevLett.116.046802>.
- [65] Guang-Wei Deng, Da Wei, J. R. Johansson, Miao-Lei Zhang, Shu-Xiao Li, Hai-Ou Li, Gang Cao, Ming Xiao, Tao Tu, Guang-Can Guo, Hong-Wen Jiang, Franco Nori, and Guo-Ping Guo. Charge Number Dependence of the Dephasing Rates of a Graphene Double Quantum Dot in a Circuit QED Architecture. *Physical Review Letters*, 115(12):126804, September 2015. ISSN 0031-9007, 1079-7114. doi:10.1103/PhysRevLett.115.126804. URL <https://link.aps.org/doi/10.1103/PhysRevLett.115.126804>.
- [66] Simon J. Devitt, Kae Nemoto, and William J. Munro. Quantum Error Correction for Beginners. *Reports on Progress in Physics*, 76(7): 076001, July 2013. ISSN 0034-4885, 1361-6633. doi:10.1088/0034-4885/76/7/076001. URL <http://arxiv.org/abs/0905.2794>. arXiv: 0905.2794.
- [67] O. E. Dial, M. D. Shulman, S. P. Harvey, H. Bluhm, V. Umansky, and A. Yacoby. Charge Noise Spectroscopy Using Coherent Exchange Oscillations in a Singlet-Triplet Qubit. *Physical Review Letters*, 110(14):146804, April 2013. ISSN 0031-9007, 1079-7114. doi: 10.1103/PhysRevLett.110.146804. URL <https://link.aps.org/doi/10.1103/PhysRevLett.110.146804>.
- [68] Y. Dovzhenko, J. Stehlik, K. D. Petersson, J. R. Petta, H. Lu, and A. C. Gossard. Nonadiabatic quantum control of a semiconductor charge qubit. *Physical Review B*, 84(16):161302, October 2011. ISSN 1098-0121, 1550-235X. doi:10.1103/PhysRevB.84.161302. URL <https://link.aps.org/doi/10.1103/PhysRevB.84.161302>.
- [69] Jingyu Duan, Michael A. Fogarty, James Williams, Louis Hutin, Maud Vinet, and John J. L. Morton. Remote Capacitive Sensing in Two-Dimensional Quantum-Dot Arrays. *Nano Letters*, 20(10):7123–7128, September 2020. ISSN 1530-6984, 1530-6992. doi: 10.1021/acs.nanolett.0c02393. URL <https://pubs.acs.org/doi/10.1021/acs.nanolett.0c02393>.
- [70] J. M. Elzerman, R. Hanson, L. H. Willems van Beveren, B. Witkamp, L. M. K. Vandersypen, and L. P. Kouwenhoven. Single-shot read-out of an individual electron spin in a quantum dot. *Nature*, 430(6998):431–435, July 2004. ISSN 0028-0836, 1476-4679. doi: 10.1038/nature02693. URL <http://www.nature.com/doifinder/10.1038/nature02693>.
- [71] K. Eng, T. D. Ladd, A. Smith, M. G. Borselli, A. A. Kiselev, B. H. Fong, K. S. Holabird, T. M. Hazard, B. Huang, P. W. Deelman, I. Milosavljevic, A. E. Schmitz, R. S. Ross, M. F. Gyure, and A. T. Hunter. Isotopically enhanced triple-quantum-dot qubit. *Science Advances*, 1(4):e1500214–e1500214, May 2015. ISSN 2375-2548. doi:10.1126/sciadv.1500214. URL <http://advances.sciencemag.org/cgi/doi/10.1126/sciadv.1500214>.
- [72] Jeffrey M. Epstein, Andrew W. Cross, Easwar Magesan, and Jay M. Gambetta. Investigating the limits of randomized benchmarking protocols. *Physical Review A*, 89(6):062321, June 2014. ISSN 1050-2947, 1094-1622. doi:10.1103/PhysRevA.89.062321. URL <https://link.aps.org/doi/10.1103/PhysRevA.89.062321>.
- [73] T.J. Evans, W. Huang, J. Yoneda, R. Harper, T. Tanttu, K.W. Chan, F.E. Hudson, K.M. Itoh, A. Saraiva, C.H. Yang, A.S. Dzurak, and S.D. Bartlett. Fast Bayesian Tomography of a Two-Qubit Gate Set in Silicon. *Physical Review Applied*, 17(2):024068, February 2022. ISSN 2331-7019. doi:10.1103/PhysRevApplied.17.024068. URL <https://link.aps.org/doi/10.1103/PhysRevApplied.17.024068>.
- [74] Rami Ezzouch, Simon Zihlmann, Vincent P. Michal, Jing Li, Agostino Aprá, Benoit Bertrand, Louis Hutin, Maud Vinet, Matias Ur-dampilleta, Tristan Meunier, Xavier Jehl, Yann-Michel Niquet, Marc Sanquer, Silvano De Franceschi, and Romain Maurand. Dispersively Probed Microwave Spectroscopy of a Silicon Hole Double Quantum Dot. *Physical Review Applied*, 16(3):034031, September 2021. ISSN 2331-7019. doi:10.1103/PhysRevApplied.16.034031. URL <https://link.aps.org/doi/10.1103/PhysRevApplied.16.034031>.
- [75] Jaroslav Fabian, Alex Matos-Abiague, Christian Ertler, Peter Stano, and Igor Žutić. Semiconductor spintronics. *Acta Physica Slovaca. Reviews and Tutorials*, 57(4-5), August 2007. ISSN 1336-040X, 0323-0465. doi:10.2478/v10155-010-0086-8. URL <https://www.degruyter.com/doi/10.2478/v10155-010-0086-8>.

- [76] Federico Fedele, Anasua Chatterjee, Saeed Fallahi, Geoffrey C. Gardner, Michael J. Manfra, and Ferdinand Kuemmeth. Simultaneous Operations in a Two-Dimensional Array of Singlet-Triplet Qubits. *PRX Quantum*, 2(4):040306, October 2021. ISSN 2691-3399. doi: 10.1103/PRXQuantum.2.040306. URL <https://link.aps.org/doi/10.1103/PRXQuantum.2.040306>.
- [77] J. Fischer and D. Loss. Dealing with Decoherence. *Science*, 324(5932):1277–1278, June 2009. ISSN 0036-8075, 1095-9203. doi: 10.1126/science.1169554. URL <https://www.sciencemag.org/lookup/doi/10.1126/science.1169554>.
- [78] H. Flentje, P.-A. Mortemousque, R. Thalineau, A. Ludwig, A. D. Wieck, C. Bäuerle, and T. Meunier. Coherent long-distance displacement of individual electron spins. *Nature Communications*, 8(1):501, September 2017. ISSN 2041-1723. doi:10.1038/s41467-017-00534-3. URL <http://www.nature.com/articles/s41467-017-00534-3>.
- [79] Hanno Flentje, Benoit Bertrand, Pierre-André Mortemousque, Vivien Thiney, Arne Ludwig, Andreas D. Wieck, Christopher Bäuerle, and Tristan Meunier. A linear triple quantum dot system in isolated configuration. *Applied Physics Letters*, 110(23):233101, June 2017. ISSN 0003-6951, 1077-3118. doi:10.1063/1.4984745. URL <http://aip.scitation.org/doi/10.1063/1.4984745>.
- [80] M. A. Fogarty, K. W. Chan, B. Hensen, W. Huang, T. Tanttu, C. H. Yang, A. Laucht, M. Veldhorst, F. E. Hudson, K. M. Itoh, D. Culcer, T. D. Ladd, A. Morello, and A. S. Dzurak. Integrated silicon qubit platform with single-spin addressability, exchange control and single-shot singlet-triplet readout. *Nature Communications*, 9(1):4370, October 2018. ISSN 2041-1723. doi:10.1038/s41467-018-06039-x. URL <http://www.nature.com/articles/s41467-018-06039-x>.
- [81] T. Frey, P. J. Leek, M. Beck, A. Blais, T. Ihn, K. Ensslin, and A. Wallraff. Dipole Coupling of a Double Quantum Dot to a Microwave Resonator. *Physical Review Letters*, 108(4):046807, January 2012. ISSN 0031-9007, 1079-7114. doi:10.1103/PhysRevLett.108.046807. URL <https://link.aps.org/doi/10.1103/PhysRevLett.108.046807>.
- [82] Stefan Fringes, Christian Volk, Caroline Norda, Bernat Terrés, Jan Dauber, Stephan Engels, Stefan Trellenkamp, and Christoph Stampfer. Charge detection in a bilayer graphene quantum dot. *physica status solidi (b)*, 248(11):2684–2687, November 2011. ISSN 03701972. doi:10.1002/pssb.201100189. URL <http://arxiv.org/abs/1110.5811>. arXiv: 1110.5811.
- [83] F. N. M. Froning, M. K. Rehmann, J. Ridderbos, M. Brauns, F. A. Zwanenburg, A. Li, E. P. A. M. Bakkers, D. M. Zumbühl, and F. R. Braakman. Single, double, and triple quantum dots in Ge/Si nanowires. *Applied Physics Letters*, 113(7):073102, August 2018. ISSN 0003-6951, 1077-3118. doi:10.1063/1.5042501. URL <http://aip.scitation.org/doi/10.1063/1.5042501>.
- [84] Florian N. M. Froning, Leon C. Camenzind, Orson A. H. van der Molen, Ang Li, Erik P. A. M. Bakkers, Dominik M. Zumbühl, and Floris R. Braakman. Ultrafast hole spin qubit with gate-tunable spin-orbit switch functionality. *Nature Nanotechnology*, 16:308–312, January 2021. ISSN 1748-3387, 1748-3395. doi:10.1038/s41565-020-00828-6. URL <http://www.nature.com/articles/s41565-020-00828-6>.
- [85] Toshimasa Fujisawa, David Guy Austing, Yasuhiro Tokura, Yoshiro Hirayama, and Seigo Tarucha. Allowed and forbidden transitions in artificial hydrogen and helium atoms. *Nature*, 419(6904):278–281, September 2002. ISSN 0028-0836, 1476-4687. doi: 10.1038/nature00976. URL <http://www.nature.com/articles/nature00976>.
- [86] Takafumi Fujita, Timothy Alexander Baart, Christian Reichl, Werner Wegscheider, and Lieven Mark Koenraad Vandersypen. Coherent shuttle of electron-spin states. *npj Quantum Information*, 3(1):22, June 2017. ISSN 2056-6387. doi:10.1038/s41534-017-0024-4. URL <http://www.nature.com/articles/s41534-017-0024-4>.
- [87] Lisa Maria Gächter, Rebekka Garreis, Chuyao Tong, Max Josef Ruckriegel, Benedikt Kratochwil, Folkert Kornelis de Vries, Annika Kurzmann, Kenji Watanabe, Takashi Taniguchi, Thomas Ihn, Klaus Ensslin, and Wister Wei Huang. Single-shot readout in graphene quantum dots. *arXiv:2112.12091 [cond-mat, physics:quant-ph]*, December 2021. URL <http://arxiv.org/abs/2112.12091>. arXiv: 2112.12091.
- [88] L. Gaudreau, A. Kam, G. Granger, S. A. Studenikin, P. Zawadzki, and A. S. Sachrajda. A tunable few electron triple quantum dot. *Applied Physics Letters*, 95(19):193101, November 2009. ISSN 0003-6951, 1077-3118. doi:10.1063/1.3258663. URL <http://aip.scitation.org/doi/10.1063/1.3258663>.
- [89] L. Gaudreau, G. Granger, A. Kam, G. C. Aers, S. A. Studenikin, P. Zawadzki, M. Pioro-Ladrière, Z. R. Wasilewski, and A. S. Sachrajda. Coherent control of three-spin states in a triple quantum dot. *Nature Physics*, 8(1):54–58, November 2011. ISSN 1745-2473, 1745-2481. doi:10.1038/nphys2149. URL <http://www.nature.com/articles/nphys2149>.
- [90] Will Gilbert, Andre Saraiva, Wee Han Lim, Chih Hwan Yang, Arne Laucht, Benoit Bertrand, Nils Rambal, Louis Hutin, Christopher C. Escott, Maud Vinet, and Andrew S. Dzurak. Single-electron operation of a silicon-CMOS 2x2 quantum dot array with integrated charge sensing. *Nano Letters*, 20(11):7882–7888, October 2020. ISSN 1530-6984, 1530-6992. doi:10.1021/acs.nanolett.0c02397. URL <http://arxiv.org/abs/2004.11558>. arXiv: 2004.11558.
- [91] Alexei Gilchrist, Nathan K. Langford, and Michael A. Nielsen. Distance measures to compare real and ideal quantum processes. *Physical Review A*, 71(6):062310, June 2005. ISSN 1050-2947, 1094-1622. doi:10.1103/PhysRevA.71.062310. URL <https://link.aps.org/doi/10.1103/PhysRevA.71.062310>.
- [92] M. F. Gonzalez-Zalba, S. Barraud, A. J. Ferguson, and A. C. Betz. Probing the limits of gate-based charge sensing. *Nature Communications*, 6(1):6084, May 2015. ISSN 2041-1723. doi:10.1038/ncomms7084. URL <http://www.nature.com/articles/ncomms7084>.
- [93] M. F. Gonzalez-Zalba, S. de Franceschi, E. Charbon, T. Meunier, M. Vinet, and A. S. Dzurak. Scaling silicon-based quantum computing using CMOS technology. *Nature Electronics*, 4(12):872–884, December 2021. ISSN 2520-1131. doi:10.1038/s41928-021-00681-y. URL <https://www.nature.com/articles/s41928-021-00681-y>.
- [94] Daniel Gottesman. Theory of fault-tolerant quantum computation. *Physical Review A*, 57(1):127–137, January 1998. ISSN 1050-2947, 1094-1622. doi:10.1103/PhysRevA.57.127. URL <https://link.aps.org/doi/10.1103/PhysRevA.57.127>.
- [95] Wonill Ha, Sieu D. Ha, Maxwell D. Choi, Yan Tang, Adele E. Schmitz, Mark P. Levendorf, Kangmu Lee, James M. Chappell, Tower S. Adams, Daniel R. Hulbert, Edwin Acuna, Ramsey S. Noah, Justine W. Matten, Michael P. Jura, Jeffrey A. Wright, Matthew T. Rakher, and Matthew G. Borselli. A Flexible Design Platform for Si/SiGe Exchange-Only Qubits with Low Disorder. *Nano Letters*, 22(3):1443–1448, November 2021. ISSN 1530-6984, 1530-6992. doi:10.1021/acs.nanolett.1c03026. URL <https://pubs.acs.org/doi/10.1021/acs.nanolett.1c03026>.
- [96] E. L. Hahn. Spin Echoes. *Physical Review*, 80(4):580–594, November 1950. ISSN 0031-899X. doi:10.1103/PhysRev.80.580. URL <https://link.aps.org/doi/10.1103/PhysRev.80.580>.

- <https://link.aps.org/doi/10.1103/PhysRev.80.580>.
- [97] R. Hanson, B. Witkamp, L. M. K. Vandersypen, L. H. Willems van Beveren, J. M. Elzerman, and L. P. Kouwenhoven. Zeeman Energy and Spin Relaxation in a One-Electron Quantum Dot. *Physical Review Letters*, 91(19):196802, November 2003. ISSN 0031-9007, 1079-7114. doi:10.1103/PhysRevLett.91.196802. URL <https://link.aps.org/doi/10.1103/PhysRevLett.91.196802>.
- [98] R. Hanson, L. P. Kouwenhoven, J. R. Petta, S. Tarucha, and L. M. K. Vandersypen. Spins in few-electron quantum dots. *Reviews of Modern Physics*, 79(4):1217–1265, October 2007. ISSN 0034-6861, 1539-0756. doi:10.1103/RevModPhys.79.1217. URL <https://link.aps.org/doi/10.1103/RevModPhys.79.1217>.
- [99] Will J Hardy, C Thomas Harris, Yi-Hsin Su, Yen Chuang, Jonathan Moussa, Leon N Maurer, Jun-Yun Li, Tzu-Ming Lu, and Dwight R Luhman. Single and double hole quantum dots in strained Ge/SiGe quantum wells. *Nanotechnology*, 30(21):215202, March 2019. ISSN 0957-4484, 1361-6528. doi:10.1088/1361-6528/ab061e. URL <https://iopscience.iop.org/article/10.1088/1361-6528/ab061e>.
- [100] Patrick Harvey-Collard, N. Tobias Jacobson, Martin Rudolph, Jason Dominguez, Gregory A. Ten Eyck, Joel R. Wendt, Tammy Pluym, John King Gamble, Michael P. Lilly, Michel Pioro-Ladrière, and Malcolm S. Carroll. Coherent coupling between a quantum dot and a donor in silicon. *Nature Communications*, 8(1):1029, October 2017. ISSN 2041-1723. doi:10.1038/s41467-017-01113-2. URL <http://www.nature.com/articles/s41467-017-01113-2>.
- [101] Patrick Harvey-Collard, Benjamin D’Anjou, Martin Rudolph, N. Tobias Jacobson, Jason Dominguez, Gregory A. Ten Eyck, Joel R. Wendt, Tammy Pluym, Michael P. Lilly, William A. Coish, Michel Pioro-Ladrière, and Malcolm S. Carroll. High-Fidelity Single-Shot Readout for a Spin Qubit via an Enhanced Latching Mechanism. *Physical Review X*, 8(2):021046, May 2018. ISSN 2160-3308. doi:10.1103/PhysRevX.8.021046. URL <https://link.aps.org/doi/10.1103/PhysRevX.8.021046>.
- [102] Patrick Harvey-Collard, N. Tobias Jacobson, Chloé Bureau-Oxton, Ryan M. Jock, Vanita Srinivasa, Andrew M. Mounce, Daniel R. Ward, John M. Anderson, Ronald P. Manginell, Joel R. Wendt, Tammy Pluym, Michael P. Lilly, Dwight R. Luhman, Michel Pioro-Ladrière, and Malcolm S. Carroll. Spin-orbit Interactions for Singlet-Triplet Qubits in Silicon. *Physical Review Letters*, 122(21):217702, May 2019. ISSN 0031-9007, 1079-7114. doi:10.1103/PhysRevLett.122.217702. URL <https://link.aps.org/doi/10.1103/PhysRevLett.122.217702>.
- [103] Patrick Harvey-Collard, Jurgen Dijkema, Guoji Zheng, Amir Sammak, Giordano Scappucci, and Lieven M. K. Vandersypen. Circuit quantum electrodynamics with two remote electron spins. *arXiv:2108.01206 [cond-mat, physics:quant-ph]*, August 2021. URL <http://arxiv.org/abs/2108.01206>. arXiv: 2108.01206.
- [104] Julian Hauss, Arkady Fedorov, Carsten Hutter, Alexander Shnirman, and Gerd Schön. Single-Qubit Lasing and Cooling at the Rabi Frequency. *Physical Review Letters*, 100(3):037003, January 2008. ISSN 0031-9007, 1079-7114. doi:10.1103/PhysRevLett.100.037003. URL <https://link.aps.org/doi/10.1103/PhysRevLett.100.037003>.
- [105] T. Hayashi, T. Fujisawa, H. D. Cheong, Y. H. Jeong, and Y. Hirayama. Coherent Manipulation of Electronic States in a Double Quantum Dot. *Physical Review Letters*, 91(22):226804, November 2003. ISSN 0031-9007, 1079-7114. doi:10.1103/PhysRevLett.91.226804. URL <https://link.aps.org/doi/10.1103/PhysRevLett.91.226804>.
- [106] Robert R. Hayes, Andrey A. Kiselev, Matthew G. Borselli, Steven S. Bui, Edward T. Croke III, Peter W. Deelman, Brett M. Maune, Ivan Milosavljevic, Jeong-Sun Moon, and Richard S. Ross. Lifetime measurements (T1) of electron spins in Si/SiGe quantum dots. *arXiv preprint arXiv:0908.0173*, August 2009. URL <http://arxiv.org/abs/0908.0173>. arXiv:0908.0173.
- [107] Y. He, S. K. Gorman, D. Keith, L. Kranz, J. G. Keizer, and M. Y. Simmons. A two-qubit gate between phosphorus donor electrons in silicon. *Nature*, 571(7765):371–375, July 2019. ISSN 0028-0836, 1476-4687. doi:10.1038/s41586-019-1381-2. URL <http://www.nature.com/articles/s41586-019-1381-2>.
- [108] Teiko Heinosaari and Mário Ziman. Guide to mathematical concepts of quantum theory. *Acta Physica Slovaca*, 58(4):487–674, 2008. ISSN 0323-0465. URL <http://www.physics.sk/aps/pubs/2008/aps-08-04/aps-08-04.pdf>.
- [109] N. W. Hendrickx, D. P. Franke, A. Sammak, G. Scappucci, and M. Veldhorst. Fast two-qubit logic with holes in germanium. *Nature*, 577(7791):487–491, January 2020. ISSN 0028-0836, 1476-4687. doi:10.1038/s41586-019-1919-3. URL <http://www.nature.com/articles/s41586-019-1919-3>.
- [110] N. W. Hendrickx, W. I. L. Lawrie, L. Petit, A. Sammak, G. Scappucci, and M. Veldhorst. A single-hole spin qubit. *Nature Communications*, 11(1):3478, July 2020. ISSN 2041-1723. doi:10.1038/s41467-020-17211-7. URL <http://www.nature.com/articles/s41467-020-17211-7>.
- [111] Nico W. Hendrickx, William I. L. Lawrie, Maximilian Russ, Floor van Riggelen, Sander L. de Snoo, Raymond N. Schouten, Amir Sammak, Giordano Scappucci, and Menno Veldhorst. A four-qubit germanium quantum processor. *Nature*, 591(7851):580–585, March 2021. ISSN 0028-0836, 1476-4687. doi:10.1038/s41586-021-03332-6. URL <http://www.nature.com/articles/s41586-021-03332-6>.
- [112] A. P. Higginbotham, F. Kuemmeth, M. P. Hanson, A. C. Gossard, and C. M. Marcus. Coherent Operations and Screening in Multielectron Spin Qubits. *Physical Review Letters*, 112(2):026801, January 2014. ISSN 0031-9007, 1079-7114. doi:10.1103/PhysRevLett.112.026801. URL <https://link.aps.org/doi/10.1103/PhysRevLett.112.026801>.
- [113] A. P. Higginbotham, T. W. Larsen, J. Yao, H. Yan, C. M. Lieber, C. M. Marcus, and F. Kuemmeth. Hole Spin Coherence in a Ge/Si Heterostructure Nanowire. *Nano Letters*, 14(6):3582–3586, May 2014. ISSN 1530-6984, 1530-6992. doi:10.1021/nl501242b. URL <http://pubs.acs.org/doi/10.1021/nl501242b>.
- [114] A. Hofmann, V. F. Maisi, T. Krähenmann, C. Reichl, W. Wegscheider, K. Ensslin, and T. Ihn. Anisotropy and Suppression of Spin-Orbit Interaction in a GaAs Double Quantum Dot. *Physical Review Letters*, 119(17):176807, October 2017. ISSN 0031-9007, 1079-7114. doi:10.1103/PhysRevLett.119.176807. URL <https://link.aps.org/doi/10.1103/PhysRevLett.119.176807>.
- [115] Arne Hollmann, Tom Struck, Veit Langrock, Andreas Schmidbauer, Floyd Schauer, Tim Leonhardt, Kentarou Sawano, Helge Riemann, Nikolay V. Abrosimov, Dominique Bougeard, and Lars R. Schreiber. Large, Tunable Valley Splitting and Single-Spin Relaxation Mechanisms in a Si / Si x Ge 1 - x Quantum Dot. *Physical Review Applied*, 13(3):034068, March 2020. ISSN 2331-7019. doi:10.1103/PhysRevApplied.13.034068. URL <https://link.aps.org/doi/10.1103/PhysRevApplied.13.034068>.

- [116] W. Huang, C. H. Yang, K. W. Chan, T. Tanttu, B. Hensen, R. C. C. Leon, M. A. Fogarty, J. C. C. Hwang, F. E. Hudson, K. M. Itoh, A. Morello, A. Laucht, and A. S. Dzurak. Fidelity benchmarks for two-qubit gates in silicon. *Nature*, 569(7757):532–536, May 2019. ISSN 0028-0836, 1476-4687. doi:10.1038/s41586-019-1197-0. URL <http://www.nature.com/articles/s41586-019-1197-0>.
- [117] David J. Ibberson, Theodor Lundberg, James A. Haigh, Louis Hutin, Benoit Bertrand, Sylvain Barraud, Chang-Min Lee, Nadia A. Stelmashenko, Giovanni A. Oakes, Laurence Cochrane, Jason W.A. Robinson, Maud Vinet, M. Fernando Gonzalez-Zalba, and Lisa A. Ibberson. Large Dispersive Interaction between a CMOS Double Quantum Dot and Microwave Photons. *PRX Quantum*, 2(2):020315, May 2021. ISSN 2691-3399. doi:10.1103/PRXQuantum.2.020315. URL <https://link.aps.org/doi/10.1103/PRXQuantum.2.020315>.
- [118] G. Ithier, E. Collin, P. Joyez, P. J. Meeson, D. Vion, D. Esteve, F. Chiarello, A. Shnirman, Y. Makhlin, J. Schriefl, and G. Schön. Decoherence in a superconducting quantum bit circuit. *Physical Review B*, 72(13), October 2005. ISSN 1098-0121, 1550-235X. doi:10.1103/PhysRevB.72.134519. URL <https://link.aps.org/doi/10.1103/PhysRevB.72.134519>.
- [119] Takumi Ito, Tomohiro Otsuka, Shinichi Amaha, Matthieu R. Delbecq, Takashi Nakajima, Jun Yoneda, Kenta Takeda, Giles Allison, Akito Noiri, Kento Kawasaki, and Seigo Tarucha. Detection and control of charge states in a quintuple quantum dot. *Scientific Reports*, 6(1):39113, December 2016. ISSN 2045-2322. doi:10.1038/srep39113. URL <http://www.nature.com/articles/srep39113>.
- [120] Takumi Ito, Tomohiro Otsuka, Takashi Nakajima, Matthieu R. Delbecq, Shinichi Amaha, Jun Yoneda, Kenta Takeda, Akito Noiri, Giles Allison, Arne Ludwig, Andreas D. Wieck, and Seigo Tarucha. Four single-spin Rabi oscillations in a quadruple quantum dot. *Applied Physics Letters*, 113(9):093102, August 2018. ISSN 0003-6951, 1077-3118. doi:10.1063/1.5040280. URL <http://aip.scitation.org/doi/10.1063/1.5040280>.
- [121] Baptiste Jadot, Pierre-André Mortemousque, Emmanuel Chanrion, Vivien Thiney, Arne Ludwig, Andreas D. Wieck, Matias Ur-dampilleta, Christopher Bäuerle, and Tristan Meunier. Distant spin entanglement via fast and coherent electron shuttling. *Nature Nanotechnology*, 16(5):570–575, February 2021. ISSN 1748-3387, 1748-3395. doi:10.1038/s41565-021-00846-y. URL <http://www.nature.com/articles/s41565-021-00846-y>.
- [122] Wonjin Jang, Min-Kyun Cho, Jehyun Kim, Hwanchul Chung, Vladimir Umansky, and Dohun Kim. Individual two-axis control of three singlet-triplet qubits in a micromagnet integrated quantum dot array. *Applied Physics Letters*, 117(23):234001, December 2020. ISSN 0003-6951, 1077-3118. doi:10.1063/5.0031231. URL <http://aip.scitation.org/doi/10.1063/5.0031231>.
- [123] Wonjin Jang, Jehyun Kim, Min-Kyun Cho, Hwanchul Chung, Sanghyeok Park, Jaeun Eom, Vladimir Umansky, Yunchul Chung, and Dohun Kim. Robust energy-selective tunneling readout of singlet-triplet qubits under large magnetic field gradient. *npj Quantum Information*, 6(1):64, July 2020. ISSN 2056-6387. doi:10.1038/s41534-020-00295-w. URL <http://www.nature.com/articles/s41534-020-00295-w>.
- [124] Wonjin Jang, Min-Kyun Cho, Hyeongyu Jang, Jehyun Kim, Jaemin Park, Gyeonghun Kim, Byoungwoo Kang, Hwanchul Jung, Vladimir Umansky, and Dohun Kim. Single-Shot Readout of a Driven Hybrid Qubit in a GaAs Double Quantum Dot. *Nano Letters*, 21(12):4999–5005, June 2021. ISSN 1530-6984, 1530-6992. doi:10.1021/acs.nanolett.1c00783. URL <https://pubs.acs.org/doi/10.1021/acs.nanolett.1c00783>.
- [125] Daniel Jirovec, Andrea Hofmann, Andrea Ballabio, Philipp M. Mutter, Giulio Tavani, Marc Botifoll, Alessandro Crippa, Josip Kukucka, Oliver Sagi, Frederico Martins, Jaime Saez-Mollejo, Ivan Prieto, Maksim Borovkov, Jordi Arbiol, Daniel Chastina, Giovanni Isella, and Georgios Katsaros. A singlet-triplet hole spin qubit in planar Ge. *Nature Materials*, 20(8):1106–1112, June 2021. ISSN 1476-1122, 1476-4660. doi:10.1038/s41563-021-01022-2. URL <http://www.nature.com/articles/s41563-021-01022-2>.
- [126] Ryan M. Jock, N. Tobias Jacobson, Patrick Harvey-Collard, Andrew M. Mounce, Vanita Srinivasa, Dan R. Ward, John Anderson, Ron Manginell, Joel R. Wendt, Martin Rudolph, Tammy Pluym, John King Gamble, Andrew D. Baczewski, Wayne M. Witzel, and Malcolm S. Carroll. A silicon metal-oxide-semiconductor electron spin-orbit qubit. *Nature Communications*, 9(1):1768, May 2018. ISSN 2041-1723. doi:10.1038/s41467-018-04200-0. URL <http://www.nature.com/articles/s41467-018-04200-0>.
- [127] Ryan M. Jock, N. Tobias Jacobson, Martin Rudolph, Daniel R. Ward, Malcolm S. Carroll, and Dwight R. Luhman. A silicon singlet-triplet qubit driven by spin-valley coupling. *Nature Communications*, 13(1):641, February 2022. ISSN 2041-1723. doi:10.1038/s41467-022-28302-y. URL <https://www.nature.com/articles/s41467-022-28302-y>.
- [128] A. C. Johnson, J. R. Petta, J. M. Taylor, A. Yacoby, M. D. Lukin, C. M. Marcus, M. P. Hanson, and A. C. Gossard. Triplet–singlet spin relaxation via nuclei in a double quantum dot. *Nature*, 435(7044):925–928, June 2005. ISSN 0028-0836, 1476-4679. doi:10.1038/nature03815. URL <http://www.nature.com/doifinder/10.1038/nature03815>.
- [129] Mark A. I. Johnson, Mateusz T. Mądzik, Fay E. Hudson, Kohéi M. Itoh, Alexander M. Jakob, David N. Jamieson, Andrew Dzurak, and Andrea Morello. Beating the thermal limit of qubit initialization with a Bayesian ‘Maxwell’s demon’. *arXiv:2110.02046 [cond-mat, physics:quant-ph]*, October 2021. URL <http://arxiv.org/abs/2110.02046>. arXiv: 2110.02046.
- [130] A.M. Jones, E.J. Pritchett, E.H. Chen, T.E. Keating, R.W. Andrews, J.Z. Blumoff, L.A. De Lorenzo, K. Eng, S.D. Ha, A.A. Kiselev, S.M. Meenehan, S.T. Merkel, J.A. Wright, L.F. Edge, R.S. Ross, M.T. Rakher, M.G. Borselli, and A. Hunter. Spin-Blockade Spectroscopy of Si / Si - Ge Quantum Dots. *Physical Review Applied*, 12(1):014026, July 2019. ISSN 2331-7019. doi:10.1103/PhysRevApplied.12.014026. URL <https://link.aps.org/doi/10.1103/PhysRevApplied.12.014026>.
- [131] Yadav P. Kandel, Haifeng Qiao, Saeed Fallahi, Geoffrey C. Gardner, Michael J. Manfra, and John M. Nichol. Coherent spin-state transfer via Heisenberg exchange. *Nature*, 573(7775):553–557, September 2019. ISSN 0028-0836, 1476-4687. doi:10.1038/s41586-019-1566-8. URL <http://www.nature.com/articles/s41586-019-1566-8>.
- [132] Yadav P. Kandel, Haifeng Qiao, Saeed Fallahi, Geoffrey C. Gardner, Michael J. Manfra, and John M. Nichol. Adiabatic quantum state transfer in a semiconductor quantum-dot spin chain. *Nature Communications*, 12(1):2156, April 2021. ISSN 2041-1723. doi:10.1038/s41467-021-22416-5. URL <http://www.nature.com/articles/s41467-021-22416-5>.
- [133] B. E. Kane. A silicon-based nuclear spin quantum computer. *Nature*, 393(6681):133–137, May 1998. ISSN 1476-4687. doi:10.1038/30156. URL <https://doi.org/10.1038/30156>.
- [134] E. Kawakami, P. Scarlino, D. R. Ward, F. R. Braakman, D. E. Savage, M. G. Lagally, Mark Friesen, S. N. Coppersmith, M. A. Eriksson, and L. M. K. Vandersypen. Electrical control of a long-lived spin qubit in a Si/SiGe quantum dot. *Nature Nanotechnology*, 9(9):666–670,

- August 2014. ISSN 1748-3387, 1748-3395. doi:10.1038/nano.2014.153. URL <http://www.nature.com/doifinder/10.1038/nano.2014.153>.
- [135] Erika Kawakami, Thibaut Jullien, Pasquale Scarlino, Daniel R. Ward, Donald E. Savage, Max G. Lagally, Viatcheslav V. Dobrovitski, Mark Friesen, Susan N. Coppersmith, Mark A. Eriksson, and Lieven M. K. Vandersypen. Gate fidelity and coherence of an electron spin in an Si/SiGe quantum dot with micromagnet. *Proceedings of the National Academy of Sciences*, 113(42):11738–11743, October 2016. ISSN 0027-8424, 1091-6490. doi:10.1073/pnas.1603251113. URL <http://www.pnas.org/lookup/doi/10.1073/pnas.1603251113>.
- [136] D. Keith, M. G. House, M. B. Donnelly, T. F. Watson, B. Weber, and M. Y. Simmons. Single-Shot Spin Readout in Semiconductors Near the Shot-Noise Sensitivity Limit. *Physical Review X*, 9(4):041003, October 2019. ISSN 2160-3308. doi:10.1103/PhysRevX.9.041003. URL <https://link.aps.org/doi/10.1103/PhysRevX.9.041003>.
- [137] J. Kerckhoff, B. Sun, B.H. Fong, C. Jones, A.A. Kiselev, D.W. Barnes, R.S. Noah, E. Acuna, M. Akmal, S.D. Ha, J.A. Wright, B.J. Thomas, C.A.C. Jackson, L.F. Edge, K. Eng, R.S. Ross, and T.D. Ladd. Magnetic Gradient Fluctuations from Quadrupolar 73 Ge in Si / Si Ge Exchange-Only Qubits. *PRX Quantum*, 2(1):010347, March 2021. ISSN 2691-3399. doi:10.1103/PRXQuantum.2.010347. URL <https://link.aps.org/doi/10.1103/PRXQuantum.2.010347>.
- [138] Alexander V. Khaetskii and Yuli V. Nazarov. Spin-flip transitions between Zeeman sublevels in semiconductor quantum dots. *Physical Review B*, 64(12), September 2001. ISSN 0163-1829, 1095-3795. doi:10.1103/PhysRevB.64.125316. URL <https://link.aps.org/doi/10.1103/PhysRevB.64.125316>.
- [139] Alexander V. Khaetskii, Daniel Loss, and Leonid Glazman. Electron Spin Decoherence in Quantum Dots due to Interaction with Nuclei. *Physical Review Letters*, 88(18), April 2002. ISSN 0031-9007, 1079-7114. doi:10.1103/PhysRevLett.88.186802. URL <https://link.aps.org/doi/10.1103/PhysRevLett.88.186802>.
- [140] Dohun Kim, Zhan Shi, C. B. Simmons, D. R. Ward, J. R. Prance, Teck Seng Koh, John King Gamble, D. E. Savage, M. G. Lagally, Mark Friesen, S. N. Coppersmith, and Mark A. Eriksson. Quantum control and process tomography of a semiconductor quantum dot hybrid qubit. *Nature*, 511(7507):70–74, July 2014. ISSN 0028-0836, 1476-4687. doi:10.1038/nature13407. URL <http://www.nature.com/doifinder/10.1038/nature13407>.
- [141] Dohun Kim, D. R. Ward, C. B. Simmons, John King Gamble, Robin Blume-Kohout, Erik Nielsen, D. E. Savage, M. G. Lagally, Mark Friesen, S. N. Coppersmith, and M. A. Eriksson. Microwave-driven coherent operation of a semiconductor quantum dot charge qubit. *Nature Nanotechnology*, 10(3):243–247, February 2015. ISSN 1748-3387, 1748-3395. doi:10.1038/nnano.2014.336. URL <http://www.nature.com/articles/nnano.2014.336>.
- [142] Dohun Kim, Daniel R Ward, Christie B Simmons, Don E Savage, Max G Lagally, Mark Friesen, Susan N Coppersmith, and Mark A Eriksson. High-fidelity resonant gating of a silicon-based quantum dot hybrid qubit. *npj Quantum Information*, 1(1):15004, December 2015. ISSN 2056-6387. doi:10.1038/npjqpi.2015.4. URL <http://www.nature.com/articles/npjqpi20154>.
- [143] H. Kiyama, T. Nakajima, S. Teraoka, A. Oiwa, and S. Tarucha. Single-Shot Ternary Readout of Two-Electron Spin States in a Quantum Dot Using Spin Filtering by Quantum Hall Edge States. *Physical Review Letters*, 117(23):236802, November 2016. ISSN 0031-9007, 1079-7114. doi:10.1103/PhysRevLett.117.236802. URL <https://link.aps.org/doi/10.1103/PhysRevLett.117.236802>.
- [144] Christoph Kloeffel and Daniel Loss. Prospects for Spin-Based Quantum Computing in Quantum Dots. *Annual Review of Condensed Matter Physics*, 4(1):51–81, April 2013. ISSN 1947-5454, 1947-5462. doi:10.1146/annurev-conmatphys-030212-184248. URL <http://www.annualreviews.org/doi/10.1146/annurev-conmatphys-030212-184248>.
- [145] Takashi Kobayashi, Joseph Salfi, Cassandra Chua, Joost van der Heijden, Matthew G. House, Dimitrie Culcer, Wayne D. Hutchison, Brett C. Johnson, Jeff C. McCallum, Helge Riemann, Nikolay V. Abrosimov, Peter Becker, Hans-Joachim Pohl, Michelle Y. Simmons, and Sven Rogge. Engineering long spin coherence times of spin-orbit qubits in silicon. *Nature Materials*, 20(1):38–42, July 2020. ISSN 1476-1122, 1476-4660. doi:10.1038/s41563-020-0743-3. URL <http://www.nature.com/articles/s41563-020-0743-3>.
- [146] Matthias Koch, Joris G. Keizer, Prasanna Pakkiam, Daniel Keith, Matthew G. House, Eldad Peretz, and Michelle Y. Simmons. Spin read-out in atomic qubits in an all-epitaxial three-dimensional transistor. *Nature Nanotechnology*, 14(2):137–140, January 2019. ISSN 1748-3387, 1748-3395. doi:10.1038/s41565-018-0338-1. URL <http://www.nature.com/articles/s41565-018-0338-1>.
- [147] Y. Kojima, T. Nakajima, A. Noiri, J. Yoneda, T. Otsuka, K. Takeda, S. Li, S. D. Bartlett, A. Ludwig, A. D. Wieck, and S. Tarucha. Probabilistic teleportation of a quantum dot spin qubit. *npj Quantum Information*, 7(1):68, May 2021. ISSN 2056-6387. doi:10.1038/s41534-021-00403-4. URL <http://www.nature.com/articles/s41534-021-00403-4>.
- [148] F. H. L. Koppens. Control and Detection of Singlet-Triplet Mixing in a Random Nuclear Field. *Science*, 309(5739):1346–1350, August 2005. ISSN 0036-8075, 1095-9203. doi:10.1126/science.1113719. URL <http://www.sciencemag.org/cgi/doi/10.1126/science.1113719>.
- [149] F. H. L. Koppens, C. Buijzer, K. J. Tielrooij, I. T. Vink, K. C. Nowack, T. Meunier, L. P. Kouwenhoven, and L. M. K. Vandersypen. Driven coherent oscillations of a single electron spin in a quantum dot. *Nature*, 442(7104):766–771, August 2006. ISSN 0028-0836, 1476-4687. doi:10.1038/nature05065. URL <http://www.nature.com/doifinder/10.1038/nature05065>.
- [150] F. H. L. Koppens, D. Klauser, W. A. Coish, K. C. Nowack, L. P. Kouwenhoven, D. Loss, and L. M. K. Vandersypen. Universal Phase Shift and Nonexponential Decay of Driven Single-Spin Oscillations. *Physical Review Letters*, 99(10):106803, September 2007. ISSN 0031-9007, 1079-7114. doi:10.1103/PhysRevLett.99.106803. URL <https://link.aps.org/doi/10.1103/PhysRevLett.99.106803>.
- [151] F. H. L. Koppens, K. C. Nowack, and L. M. K. Vandersypen. Spin Echo of a Single Electron Spin in a Quantum Dot. *Physical Review Letters*, 100(23):236802, June 2008. ISSN 0031-9007, 1079-7114. doi:10.1103/PhysRevLett.100.236802. URL <https://link.aps.org/doi/10.1103/PhysRevLett.100.236802>.
- [152] J. V. Koski, A. J. Landig, M. Russ, J. C. Abadillo-Uriel, P. Scarlino, B. Kratochwil, C. Reichl, W. Wegscheider, Guido Burkard, Mark Friesen, S. N. Coppersmith, A. Wallraff, K. Ensslin, and T. Ihn. Strong photon coupling to the quadrupole moment of an electron in a solid-state qubit. *Nature Physics*, 16(6):642–646, May 2020. ISSN 1745-2473, 1745-2481. doi:10.1038/s41567-020-0862-4. URL <http://www.nature.com/articles/s41567-020-0862-4>.
- [153] B. Kratochwil, J. V. Koski, A. J. Landig, P. Scarlino, J. C. Abadillo-Uriel, C. Reichl, S. N. Coppersmith, W. Wegscheider, Mark Friesen,

- A. Wallraff, T. Ihn, and K. Ensslin. Charge qubit in a triple quantum dot with tunable coherence. *Physical Review Research*, 3(1):013171, February 2021. ISSN 2643-1564. doi:10.1103/PhysRevResearch.3.013171. URL <https://link.aps.org/doi/10.1103/PhysRevResearch.3.013171>.
- [154] Ferdinand Kuemmeth and Hendrik Bluhm. Roadmap for gallium arsenide spin qubits. *arXiv:2011.13907 [cond-mat, physics:quant-ph]*, November 2020. URL <http://arxiv.org/abs/2011.13907>. arXiv: 2011.13907.
- [155] E. A. Laird, J. R. Petta, A. C. Johnson, C. M. Marcus, A. Yacoby, M. P. Hanson, and A. C. Gossard. Effect of Exchange Interaction on Spin Dephasing in a Double Quantum Dot. *Physical Review Letters*, 97(5):056801, July 2006. ISSN 0031-9007, 1079-7114. doi:10.1103/PhysRevLett.97.056801. URL <https://link.aps.org/doi/10.1103/PhysRevLett.97.056801>.
- [156] E. A. Laird, C. Barthel, E. I. Rashba, C. M. Marcus, M. P. Hanson, and A. C. Gossard. Hyperfine-Mediated Gate-Driven Electron Spin Resonance. *Physical Review Letters*, 99(24):246601, December 2007. ISSN 0031-9007, 1079-7114. doi:10.1103/PhysRevLett.99.246601. URL <http://link.aps.org/doi/10.1103/PhysRevLett.99.246601>.
- [157] E. A. Laird, J. M. Taylor, D. P. DiVincenzo, C. M. Marcus, M. P. Hanson, and A. C. Gossard. Coherent spin manipulation in an exchange-only qubit. *Physical Review B*, 82(7):075403, August 2010. ISSN 1098-0121, 1550-235X. doi:10.1103/PhysRevB.82.075403. URL <https://link.aps.org/doi/10.1103/PhysRevB.82.075403>.
- [158] E. A. Laird, F. Pei, and L. P. Kouwenhoven. A valley–spin qubit in a carbon nanotube. *Nature Nanotechnology*, 8(8):565–568, July 2013. ISSN 1748-3387, 1748-3395. doi:10.1038/nnano.2013.140. URL <http://www.nature.com/articles/nnano.2013.140>.
- [159] A. J. Landig, J. V. Koski, P. Scarlino, U. C. Mendes, A. Blais, C. Reichl, W. Wegscheider, A. Wallraff, K. Ensslin, and T. Ihn. Coherent spin–photon coupling using a resonant exchange qubit. *Nature*, 560(7717):179–184, July 2018. ISSN 0028-0836, 1476-4687. doi:10.1038/s41586-018-0365-y. URL <http://www.nature.com/articles/s41586-018-0365-y>.
- [160] A. J. Landig, J. V. Koski, P. Scarlino, C. Müller, J. C. Abadillo-Uriel, B. Kratochwil, C. Reichl, W. Wegscheider, S. N. Coppersmith, Mark Friesen, A. Wallraff, T. Ihn, and K. Ensslin. Virtual-photon-mediated spin-qubit-transmon coupling. *Nature Communications*, 10(1):5037, November 2019. ISSN 2041-1723. doi:10.1038/s41467-019-13000-z. URL <http://www.nature.com/articles/s41467-019-13000-z>.
- [161] A. J. Landig, J. V. Koski, P. Scarlino, C. Reichl, W. Wegscheider, A. Wallraff, K. Ensslin, and T. Ihn. Microwave-Cavity-Detected Spin Blockade in a Few-Electron Double Quantum Dot. *Physical Review Letters*, 122(21):213601, May 2019. ISSN 0031-9007, 1079-7114. doi:10.1103/PhysRevLett.122.213601. URL <https://link.aps.org/doi/10.1103/PhysRevLett.122.213601>.
- [162] A. Laucht, J. T. Muhonen, F. A. Mohiyaddin, R. Kalra, J. P. Dehollain, S. Freer, F. E. Hudson, M. Veldhorst, R. Rahman, G. Klimeck, K. M. Itoh, D. N. Jamieson, J. C. McCallum, A. S. Dzurak, and A. Morello. Electrically controlling single-spin qubits in a continuous microwave field. *Science Advances*, 1(3):e1500022–e1500022, April 2015. ISSN 2375-2548. doi:10.1126/sciadv.1500022. URL <http://advances.sciencemag.org/cgi/doi/10.1126/sciadv.1500022>.
- [163] Arne Laucht, Rachpon Kalra, Stephanie Simmons, Juan P. Dehollain, Juha T. Muhonen, Fahd A. Mohiyaddin, Solomon Freer, Fay E. Hudson, Kohei M. Itoh, David N. Jamieson, Jeffrey C. McCallum, Andrew S. Dzurak, and A. Morello. A dressed spin qubit in silicon. *Nature Nanotechnology*, 12(1):61–66, October 2016. ISSN 1748-3387, 1748-3395. doi:10.1038/nnano.2016.178. URL <http://www.nature.com/doifinder/10.1038/nnano.2016.178>.
- [164] W. I. L. Lawrie, H. G. J. Eenink, N. W. Hendrickx, J. M. Boter, L. Petit, S. V. Amitonov, M. Lodari, B. Paquelet Wuetz, C. Volk, S. G. J. Philips, G. Droulers, N. Kalhor, F. van Riggelen, D. Brousse, A. Sammak, L. M. K. Vandersypen, G. Scappucci, and M. Veldhorst. Quantum dot arrays in silicon and germanium. *Applied Physics Letters*, 116(8):080501, February 2020. ISSN 0003-6951, 1077-3118. doi:10.1063/5.0002013. URL <http://aip.scitation.org/doi/10.1063/5.0002013>.
- [165] W. I. L. Lawrie, N. W. Hendrickx, F. van Riggelen, M. Russ, L. Petit, A. Sammak, G. Scappucci, and M. Veldhorst. Spin relaxation benchmarks and individual qubit addressability for holes in quantum dots. *Nano Letters*, 20(10):7237–7242, August 2020. ISSN 1530-6984, 1530-6992. doi:10.1021/acs.nanolett.0c02589. URL <http://arxiv.org/abs/2006.12563>. arXiv: 2006.12563.
- [166] W. I. L. Lawrie, M. Russ, F. van Riggelen, N. W. Hendrickx, S. L. de Snoo, A. Sammak, G. Scappucci, and M. Veldhorst. Simultaneous driving of semiconductor spin qubits at the fault-tolerant threshold. *arXiv:2109.07837 [cond-mat]*, September 2021. URL <http://arxiv.org/abs/2109.07837>. arXiv: 2109.07837.
- [167] R. C. C. Leon, C. H. Yang, J. C. C. Hwang, J. Camirand Lemyre, T. Tanttu, W. Huang, K. W. Chan, K. Y. Tan, F. E. Hudson, K. M. Itoh, A. Morello, A. Laucht, M. Pioro-Ladrière, A. Saraiva, and A. S. Dzurak. Coherent spin control of s-, p-, d- and f-electrons in a silicon quantum dot. *Nature Communications*, 11(1):797, February 2020. ISSN 2041-1723. doi:10.1038/s41467-019-14053-w. URL <http://www.nature.com/articles/s41467-019-14053-w>.
- [168] Ross C. C. Leon, Chih Hwan Yang, Jason C. C. Hwang, Julien Camirand Lemyre, Tuomo Tanttu, Wei Huang, Jonathan Y. Huang, Fay E. Hudson, Kohei M. Itoh, Arne Laucht, Michel Pioro-Ladrière, Andre Saraiva, and Andrew S. Dzurak. Bell-state tomography in a silicon many-electron artificial molecule. *Nature Communications*, 12(1):3228, May 2021. ISSN 2041-1723. doi:10.1038/s41467-021-23437-w. URL <http://www.nature.com/articles/s41467-021-23437-w>.
- [169] Jeremy Levy. Universal Quantum Computation with Spin- 1 / 2 Pairs and Heisenberg Exchange. *Physical Review Letters*, 89(14), September 2002. ISSN 0031-9007, 1079-7114. doi:10.1103/PhysRevLett.89.147902. URL <http://link.aps.org/doi/10.1103/PhysRevLett.89.147902>.
- [170] Hai-Ou Li, Gang Cao, Guo-Dong Yu, Ming Xiao, Guang-Can Guo, Hong-Wen Jiang, and Guo-Ping Guo. Conditional rotation of two strongly coupled semiconductor charge qubits. *Nature Communications*, 6(1):7681, July 2015. ISSN 2041-1723. doi:10.1038/ncomms8681. URL <http://www.nature.com/articles/ncomms8681>.
- [171] Y.-Y. Liu, L.A. Orona, Samuel F. Neyens, E.R. MacQuarrie, M.A. Eriksson, and A. Yacoby. Magnetic-Gradient-Free Two-Axis Control of a Valley Spin Qubit in Si x Ge 1 - x. *Physical Review Applied*, 16(2):024029, August 2021. ISSN 2331-7019. doi:10.1103/PhysRevApplied.16.024029. URL <https://link.aps.org/doi/10.1103/PhysRevApplied.16.024029>.
- [172] Daniel Loss and David P. DiVincenzo. Quantum computation with quantum dots. *Physical Review A*, 57(1):120–126, January 1998. ISSN 1050-2947, 1094-1622. doi:10.1103/PhysRevA.57.120. URL <https://link.aps.org/doi/10.1103/PhysRevA.57.120>.
- [173] E. R. MacQuarrie, Samuel F. Neyens, J. P. Dodson, J. Corrigan, Brandur Thorgrimsson, Nathan Holman, M. Palma, L. F. Edge, Mark

- Friesen, S. N. Coppersmith, and M. A. Eriksson. Progress toward a capacitively mediated CNOT between two charge qubits in Si/SiGe. *npj Quantum Information*, 6(1):81, September 2020. ISSN 2056-6387. doi:10.1038/s41534-020-00314-w. URL <http://www.nature.com/articles/s41534-020-00314-w>.
- [174] Mateusz T. Mądzik, Thaddeus D. Ladd, Fay E. Hudson, Kohei M. Itoh, Alexander M. Jakob, Brett C. Johnson, Jeffrey C. McCallum, David N. Jamieson, Andrew S. Dzurak, Arne Laucht, and Andrea Morello. Controllable freezing of the nuclear spin bath in a single-atom spin qubit. *Science Advances*, 6(27):eaba3442, July 2020. ISSN 2375-2548. doi:10.1126/sciadv.aba3442. URL <https://advances.sciencemag.org/lookup/doi/10.1126/sciadv.aba3442>.
- [175] Mateusz T. Mądzik, Arne Laucht, Fay E. Hudson, Alexander M. Jakob, Brett C. Johnson, David N. Jamieson, Kohei M. Itoh, Andrew S. Dzurak, and Andrea Morello. Conditional quantum operation of two exchange-coupled single-donor spin qubits in a MOS-compatible silicon device. *Nature Communications*, 12(1):181, January 2021. ISSN 2041-1723. doi:10.1038/s41467-020-20424-5. URL <http://www.nature.com/articles/s41467-020-20424-5>.
- [176] Mateusz T. Mądzik, Serwan Asaad, Akram Youssry, Benjamin Joecker, Kenneth M. Rudinger, Erik Nielsen, Kevin C. Young, Timothy J. Proctor, Andrew D. Baczewski, Arne Laucht, Vivien Schmitt, Fay E. Hudson, Kohei M. Itoh, Alexander M. Jakob, Brett C. Johnson, David N. Jamieson, Andrew S. Dzurak, Christopher Ferrie, Robin Blume-Kohout, and Andrea Morello. Precision tomography of a three-qubit donor quantum processor in silicon. *Nature*, 601(7893):348–353, January 2022. ISSN 0028-0836, 1476-4687. doi:10.1038/s41586-021-04292-7. URL <https://www.nature.com/articles/s41586-021-04292-7>.
- [177] Easwar Magesan, Jay M. Gambetta, and Joseph Emerson. Characterizing quantum gates via randomized benchmarking. *Physical Review A*, 85(4):042311, April 2012. ISSN 1050-2947, 1094-1622. doi:10.1103/PhysRevA.85.042311. URL <https://link.aps.org/doi/10.1103/PhysRevA.85.042311>.
- [178] Easwar Magesan, Jay M. Gambetta, B. R. Johnson, Colm A. Ryan, Jerry M. Chow, Seth T. Merkel, Marcus P. da Silva, George A. Keefe, Mary B. Rothwell, Thomas A. Ohki, Mark B. Ketchen, and M. Steffen. Efficient Measurement of Quantum Gate Error by Interleaved Randomized Benchmarking. *Physical Review Letters*, 109(8):080505, August 2012. ISSN 0031-9007, 1079-7114. doi:10.1103/PhysRevLett.109.080505. URL <https://link.aps.org/doi/10.1103/PhysRevLett.109.080505>.
- [179] Filip K. Malinowski, Frederico Martins, Peter D. Nissen, Edwin Barnes, Łukasz Cywiński, Mark S. Rudner, Saeed Fallahi, Geoffrey C. Gardner, Michael J. Manfra, Charles M. Marcus, and Ferdinand Kuemmeth. Notch filtering the nuclear environment of a spin qubit. *Nature Nanotechnology*, 12(1):16–20, October 2016. ISSN 1748-3387, 1748-3395. doi:10.1038/nnano.2016.170. URL <http://www.nature.com/doifinder/10.1038/nnano.2016.170>.
- [180] Filip K. Malinowski, Frederico Martins, Łukasz Cywiński, Mark S. Rudner, Peter D. Nissen, Saeed Fallahi, Geoffrey C. Gardner, Michael J. Manfra, Charles M. Marcus, and Ferdinand Kuemmeth. Spectrum of the Nuclear Environment for GaAs Spin Qubits. *Physical Review Letters*, 118(17):177702, April 2017. ISSN 0031-9007, 1079-7114. doi:10.1103/PhysRevLett.118.177702. URL <http://link.aps.org/doi/10.1103/PhysRevLett.118.177702>.
- [181] Filip K. Malinowski, Frederico Martins, Peter D. Nissen, Saeed Fallahi, Geoffrey C. Gardner, Michael J. Manfra, Charles M. Marcus, and Ferdinand Kuemmeth. Symmetric operation of the resonant exchange qubit. *Physical Review B*, 96(4):045443, July 2017. ISSN 2469-9950, 2469-9969. doi:10.1103/PhysRevB.96.045443. URL <http://link.aps.org/doi/10.1103/PhysRevB.96.045443>.
- [182] Filip K. Malinowski, Frederico Martins, Thomas B. Smith, Stephen D. Bartlett, Andrew C. Doherty, Peter D. Nissen, Saeed Fallahi, Geoffrey C. Gardner, Michael J. Manfra, Charles M. Marcus, and Ferdinand Kuemmeth. Fast spin exchange across a multielectron mediator. *Nature Communications*, 10(1):1196, March 2019. ISSN 2041-1723. doi:10.1038/s41467-019-09194-x. URL <http://www.nature.com/articles/s41467-019-09194-x>.
- [183] Frederico Martins, Filip K. Malinowski, Peter D. Nissen, Edwin Barnes, Saeed Fallahi, Geoffrey C. Gardner, Michael J. Manfra, Charles M. Marcus, and Ferdinand Kuemmeth. Noise Suppression Using Symmetric Exchange Gates in Spin Qubits. *Physical Review Letters*, 116(11):116801, March 2016. ISSN 0031-9007, 1079-7114. doi:10.1103/PhysRevLett.116.116801. URL <https://link.aps.org/doi/10.1103/PhysRevLett.116.116801>.
- [184] B. M. Maune, M. G. Borselli, B. Huang, T. D. Ladd, P. W. Deelman, K. S. Holabird, A. A. Kiselev, I. Alvarado-Rodriguez, R. S. Ross, A. E. Schmitz, M. Sokolich, C. A. Watson, M. F. Gyure, and A. T. Hunter. Coherent singlet-triplet oscillations in a silicon-based double quantum dot. *Nature*, 481(7381):344–347, January 2012. ISSN 0028-0836, 1476-4687. doi:10.1038/nature10707. URL <http://www.nature.com/articles/nature10707>.
- [185] R. Maurand, X. Jehl, D. Kotekar-Patil, A. Corra, H. Bohuslavskyi, R. Laviéville, L. Hutin, S. Barraud, M. Vinet, M. Sanquer, and S. De Franceschi. A CMOS silicon spin qubit. *Nature Communications*, 7:13575, November 2016. ISSN 2041-1723. doi:10.1038/ncomms13575. URL <http://www.nature.com/doifinder/10.1038/ncomms13575>.
- [186] J. Medford, Ł. Cywiński, C. Barthel, C. M. Marcus, M. P. Hanson, and A. C. Gossard. Scaling of Dynamical Decoupling for Spin Qubits. *Physical Review Letters*, 108(8):086802, February 2012. ISSN 0031-9007, 1079-7114. doi:10.1103/PhysRevLett.108.086802. URL <https://link.aps.org/doi/10.1103/PhysRevLett.108.086802>.
- [187] J. Medford, J. Beil, J. M. Taylor, S. D. Bartlett, A. C. Doherty, E. I. Rashba, D. P. DiVincenzo, H. Lu, A. C. Gossard, and C. M. Marcus. Self-consistent measurement and state tomography of an exchange-only spin qubit. *Nature Nanotechnology*, 8(9):654–659, September 2013. ISSN 1748-3387, 1748-3395. doi:10.1038/nnano.2013.168. URL <http://www.nature.com/doifinder/10.1038/nnano.2013.168>.
- [188] J. Medford, J. Beil, J. M. Taylor, E. I. Rashba, H. Lu, A. C. Gossard, and C. M. Marcus. Quantum-Dot-Based Resonant Exchange Qubit. *Physical Review Letters*, 111(5):050501, July 2013. ISSN 0031-9007, 1079-7114. doi:10.1103/PhysRevLett.111.050501. URL <https://link.aps.org/doi/10.1103/PhysRevLett.111.050501>.
- [189] I. A. Merkulov, Al. L. Efros, and M. Rosen. Electron spin relaxation by nuclei in semiconductor quantum dots. *Physical Review B*, 65(20), April 2002. ISSN 0163-1829, 1095-3795. doi:10.1103/PhysRevB.65.205309. URL <https://link.aps.org/doi/10.1103/PhysRevB.65.205309>.
- [190] N. David Mermin. *Quantum computer science: an introduction*. Cambridge University Press, Cambridge, 2007. ISBN 978-0-521-87658-2. OCLC: ocn137221653.

- [191] T. Meunier, K.-J. Tielrooij, I. T. Vink, F. H. L. Koppens, H. P. Tranitz, W. Wegscheider, L. P. Kouwenhoven, and L. M. K. Vandersypen. High fidelity measurement of singlet–triplet state in a quantum dot. *physica status solidi (b)*, 243(15):3855–3858, November 2006. ISSN 03701972, 15213951. doi:10.1002/pssb.200671503. URL <http://doi.wiley.com/10.1002/pssb.200671503>.
- [192] T. Meunier, I. T. Vink, L. H. Willems van Beveren, F. H. L. Koppens, H. P. Tranitz, W. Wegscheider, L. P. Kouwenhoven, and L. M. K. Vandersypen. Nondestructive measurement of electron spins in a quantum dot. *Physical Review B*, 74(19):195303, November 2006. ISSN 1098-0121, 1550-235X. doi:10.1103/PhysRevB.74.195303. URL <https://link.aps.org/doi/10.1103/PhysRevB.74.195303>.
- [193] T. Meunier, I. T. Vink, L. H. Willems van Beveren, K.-J. Tielrooij, R. Hanson, F. H. L. Koppens, H. P. Tranitz, W. Wegscheider, L. P. Kouwenhoven, and L. M. K. Vandersypen. Experimental Signature of Phonon-Mediated Spin Relaxation in a Two-Electron Quantum Dot. *Physical Review Letters*, 98(12):126601, March 2007. ISSN 0031-9007, 1079-7114. doi:10.1103/PhysRevLett.98.126601. URL <http://link.aps.org/doi/10.1103/PhysRevLett.98.126601>.
- [194] X. Mi, J. V. Cady, D. M. Zajac, P. W. Deelman, and J. R. Petta. Strong coupling of a single electron in silicon to a microwave photon. *Science*, 355(6321):156–158, December 2016. ISSN 0036-8075, 1095-9203. doi:10.1126/science.aal2469. URL <http://www.sciencemag.org/lookup/doi/10.1126/science.aal2469>.
- [195] X. Mi, J. V. Cady, D. M. Zajac, J. Stehlík, L. F. Edge, and J. R. Petta. Circuit quantum electrodynamics architecture for gate-defined quantum dots in silicon. *Applied Physics Letters*, 110(4):043502, January 2017. ISSN 0003-6951, 1077-3118. doi:10.1063/1.4974536. URL <http://aip.scitation.org/doi/10.1063/1.4974536>.
- [196] X. Mi, M. Benito, S. Putz, D. M. Zajac, J. M. Taylor, Guido Burkard, and J. R. Petta. A coherent spin–photon interface in silicon. *Nature*, 555(7698):599–603, February 2018. ISSN 0028-0836, 1476-4687. doi:10.1038/nature25769. URL <http://www.nature.com/doifinder/10.1038/nature25769>.
- [197] A. R. Mills, D. M. Zajac, M. J. Gullans, F. J. Schupp, T. M. Hazard, and J. R. Petta. Shutting a single charge across a one-dimensional array of silicon quantum dots. *Nature Communications*, 10(1):1063, March 2019. ISSN 2041-1723. doi:10.1038/s41467-019-08970-z. URL <http://www.nature.com/articles/s41467-019-08970-z>.
- [198] A. R. Mills, C. R. Guinn, M. J. Gullans, A. J. Sigillito, M. M. Feldman, E. Nielsen, and J. R. Petta. Two-qubit silicon quantum processor with operation fidelity exceeding 99%. *arXiv:2111.11937 [cond-mat, physics:quant-ph]*, November 2021. URL <http://arxiv.org/abs/2111.11937>. arXiv: 2111.11937.
- [199] Andrea Morello, Jarryd J. Pla, Floris A. Zwanenburg, Kok W. Chan, Kuan Y. Tan, Hans Huebl, Mikko Möttönen, Christopher D. Nugroho, Changyi Yang, Jessica A. van Donkelaar, Andrew D. C. Alves, David N. Jamieson, Christopher C. Escott, Lloyd C. L. Hollenberg, Robert G. Clark, and Andrew S. Dzurak. Single-shot readout of an electron spin in silicon. *Nature*, 467(7316):687–691, September 2010. ISSN 0028-0836, 1476-4687. doi:10.1038/nature09392. URL <http://www.nature.com/articles/nature09392>.
- [200] Pierre-André Mortemousque, Emmanuel Chanrion, Baptiste Jadot, Hanno Flentje, Arne Ludwig, Andreas D. Wieck, Matias Urdampilleta, Christopher Bäuerle, and Tristan Meunier. Coherent control of individual electron spins in a two-dimensional quantum dot array. *Nature Nanotechnology*, 16:296–301, December 2020. ISSN 1748-3387, 1748-3395. doi:10.1038/s41565-020-00816-w. URL <http://www.nature.com/articles/s41565-020-00816-w>.
- [201] Pierre-André Mortemousque, Baptiste Jadot, Emmanuel Chanrion, Vivien Thiney, Christopher Bäuerle, Arne Ludwig, Andreas D. Wieck, Matias Urdampilleta, and Tristan Meunier. Enhanced Spin Coherence while Displacing Electron in a Two-Dimensional Array of Quantum Dots. *PRX Quantum*, 2(3):030331, August 2021. ISSN 2691-3399. doi:10.1103/PRXQuantum.2.030331. URL <https://link.aps.org/doi/10.1103/PRXQuantum.2.030331>.
- [202] J T Muhonen, A Laucht, S Simmons, J P Dehollain, R Kalra, F E Hudson, S Freer, K M Itoh, D N Jamieson, J C McCallum, A S Dzurak, and A Morello. Quantifying the quantum gate fidelity of single-atom spin qubits in silicon by randomized benchmarking. *Journal of Physics: Condensed Matter*, 27(15):154205, March 2015. ISSN 0953-8984, 1361-648X. doi:10.1088/0953-8984/27/15/154205. URL <https://iopscience.iop.org/article/10.1088/0953-8984/27/15/154205>.
- [203] Juha T. Muhonen, Juan P. Dehollain, Arne Laucht, Fay E. Hudson, Rachpon Kalra, Takeharu Sekiguchi, Kohei M. Itoh, David N. Jamieson, Jeffrey C. McCallum, Andrew S. Dzurak, and Andrea Morello. Storing quantum information for 30 seconds in a nanoelectronic device. *Nature Nanotechnology*, 9(12):986–991, October 2014. ISSN 1748-3387, 1748-3395. doi:10.1038/nnano.2014.211. URL <http://www.nature.com/doifinder/10.1038/nnano.2014.211>.
- [204] Uditendu Mukhopadhyay, Juan Pablo Dehollain, Christian Reichl, Werner Wegscheider, and Lieven M. K. Vandersypen. A 2x2 quantum dot array with controllable inter-dot tunnel couplings. *Applied Physics Letters*, 112(18):183505, April 2018. ISSN 0003-6951, 1077-3118. doi:10.1063/1.5025928. URL <http://arxiv.org/abs/1802.05446>. arXiv: 1802.05446.
- [205] S. Nadj-Perge, S. M. Frolov, E. P. A. M. Bakkers, and L. P. Kouwenhoven. Spin–orbit qubit in a semiconductor nanowire. *Nature*, 468(7327):1084–1087, December 2010. ISSN 0028-0836, 1476-4687. doi:10.1038/nature09682. URL <http://www.nature.com/doifinder/10.1038/nature09682>.
- [206] Takashi Nakajima, Matthieu R. Delbecq, Tomohiro Otsuka, Peter Stano, Shinichi Amaha, Jun Yoneda, Akito Noiri, Kento Kawasaki, Kenta Takeda, Giles Allison, Arne Ludwig, Andreas D. Wieck, Daniel Loss, and Seigo Tarucha. Robust Single-Shot Spin Measurement with 99.5% Fidelity in a Quantum Dot Array. *Physical Review Letters*, 119(1):017701, July 2017. ISSN 0031-9007, 1079-7114. doi:10.1103/PhysRevLett.119.017701. URL <https://link.aps.org/doi/10.1103/PhysRevLett.119.017701>.
- [207] Takashi Nakajima, Akito Noiri, Jun Yoneda, Matthieu R. Delbecq, Peter Stano, Tomohiro Otsuka, Kenta Takeda, Shinichi Amaha, Giles Allison, Kento Kawasaki, Arne Ludwig, Andreas D. Wieck, Daniel Loss, and Seigo Tarucha. Quantum non-demolition measurement of an electron spin qubit. *Nature Nanotechnology*, 14(6):555–560, April 2019. ISSN 1748-3387, 1748-3395. doi:10.1038/s41565-019-0426-x. URL <http://www.nature.com/articles/s41565-019-0426-x>.
- [208] Takashi Nakajima, Akito Noiri, Kento Kawasaki, Jun Yoneda, Peter Stano, Shinichi Amaha, Tomohiro Otsuka, Kenta Takeda, Matthieu R. Delbecq, Giles Allison, Arne Ludwig, Andreas D. Wieck, Daniel Loss, and Seigo Tarucha. Coherence of a Driven Electron Spin Qubit Actively Decoupled from Quasistatic Noise. *Physical Review X*, 10(1):011060, March 2020. ISSN 2160-3308. doi:10.1103/PhysRevX.10.011060. URL <https://link.aps.org/doi/10.1103/PhysRevX.10.011060>.
- [209] John M. Nichol, Lucas A. Orona, Shannon P. Harvey, Saeed Fallahi, Geoffrey C. Gardner, Michael J. Manfra, and Amir Yacoby. High-

- fidelity entangling gate for double-quantum-dot spin qubits. *npj Quantum Information*, 3(1):3, January 2017. ISSN 2056-6387. doi: 10.1038/s41534-016-0003-1. URL <http://www.nature.com/articles/s41534-016-0003-1>.
- [210] A. Noiri, T. Takakura, T. Obata, T. Otsuka, T. Nakajima, J. Yoneda, and S. Tarucha. Cotunneling spin blockade observed in a three-terminal triple quantum dot. *Physical Review B*, 96(15):155414, October 2017. ISSN 2469-9950, 2469-9969. doi: 10.1103/PhysRevB.96.155414. URL <https://link.aps.org/doi/10.1103/PhysRevB.96.155414>.
- [211] A. Noiri, T. Nakajima, J. Yoneda, M. R. Delbecq, P. Stano, T. Otsuka, K. Takeda, S. Amaha, G. Allison, K. Kawasaki, Y. Kojima, A. Ludwig, A. D. Wieck, D. Loss, and S. Tarucha. A fast quantum interface between different spin qubit encodings. *Nature Communications*, 9(1):5066, November 2018. ISSN 2041-1723. doi:10.1038/s41467-018-07522-1. URL <http://www.nature.com/articles/s41467-018-07522-1>.
- [212] Akito Noiri, Jun Yoneda, Takashi Nakajima, Tomohiro Otsuka, Matthieu R. Delbecq, Kenta Takeda, Shinichi Amaha, Giles Allison, Arne Ludwig, Andreas D. Wieck, and others. Coherent electron-spin-resonance manipulation of three individual spins in a triple quantum dot. *Applied Physics Letters*, 108(15):153101, April 2016. doi:10.1063/1.4945592. URL <http://scitation.aip.org/content/aip/journal/apl/108/15/10.1063/1.4945592>.
- [213] Akito Noiri, Kenta Takeda, Jun Yoneda, Takashi Nakajima, Tetsuo Kodera, and Seigo Tarucha. Radio-Frequency-Detected Fast Charge Sensing in Undoped Silicon Quantum Dots. *Nano Letters*, 20(2):947–952, January 2020. ISSN 1530-6984, 1530-6992. doi: 10.1021/acs.nanolett.9b03847. URL <https://pubs.acs.org/doi/10.1021/acs.nanolett.9b03847>.
- [214] Akito Noiri, Kenta Takeda, Takashi Nakajima, Takashi Kobayashi, Amir Sammak, Giordano Scappucci, and Seigo Tarucha. Fast universal quantum gate above the fault-tolerance threshold in silicon. *Nature*, 601(7893):338–342, January 2022. ISSN 0028-0836, 1476-4687. doi:10.1038/s41586-021-04182-y. URL <https://www.nature.com/articles/s41586-021-04182-y>.
- [215] K. C. Nowack, F. H. L. Koppens, Yu. V. Nazarov, and L. M. K. Vandersypen. Coherent Control of a Single Electron Spin with Electric Fields. *Science*, 318(5855):1430–1433, November 2007. ISSN 0036-8075, 1095-9203. doi:10.1126/science.1148092. URL <http://www.sciencemag.org/cgi/doi/10.1126/science.1148092>.
- [216] K. C. Nowack, M. Shafiei, M. Laforest, G. E. D. K. Prawiroatmodjo, L. R. Schreiber, C. Reichl, W. Wegscheider, and L. M. K. Vandersypen. Single-Shot Correlations and Two-Qubit Gate of Solid-State Spins. *Science*, 333(6047):1269–1272, August 2011. ISSN 0036-8075, 1095-9203. doi:10.1126/science.1209524. URL <http://www.sciencemag.org/cgi/doi/10.1126/science.1209524>.
- [217] Akira Oiwa, Takafumi Fujita, Haruki Kiyama, Giles Allison, Arne Ludwig, Andreas D. Wieck, and Seigo Tarucha. Conversion from Single Photon to Single Electron Spin Using Electrically Controllable Quantum Dots. *Journal of the Physical Society of Japan*, 86(1): 011008, January 2017. ISSN 0031-9015, 1347-4073. doi:10.7566/JPSJ.86.011008. URL <http://journals.jps.jp/doi/10.7566/JPSJ.86.011008>.
- [218] K. Ono, D. G. Austing, Y. Tokura, and S. Tarucha. Current Rectification by Pauli Exclusion in a Weakly Coupled Double Quantum Dot System. *Science*, 297(5585):1313–1317, August 2002. ISSN 00368075, 10959203. doi:10.1126/science.1070958. URL <http://www.sciencemag.org/cgi/doi/10.1126/science.1070958>.
- [219] T. OOSTERKAMP, W. VAN DER WIEL, S. DeFRANCESCHI, CJPM Harmans, and L. KOUWENHOVEN. Photon Assisted Tunneling in Quantum Dots. *arXiv: cond-mat*, 9904359, 1999. URL <https://doi.org/10.48550/arXiv.cond-mat/9904359>.
- [220] Lucas A. Orona, John M. Nichol, Shannon P. Harvey, Charlotte G. L. Böttcher, Saeed Fallahi, Geoffrey C. Gardner, Michael J. Manfra, and Amir Yacoby. Readout of singlet-triplet qubits at large magnetic field gradients. *Physical Review B*, 98(12):125404, September 2018. ISSN 2469-9950, 2469-9969. doi:10.1103/PhysRevB.98.125404. URL <https://link.aps.org/doi/10.1103/PhysRevB.98.125404>.
- [221] Tomohiro Otsuka, Takashi Nakajima, Matthieu R. Delbecq, Shinichi Amaha, Jun Yoneda, Kenta Takeda, Giles Allison, Takumi Ito, Retsu Sugawara, Akito Noiri, Arne Ludwig, Andreas D. Wieck, and Seigo Tarucha. Single-electron Spin Resonance in a Quadruple Quantum Dot. *Scientific Reports*, 6(1):31820, August 2016. ISSN 2045-2322. doi:10.1038/srep31820. URL <http://www.nature.com/articles/srep31820>.
- [222] P. Pakkiam, A. V. Timofeev, M. G. House, M. R. Hogg, T. Kobayashi, M. Koch, S. Rogge, and M. Y. Simmons. Single-Shot Single-Gate rf Spin Readout in Silicon. *Physical Review X*, 8(4):041032, November 2018. ISSN 2160-3308. doi:10.1103/PhysRevX.8.041032. URL <https://link.aps.org/doi/10.1103/PhysRevX.8.041032>.
- [223] Z. V. Penfold-Fitch, F. Sfigakis, and M. R. Buitelaar. Microwave Spectroscopy of a Carbon Nanotube Charge Qubit. *Physical Review Applied*, 7(5):054017, May 2017. ISSN 2331-7019. doi:10.1103/PhysRevApplied.7.054017. URL <http://link.aps.org/doi/10.1103/PhysRevApplied.7.054017>.
- [224] Nicholas E. Penthorn, Joshua S. Schoenfield, John D. Rooney, Lisa F. Edge, and HongWen Jiang. Two-axis quantum control of a fast valley qubit in silicon. *npj Quantum Information*, 5(1):94, November 2019. ISSN 2056-6387. doi:10.1038/s41534-019-0212-5. URL <http://www.nature.com/articles/s41534-019-0212-5>.
- [225] K. D. Petersson, J. R. Petta, H. Lu, and A. C. Gossard. Quantum Coherence in a One-Electron Semiconductor Charge Qubit. *Physical Review Letters*, 105(24):246804, December 2010. ISSN 0031-9007, 1079-7114. doi:10.1103/PhysRevLett.105.246804. URL <https://link.aps.org/doi/10.1103/PhysRevLett.105.246804>.
- [226] K. D. Petersson, C. G. Smith, D. Anderson, P. Atkinson, G. A. C. Jones, and D. A. Ritchie. Charge and Spin State Readout of a Double Quantum Dot Coupled to a Resonator. *Nano Letters*, 10(8):2789–2793, July 2010. ISSN 1530-6984, 1530-6992. doi:10.1021/nl100663w. URL <http://pubs.acs.org/doi/abs/10.1021/nl100663w>.
- [227] K. D. Petersson, L. W. McFaul, M. D. Schroer, M. Jung, J. M. Taylor, A. A. Houck, and J. R. Petta. Circuit quantum electrodynamics with a spin qubit. *Nature*, 490(7420):380–383, October 2012. ISSN 0028-0836, 1476-4687. doi:10.1038/nature11559. URL <http://www.nature.com/doifinder/10.1038/nature11559>.
- [228] L. Petit, J. M. Boter, H. G. J. Eeenink, G. Droulers, M. L. V. Tagliaferri, R. Li, D. P. Franke, K. J. Singh, J. S. Clarke, R. N. Schouten, V. V. Dobrovitski, L. M. K. Vandersypen, and M. Veldhorst. Spin Lifetime and Charge Noise in Hot Silicon Quantum Dot Qubits. *Physical Review Letters*, 121(7):076801, August 2018. ISSN 0031-9007, 1079-7114. doi:10.1103/PhysRevLett.121.076801. URL <https://link.aps.org/doi/10.1103/PhysRevLett.121.076801>.

- [229] L. Petit, H. G. J. Eenink, M. Russ, W. I. L. Lawrie, N. W. Hendrickx, S. G. J. Philips, J. S. Clarke, L. M. K. Vandersypen, and M. Veldhorst. Universal quantum logic in hot silicon qubits. *Nature*, 580(7803):355–359, April 2020. ISSN 0028-0836, 1476-4687. doi: 10.1038/s41586-020-2170-7. URL <http://www.nature.com/articles/s41586-020-2170-7>.
- [230] J. R. Petta, A. C. Johnson, C. M. Marcus, M. P. Hanson, and A. C. Gossard. Manipulation of a Single Charge in a Double Quantum Dot. *Physical Review Letters*, 93(18):186802, October 2004. ISSN 0031-9007, 1079-7114. doi:10.1103/PhysRevLett.93.186802. URL <http://link.aps.org/doi/10.1103/PhysRevLett.93.186802>.
- [231] Jason R. Petta, Alexander Comstock Johnson, Jacob M. Taylor, Edward A. Laird, Amir Yacoby, Mikhail D. Lukin, Charles M. Marcus, Micah P. Hanson, and Arthur C. Gossard. Coherent manipulation of coupled electron spins in semiconductor quantum dots. *Science*, 309(5744):2180–2184, September 2005. doi:10.1126/science.1116955. URL <http://science.sciencemag.org/content/309/5744/2180.short>.
- [232] Jarryd J. Pla, Kuan Y. Tan, Juan P. Dehollain, Wee H. Lim, John J. L. Morton, David N. Jamieson, Andrew S. Dzurak, and Andrea Morello. A single-atom electron spin qubit in silicon. *Nature*, 489(7417):541–545, September 2012. ISSN 0028-0836, 1476-4687. doi:10.1038/nature11449. URL <http://www.nature.com/doifinder/10.1038/nature11449>.
- [233] J. R. Prance, Zhan Shi, C. B. Simmons, D. E. Savage, M. G. Lagally, L. R. Schreiber, L. M. K. Vandersypen, Mark Friesen, Robert Joynt, S. N. Coppersmith, and M. A. Eriksson. Single-Shot Measurement of Triplet-Singlet Relaxation in a Si / SiGe Double Quantum Dot. *Physical Review Letters*, 108(4):046808, January 2012. ISSN 0031-9007, 1079-7114. doi:10.1103/PhysRevLett.108.046808. URL <https://link.aps.org/doi/10.1103/PhysRevLett.108.046808>.
- [234] Haifeng Qiao, Yadav P. Kandel, Kuangyin Deng, Saeed Fallahi, Geoffrey C. Gardner, Michael J. Manfra, Edwin Barnes, and John M. Nichol. Coherent Multispin Exchange Coupling in a Quantum-Dot Spin Chain. *Physical Review X*, 10(3):031006, July 2020. ISSN 2160-3308. doi:10.1103/PhysRevX.10.031006. URL <https://link.aps.org/doi/10.1103/PhysRevX.10.031006>.
- [235] Haifeng Qiao, Yadav P. Kandel, Sreenath K. Manikandan, Andrew N. Jordan, Saeed Fallahi, Geoffrey C. Gardner, Michael J. Manfra, and John M. Nichol. Conditional teleportation of quantum-dot spin states. *Nature Communications*, 11(1):3022, June 2020. ISSN 2041-1723. doi:10.1038/s41467-020-16745-0. URL <http://www.nature.com/articles/s41467-020-16745-0>.
- [236] Haifeng Qiao, Yadav P. Kandel, Saeed Fallahi, Geoffrey C. Gardner, Michael J. Manfra, Xuedong Hu, and John M. Nichol. Long-Distance Superexchange between Semiconductor Quantum-Dot Electron Spins. *Physical Review Letters*, 126(1):017701, January 2021. ISSN 0031-9007, 1079-7114. doi:10.1103/PhysRevLett.126.017701. URL <https://link.aps.org/doi/10.1103/PhysRevLett.126.017701>.
- [237] V. Ranjan, G. Puebla-Hellmann, M. Jung, T. Hasler, A. Nunnenkamp, M. Muoth, C. Hierold, A. Wallraff, and C. Schönenberger. Clean carbon nanotubes coupled to superconducting impedance-matching circuits. *Nature Communications*, 6(1):7165, May 2015. ISSN 2041-1723. doi:10.1038/ncomms8165. URL <http://www.nature.com/articles/ncomms8165>.
- [238] Alfred G. Redfield. Nuclear Magnetic Resonance Saturation and Rotary Saturation in Solids. *Physical Review*, 98(6):1787–1809, June 1955. ISSN 0031-899X. doi:10.1103/PhysRev.98.1787. URL <https://link.aps.org/doi/10.1103/PhysRev.98.1787>.
- [239] M. D. Reed, B. M. Maune, R. W. Andrews, M. G. Borselli, K. Eng, M. P. Jura, A. A. Kiselev, T. D. Ladd, S. T. Merkel, I. Milosavljevic, E. J. Pritchett, M. T. Rakher, R. S. Ross, A. E. Schmitz, A. Smith, J. A. Wright, M. F. Gyure, and A. T. Hunter. Reduced Sensitivity to Charge Noise in Semiconductor Spin Qubits via Symmetric Operation. *Physical Review Letters*, 116(11):110402, March 2016. ISSN 0031-9007, 1079-7114. doi:10.1103/PhysRevLett.116.110402. URL <https://link.aps.org/doi/10.1103/PhysRevLett.116.110402>.
- [240] D. J. Reilly, C. M. Marcus, M. P. Hanson, and A. C. Gossard. Fast single-charge sensing with a rf quantum point contact. *Applied Physics Letters*, 91(16):162101, October 2007. ISSN 0003-6951, 1077-3118. doi:10.1063/1.2794995. URL <http://aip.scitation.org/doi/10.1063/1.2794995>.
- [241] D. J. Reilly, J. M. Taylor, E. A. Laird, J. R. Petta, C. M. Marcus, M. P. Hanson, and A. C. Gossard. Measurement of Temporal Correlations of the Overhauser Field in a Double Quantum Dot. *Physical Review Letters*, 101(23):236803, December 2008. ISSN 0031-9007, 1079-7114. doi:10.1103/PhysRevLett.101.236803. URL <https://link.aps.org/doi/10.1103/PhysRevLett.101.236803>.
- [242] D. J. Reilly, J. M. Taylor, J. R. Petta, C. M. Marcus, M. P. Hanson, and A. C. Gossard. Exchange Control of Nuclear Spin Diffusion in a Double Quantum Dot. *Physical Review Letters*, 104(23):236802, June 2010. ISSN 0031-9007, 1079-7114. doi:10.1103/PhysRevLett.104.236802. URL <https://link.aps.org/doi/10.1103/PhysRevLett.104.236802>.
- [243] Andrea Ruffino, Tsung-Yeh Yang, John Michniewicz, Yatao Peng, Edoardo Charbon, and Miguel Fernando Gonzalez-Zalba. Integrated multiplexed microwave readout of silicon quantum dots in a cryogenic CMOS chip. *arXiv:2101.08295 [cond-mat, physics:physics, physics:quant-ph]*, January 2021. URL <http://arxiv.org/abs/2101.08295>. arXiv: 2101.08295.
- [244] N. Samkharadze, G. Zheng, N. Kalhor, D. Brousse, A. Sammak, U. C. Mendes, A. Blais, G. Scappucci, and L. M. K. Vandersypen. Strong spin-photon coupling in silicon. *Science*, 359(6380):1123–1127, January 2018. ISSN 0036-8075, 1095-9203. doi:10.1126/science.aar4054. URL <http://www.sciencemag.org/lookup/doi/10.1126/science.aar4054>.
- [245] Yuval R Sanders, Joel J Wallman, and Barry C Sanders. Bounding quantum gate error rate based on reported average fidelity. *New Journal of Physics*, 18(1):012002, December 2015. ISSN 1367-2630. doi:10.1088/1367-2630/18/1/012002. URL <https://iopscience.iop.org/article/10.1088/1367-2630/18/1/012002>.
- [246] Giordano Scappucci, Christoph Kloeffel, Floris A. Zwanenburg, Daniel Loss, Maksym Myronov, Jian-Jun Zhang, Silvano De Franceschi, Georgios Katsaros, and Menno Veldhorst. The germanium quantum information route. *Nature Reviews Materials*, 6(10):926–943, October 2021. ISSN 2058-8437. doi:10.1038/s41578-020-00262-z. URL <https://www.nature.com/articles/s41578-020-00262-z>.
- [247] P. Scarlino, E. Kawakami, P. Stano, M. Shafiei, C. Reichl, W. Wegscheider, and L. M. K. Vandersypen. Spin-Relaxation Anisotropy in a GaAs Quantum Dot. *Physical Review Letters*, 113(25):256802, December 2014. ISSN 0031-9007, 1079-7114. doi:10.1103/PhysRevLett.113.256802. URL <https://link.aps.org/doi/10.1103/PhysRevLett.113.256802>.
- [248] P. Scarlino, E. Kawakami, T. Jullien, D. R. Ward, D. E. Savage, M. G. Lagally, Mark Friesen, S. N. Coppersmith, M. A. Eriksson, and L. M. K. Vandersypen. Dressed photon-orbital states in a quantum dot: Intervallevalley spin resonance. *Physical Review B*, 95(16):165429, April 2017. ISSN 2469-9950, 2469-9969. doi:10.1103/PhysRevB.95.165429. URL <http://link.aps.org/doi/10.1103/PhysRevB.95.165429>.

- PhysRevB.95.165429.
- [249] P. Scarlino, D. J. van Woerkom, U. C. Mendes, J. V. Koski, A. J. Landig, C. K. Andersen, S. Gasparinetti, C. Reichl, W. Wegscheider, K. Ensslin, T. Ihn, A. Blais, and A. Wallraff. Coherent microwave-photon-mediated coupling between a semiconductor and a superconducting qubit. *Nature Communications*, 10(1):3011, July 2019. ISSN 2041-1723. doi:10.1038/s41467-019-10798-6. URL <http://www.nature.com/articles/s41467-019-10798-6>.
- [250] P. Scarlino, D. J. van Woerkom, A. Stockklauser, J. V. Koski, M. C. Collodo, S. Gasparinetti, C. Reichl, W. Wegscheider, T. Ihn, K. Ensslin, and A. Wallraff. All-Microwave Control and Dispersive Readout of Gate-Defined Quantum Dot Qubits in Circuit Quantum Electrodynamics. *Physical Review Letters*, 122(20):206802, May 2019. ISSN 0031-9007, 1079-7114. doi:10.1103/PhysRevLett.122.206802. URL <https://link.aps.org/doi/10.1103/PhysRevLett.122.206802>.
- [251] S. Schaal, I. Ahmed, J. A. Haigh, L. Hutin, B. Bertrand, S. Barraud, M. Vinet, C.-M. Lee, N. Stelmashenko, J. W. A. Robinson, J. Y. Qiu, S. Hacohen-Gourgy, I. Siddiqi, M. F. Gonzalez-Zalba, and J. J. L. Morton. Fast Gate-Based Readout of Silicon Quantum Dots Using Josephson Parametric Amplification. *Physical Review Letters*, 124(6):067701, February 2020. ISSN 0031-9007, 1079-7114. doi:10.1103/PhysRevLett.124.067701. URL <https://link.aps.org/doi/10.1103/PhysRevLett.124.067701>.
- [252] John Schliemann, Alexander Khaetskii, and Daniel Loss. Electron spin dynamics in quantum dots and related nanostructures due to hyperfine interaction with nuclei. *Journal of Physics: Condensed Matter*, 15(50):R1809–R1833, December 2003. ISSN 0953-8984, 1361-648X. doi:10.1088/0953-8984/15/50/R01. URL <https://doi.org/10.1088/0953-8984/15/50/R01>.
- [253] Lars R. Schreiber and Hendrik Bluhm. Quantum computation: Silicon comes back. *Nature nanotechnology*, 9(12):966, 2014. URL <https://doi.org/10.1038/nnano.2014.249>.
- [254] F. J. Schupp, F. Vigneau, Y. Wen, A. Mavalankar, J. Griffiths, G. A. C. Jones, I. Farrer, D. A. Ritchie, C. G. Smith, L. C. Camenzind, L. Yu, D. M. Zumbühl, G. A. D. Briggs, N. Ares, and E. A. Laird. Sensitive radiofrequency readout of quantum dots using an ultra-low-noise SQUID amplifier. *Journal of Applied Physics*, 127(24):244503, June 2020. ISSN 0021-8979, 1089-7550. doi:10.1063/5.0005886. URL <http://aip.scitation.org/doi/10.1063/5.0005886>.
- [255] Amanda E. Seedhouse, Tuomo Tanttu, Ross C.C. Leon, Ruichen Zhao, Kuan Yen Tan, Bas Hensen, Fay E. Hudson, Kohei M. Itoh, Jun Yoneda, Chih Hwan Yang, Andrea Morello, Arne Laucht, Susan N. Coppersmith, Andre Saraiva, and Andrew S. Dzurak. Pauli Blockade in Silicon Quantum Dots with Spin-Orbit Control. *PRX Quantum*, 2(1):010303, January 2021. ISSN 2691-3399. doi:10.1103/PRXQuantum.2.010303. URL <https://link.aps.org/doi/10.1103/PRXQuantum.2.010303>.
- [256] M. Shafiei, K. C. Nowack, C. Reichl, W. Wegscheider, and L. M. K. Vandersypen. Resolving Spin-Orbit- and Hyperfine-Mediated Electric Dipole Spin Resonance in a Quantum Dot. *Physical Review Letters*, 110(10):107601, March 2013. ISSN 0031-9007, 1079-7114. doi:10.1103/PhysRevLett.110.107601. URL <https://link.aps.org/doi/10.1103/PhysRevLett.110.107601>.
- [257] Zhan Shi, C. B. Simmons, J. R. Prance, John King Gamble, Teck Seng Koh, Yun-Pil Shim, Xuedong Hu, D. E. Savage, M. G. Lagally, M. A. Eriksson, Mark Friesen, and S. N. Coppersmith. Fast Hybrid Silicon Double-Quantum-Dot Qubit. *Physical Review Letters*, 108(14):140503, April 2012. ISSN 0031-9007, 1079-7114. doi:10.1103/PhysRevLett.108.140503. URL <https://link.aps.org/doi/10.1103/PhysRevLett.108.140503>.
- [258] Zhan Shi, C. B. Simmons, Daniel R. Ward, J. R. Prance, R. T. Mohr, Teck Seng Koh, John King Gamble, Xian Wu, D. E. Savage, M. G. Lagally, Mark Friesen, S. N. Coppersmith, and M. A. Eriksson. Coherent quantum oscillations and echo measurements of a Si charge qubit. *Physical Review B*, 88(7):075416, August 2013. ISSN 1098-0121, 1550-235X. doi:10.1103/PhysRevB.88.075416. URL <https://link.aps.org/doi/10.1103/PhysRevB.88.075416>.
- [259] Zhan Shi, C. B. Simmons, Daniel R. Ward, J. R. Prance, Xian Wu, Teck Seng Koh, John King Gamble, D. E. Savage, M. G. Lagally, Mark Friesen, S. N. Coppersmith, and M. A. Eriksson. Fast coherent manipulation of three-electron states in a double quantum dot. *Nature Communications*, 5:3020, January 2014. ISSN 2041-1723. doi:10.1038/ncomms4020. URL <http://www.nature.com/doifinder/10.1038/ncomms4020>.
- [260] K. N. Shrivastava. Theory of Spin-Lattice Relaxation. *physica status solidi (b)*, 117(2):437–458, June 1983. ISSN 03701972, 15213951. doi:10.1002/pssb.2221170202. URL <http://doi.wiley.com/10.1002/pssb.2221170202>.
- [261] M. D. Shulman, O. E. Dial, S. P. Harvey, H. Bluhm, V. Umansky, and A. Yacoby. Demonstration of Entanglement of Electrostatically Coupled Singlet-Triplet Qubits. *Science*, 336(6078):202–205, April 2012. ISSN 0036-8075, 1095-9203. doi:10.1126/science.1217692. URL <http://www.sciencemag.org/cgi/doi/10.1126/science.1217692>.
- [262] M. D. Shulman, S. P. Harvey, J. M. Nichol, S. D. Bartlett, A. C. Doherty, V. Umansky, and A. Yacoby. Suppressing qubit dephasing using real-time Hamiltonian estimation. *Nature Communications*, 5:5156, October 2014. ISSN 2041-1723. doi:10.1038/ncomms6156. URL <http://www.nature.com/doifinder/10.1038/ncomms6156>.
- [263] A. J. Sigillito, M. J. Gullans, L. F. Edge, M. Borselli, and J. R. Petta. Coherent transfer of quantum information in a silicon double quantum dot using resonant SWAP gates. *npj Quantum Information*, 5(1):110, November 2019. ISSN 2056-6387. doi:10.1038/s41534-019-0225-0. URL <http://www.nature.com/articles/s41534-019-0225-0>.
- [264] A.J. Sigillito, J.C. Loy, D.M. Zajac, M.J. Gullans, L.F. Edge, and J.R. Petta. Site-Selective Quantum Control in an Isotopically Enriched Si 28 / Si 0.7 Ge 0.3 Quadruple Quantum Dot. *Physical Review Applied*, 11(6):061006, June 2019. ISSN 2331-7019. doi:10.1103/PhysRevApplied.11.061006. URL <https://link.aps.org/doi/10.1103/PhysRevApplied.11.061006>.
- [265] C. B. Simmons, J. R. Prance, B. J. Van Bael, Teck Seng Koh, Zhan Shi, D. E. Savage, M. G. Lagally, R. Joynt, Mark Friesen, S. N. Coppersmith, and M. A. Eriksson. Tunable Spin Loading and T 1 of a Silicon Spin Qubit Measured by Single-Shot Readout. *Physical Review Letters*, 106(15):156804, April 2011. ISSN 0031-9007, 1079-7114. doi:10.1103/PhysRevLett.106.156804. URL <https://link.aps.org/doi/10.1103/PhysRevLett.106.156804>.
- [266] Charles P. Slichter. *Principles of magnetic resonance*. Number 1 in Springer series in solid-state sciences. Springer, Berlin ; New York, 3rd enl. and updated ed edition, 1996. ISBN 978-3-540-50157-2 978-0-387-50157-4.
- [267] Cameron Spence, Bruna Cardoso Paz, Bernhard Klemt, Emmanuel Chanrion, David J. Niegemann, Baptiste Jadot, Vivien Thiney, Benoit Bertrand, Heimanu Niebojewski, Pierre-André Mortemousque, Xavier Jehl, Romain Maurand, Silvano De Franceschi, Maud Vinet, Franck Balestro, Christopher B äuerle, Yann-Michel Niquet, Tristan Meunier, and Matias Urdampilleta. Spin-valley coupling anisotropy

- and noise in CMOS quantum dots. *arXiv:2109.13557 [cond-mat]*, September 2021. URL <http://arxiv.org/abs/2109.13557>. arXiv: 2109.13557.
- [268] J. Stehlik, Y.-Y. Liu, C. M. Quintana, C. Eichler, T. R. Hartke, and J. R. Petta. Fast Charge Sensing of a Cavity-Coupled Double Quantum Dot Using a Josephson Parametric Amplifier. *Physical Review Applied*, 4(1):014018, July 2015. ISSN 2331-7019. doi: 10.1103/PhysRevApplied.4.014018. URL <https://link.aps.org/doi/10.1103/PhysRevApplied.4.014018>.
- [269] A. Stockklauser, V. F. Maisi, J. Bassett, K. Cujia, C. Reichl, W. Wegscheider, T. Ihn, A. Wallraff, and K. Ensslin. Microwave Emission from Hybridized States in a Semiconductor Charge Qubit. *Physical Review Letters*, 115(4):046802, July 2015. ISSN 0031-9007, 1079-7114. doi:10.1103/PhysRevLett.115.046802. URL <https://link.aps.org/doi/10.1103/PhysRevLett.115.046802>.
- [270] A. Stockklauser, P. Scarlino, J. V. Koski, S. Gasparinetti, C. K. Andersen, C. Reichl, W. Wegscheider, T. Ihn, K. Ensslin, and A. Wallraff. Strong Coupling Cavity QED with Gate-Defined Double Quantum Dots Enabled by a High Impedance Resonator. *Physical Review X*, 7(1):011030, March 2017. ISSN 2160-3308. doi:10.1103/PhysRevX.7.011030. URL <https://link.aps.org/doi/10.1103/PhysRevX.7.011030>.
- [271] Tom Struck, Arne Hollmann, Floyd Schauer, Olexiy Fedorets, Andreas Schmidbauer, Kentarou Sawano, Helge Riemann, Nikolay V. Abrosimov, Łukasz Cywiński, Dominique Bougeard, and Lars R. Schreiber. Low-frequency spin qubit energy splitting noise in highly purified 28Si/SiGe. *npj Quantum Information*, 6(1):40, May 2020. ISSN 2056-6387. doi:10.1038/s41534-020-0276-2. URL <http://www.nature.com/articles/s41534-020-0276-2>.
- [272] Charles Tahan. Opinion: Democratizing Spin Qubits. *Quantum*, 5:584, November 2021. ISSN 2521-327X. doi:10.22331/q-2021-11-18-584. URL <https://quantum-journal.org/papers/q-2021-11-18-584/>.
- [273] T. Takakura, A. Noiri, T. Obata, T. Otsuka, J. Yoneda, K. Yoshida, and S. Tarucha. Single to quadruple quantum dots with tunable tunnel couplings. *Applied Physics Letters*, 104(11):113109, March 2014. ISSN 0003-6951, 1077-3118. doi:10.1063/1.4869108. URL <http://aip.scitation.org/doi/10.1063/1.4869108>.
- [274] K. Takeda, J. Kamioka, T. Otsuka, J. Yoneda, T. Nakajima, M. R. Delbecq, S. Amaha, G. Allison, T. Kodera, S. Oda, and S. Tarucha. A fault-tolerant addressable spin qubit in a natural silicon quantum dot. *Science Advances*, 2(8):e1600694–e1600694, August 2016. ISSN 2375-2548. doi:10.1126/sciadv.1600694. URL <http://advances.sciencemag.org/cgi/doi/10.1126/sciadv.1600694>.
- [275] K. Takeda, J. Yoneda, T. Otsuka, T. Nakajima, M. R. Delbecq, G. Allison, Y. Hoshi, N. Usami, K. M. Itoh, S. Oda, T. Kodera, and S. Tarucha. Optimized electrical control of a Si/SiGe spin qubit in the presence of an induced frequency shift. *npj Quantum Information*, 4(1):54, October 2018. ISSN 2056-6387. doi:10.1038/s41534-018-0105-z. URL <http://www.nature.com/articles/s41534-018-0105-z>.
- [276] K. Takeda, A. Noiri, J. Yoneda, T. Nakajima, and S. Tarucha. Resonantly Driven Singlet-Triplet Spin Qubit in Silicon. *Physical Review Letters*, 124(11):117701, March 2020. ISSN 0031-9007, 1079-7114. doi:10.1103/PhysRevLett.124.117701. URL <https://link.aps.org/doi/10.1103/PhysRevLett.124.117701>.
- [277] Kenta Takeda, Akito Noiri, Takashi Nakajima, Jun Yoneda, Takashi Kobayashi, and Seigo Tarucha. Quantum tomography of an entangled three-qubit state in silicon. *Nature Nanotechnology*, 16:965–969, June 2021. ISSN 1748-3387, 1748-3395. doi:10.1038/s41565-021-00925-0. URL <http://www.nature.com/articles/s41565-021-00925-0>.
- [278] Kenta Takeda, Akito Noiri, Takashi Nakajima, Takashi Kobayashi, and Seigo Tarucha. Quantum error correction with silicon spin qubits. *arXiv:2201.08581 [cond-mat, physics:quant-ph]*, January 2022. URL <http://arxiv.org/abs/2201.08581>. arXiv: 2201.08581.
- [279] Tuomo Tanttu, Bas Hensen, Kok Wai Chan, Chih Hwan Yang, Wister Wei Huang, Michael Fogarty, Fay Hudson, Kohei Itoh, Dimitrie Culcer, Arne Laucht, Andrea Morello, and Andrew Dzurak. Controlling Spin-Orbit Interactions in Silicon Quantum Dots Using Magnetic Field Direction. *Physical Review X*, 9(2):021028, May 2019. ISSN 2160-3308. doi:10.1103/PhysRevX.9.021028. URL <https://link.aps.org/doi/10.1103/PhysRevX.9.021028>.
- [280] Stefanie B. Tenberg, Serwan Asaad, Mateusz T. Małzik, Mark A. I. Johnson, Benjamin Joecker, Arne Laucht, Fay E. Hudson, Kohei M. Itoh, A. Malwin Jakob, Brett C. Johnson, David N. Jamieson, Jeffrey C. McCallum, Andrew S. Dzurak, Robert Joyst, and Andrea Morello. Electron spin relaxation of single phosphorus donors in metal-oxide-semiconductor nanoscale devices. *Physical Review B*, 99(20):205306, May 2019. ISSN 2469-9950, 2469-9969. doi:10.1103/PhysRevB.99.205306. URL <https://link.aps.org/doi/10.1103/PhysRevB.99.205306>.
- [281] Romain Thalineau, Sylvain Hermelin, Andreas D. Wieck, Christopher Bäuerle, Laurent Saminadayar, and Tristan Meunier. A few-electron quadruple quantum dot in a closed loop. *Applied Physics Letters*, 101(10):103102, September 2012. ISSN 0003-6951, 1077-3118. doi:10.1063/1.4749811. URL <http://aip.scitation.org/doi/10.1063/1.4749811>.
- [282] Brandur Thorgrimsson, Dohun Kim, Yuan-Chi Yang, L. W. Smith, C. B. Simmons, Daniel R. Ward, Ryan H. Foote, J. Corrigan, D. E. Savage, M. G. Lagally, Mark Friesen, S. N. Coppersmith, and M. A. Eriksson. Extending the coherence of a quantum dot hybrid qubit. *npj Quantum Information*, 3(1):32, August 2017. ISSN 2056-6387. doi:10.1038/s41534-017-0034-2. URL <http://www.nature.com/articles/s41534-017-0034-2>.
- [283] L. A. Tracy, D. R. Luhman, S. M. Carr, N. C. Bishop, G. A. Ten Eyck, T. Pluym, J. R. Wendt, M. P. Lilly, and M. S. Carroll. Single shot spin readout using a cryogenic high-electron-mobility transistor amplifier at sub-Kelvin temperatures. *Applied Physics Letters*, 108(6):063101, February 2016. ISSN 0003-6951, 1077-3118. doi:10.1063/1.4941421. URL <http://aip.scitation.org/doi/10.1063/1.4941421>.
- [284] Matias Urdampilleta, David J. Niegemann, Emmanuel Chanrion, Baptiste Jadot, Cameron Spence, Pierre-André Mortemousque, Christopher Bäuerle, Louis Hutin, Benoit Bertrand, Sylvain Barraud, Romain Maurand, Marc Sanquer, Xavier Jehl, Silvano De Franceschi, Maud Vinet, and Tristan Meunier. Gate-based high fidelity spin readout in a CMOS device. *Nature Nanotechnology*, 14(8):737–741, May 2019. ISSN 1748-3387, 1748-3395. doi:10.1038/s41565-019-0443-9. URL <http://www.nature.com/articles/s41565-019-0443-9>.
- [285] J. W. G. van den Berg, S. Nadj-Perge, V. S. Pribiag, S. R. Plissard, E. P. A. M. Bakkers, S. M. Frolov, and L. P. Kouwenhoven. Fast Spin-Orbit Qubit in an Indium Antimonide Nanowire. *Physical Review Letters*, 110(6):066806, February 2013. ISSN 0031-9007, 1079-7114. doi:10.1103/PhysRevLett.110.066806. URL <https://link.aps.org/doi/10.1103/PhysRevLett.110.066806>.
- [286] Wilfred G. Van der Wiel, Silvano De Franceschi, Jeroen M. Elzerman, Toshimasa Fujisawa, Seigo Tarucha, and Leo P. Kouwenhoven.

- Electron transport through double quantum dots. *Reviews of Modern Physics*, 75(1):1, 2002. URL <https://journals.aps.org/rmp/abstract/10.1103/RevModPhys.75.1>.
- [287] C. J. van Diepen, T.-K. Hsiao, U. Mukhopadhyay, C. Reichl, W. Wegscheider, and L. M. K. Vandersypen. Quantum Simulation of Antiferromagnetic Heisenberg Chain with Gate-Defined Quantum Dots. *Physical Review X*, 11(4):041025, November 2021. ISSN 2160-3308. doi:10.1103/PhysRevX.11.041025. URL <https://link.aps.org/doi/10.1103/PhysRevX.11.041025>.
- [288] Cornelis J. van Diepen, Tzu-Kan Hsiao, Uditendu Mukhopadhyay, Christian Reichl, Werner Wegscheider, and Lieven M. K. Vandersypen. Electron cascade for distant spin readout. *Nature Communications*, 12(1):77, January 2021. ISSN 2041-1723. doi:10.1038/s41467-020-20388-6. URL <http://www.nature.com/articles/s41467-020-20388-6>.
- [289] F. van Riggelen, N. W. Hendrickx, W. I. L. Lawrie, M. Russ, A. Sammak, G. Scappucci, and M. Veldhorst. A two-dimensional array of single-hole quantum dots. *Applied Physics Letters*, 118(4):044002, January 2021. ISSN 0003-6951, 1077-3118. doi:10.1063/5.0037330. URL <http://aip.scitation.org/doi/10.1063/5.0037330>.
- [290] I. van Weperen, B. D. Armstrong, E. A. Laird, J. Medford, C. M. Marcus, M. P. Hanson, and A. C. Gossard. Charge-State Conditional Operation of a Spin Qubit. *Physical Review Letters*, 107(3):030506, July 2011. ISSN 0031-9007, 1079-7114. doi:10.1103/PhysRevLett.107.030506. URL <https://link.aps.org/doi/10.1103/PhysRevLett.107.030506>.
- [291] D. J. van Woerkom, P. Scarlino, J. H. Ungerer, C. Müller, J. V. Koski, A. J. Landig, C. Reichl, W. Wegscheider, T. Ihn, K. Ensslin, and A. Wallraff. Microwave Photon-Mediated Interactions between Semiconductor Qubits. *Physical Review X*, 8(4):041018, October 2018. ISSN 2160-3308. doi:10.1103/PhysRevX.8.041018. URL <https://link.aps.org/doi/10.1103/PhysRevX.8.041018>.
- [292] Lieven M. K. Vandersypen and Mark A. Eriksson. Quantum computing with semiconductor spins. *Physics Today*, 72(8):38–45, August 2019. ISSN 0031-9228, 1945-0699. doi:10.1063/PT.3.4270. URL <http://physicstoday.scitation.org/doi/10.1063/PT.3.4270>.
- [293] M. Veldhorst, J. C. C. Hwang, C. H. Yang, A. W. Leenstra, B. de Ronde, J. P. Dehollain, J. T. Muñonen, F. E. Hudson, K. M. Itoh, A. Morello, and A. S. Dzurak. An addressable quantum dot qubit with fault-tolerant control-fidelity. *Nature Nanotechnology*, 9(12):981–985, October 2014. ISSN 1748-3387, 1748-3395. doi:10.1038/nnano.2014.216. URL <http://www.nature.com/doifinder/10.1038/nnano.2014.216>.
- [294] M. Veldhorst, R. Ruskov, C. H. Yang, J. C. C. Hwang, F. E. Hudson, M. E. Flatté, C. Tahan, K. M. Itoh, A. Morello, and A. S. Dzurak. Spin-orbit coupling and operation of multivalley spin qubits. *Physical Review B*, 92(20):201401, November 2015. ISSN 1098-0121, 1550-235X. doi:10.1103/PhysRevB.92.201401. URL <https://link.aps.org/doi/10.1103/PhysRevB.92.201401>.
- [295] M. Veldhorst, C. H. Yang, J. C. C. Hwang, W. Huang, J. P. Dehollain, J. T. Muñonen, S. Simmons, A. Laucht, F. E. Hudson, K. M. Itoh, A. Morello, and A. S. Dzurak. A two-qubit logic gate in silicon. *Nature*, 526(7573):410–414, October 2015. ISSN 0028-0836, 1476-4687. doi:10.1038/nature15263. URL <http://www.nature.com/doifinder/10.1038/nature15263>.
- [296] J. J. Viennot, M. R. Delbecq, M. C. Dartailh, A. Cottet, and T. Kontos. Out-of-equilibrium charge dynamics in a hybrid circuit quantum electrodynamics architecture. *Physical Review B*, 89(16):165404, April 2014. ISSN 1098-0121, 1550-235X. doi:10.1103/PhysRevB.89.165404. URL <https://link.aps.org/doi/10.1103/PhysRevB.89.165404>.
- [297] J. J. Viennot, M. C. Dartailh, A. Cottet, and T. Kontos. Coherent coupling of a single spin to microwave cavity photons. *Science*, 349(6246):408–411, July 2015. ISSN 0036-8075, 1095-9203. doi:10.1126/science.aaa3786. URL <http://www.sciencemag.org/cgi/doi/10.1126/science.aaa3786>.
- [298] B. Voisin, R. Maurand, S. Barraud, M. Vinet, X. Jehl, M. Sanquer, J. Renard, and S. De Franceschi. Electrical Control of g -Factor in a Few-Hole Silicon Nanowire MOSFET. *Nano Letters*, 16(1):88–92, January 2016. ISSN 1530-6984, 1530-6992. doi:10.1021/acs.nanolett.5b02920. URL <http://pubs.acs.org/doi/10.1021/acs.nanolett.5b02920>.
- [299] C. Volk, A. M. J. Zwerver, U. Mukhopadhyay, P. T. Eendebak, C. J. van Diepen, J. P. Dehollain, T. Hensgens, T. Fujita, C. Reichl, W. Wegscheider, and L. M. K. Vandersypen. Loading a quantum-dot based “Qubyte” register. *npj Quantum Information*, 5(1):29, April 2019. ISSN 2056-6387. doi:10.1038/s41534-019-0146-y. URL <http://www.nature.com/articles/s41534-019-0146-y>.
- [300] Christian Volk, Christoph Neumann, Sebastian Kazarski, Stefan Fringes, Stephan Engels, Federica Haupt, André Müller, and Christoph Stampfer. Probing relaxation times in graphene quantum dots. *Nature Communications*, 4(1):1753, April 2013. ISSN 2041-1723. doi:10.1038/ncomms2738. URL <http://www.nature.com/articles/ncomms2738>.
- [301] Christian Volk, Anasua Chatterjee, Fabio Ansaloni, Charles M. Marcus, and Ferdinand Kuemmeth. Fast Charge Sensing of Si/SiGe Quantum Dots via a High-Frequency Accumulation Gate. *Nano Letters*, 19(8):5628–5633, August 2019. ISSN 1530-6984, 1530-6992. doi:10.1021/acs.nanolett.9b02149. URL <https://pubs.acs.org/doi/10.1021/acs.nanolett.9b02149>.
- [302] Lada Vukušić, Josip Kukucka, Hannes Watzinger, Joshua Michael Milem, Friedrich Schäffler, and Georgios Katsaros. Single-Shot Readout of Hole Spins in Ge. *Nano Letters*, 18(11):7141–7145, October 2018. ISSN 1530-6984, 1530-6992. doi:10.1021/acs.nanolett.8b03217. URL <http://pubs.acs.org/doi/10.1021/acs.nanolett.8b03217>.
- [303] Baochuan Wang, Ting Lin, Haiou Li, Sisi Gu, Mingbo Chen, Guangcan Guo, Hongwen Jiang, Xuedong Hu, Gang Cao, and Guoping Guo. Correlated spectrum of distant semiconductor qubits coupled by microwave photons. *Science Bulletin*, 66(4):332–338, February 2021. ISSN 20959273. doi:10.1016/j.scib.2020.10.005. URL <https://linkinghub.elsevier.com/retrieve/pii/S2095927320306587>.
- [304] Daisy Q. Wang, Oleh Klochan, Jo-Tzu Hung, Dimitrie Culcer, Ian Farrer, David A. Ritchie, and Alex R. Hamilton. Anisotropic Pauli Spin Blockade of Holes in a GaAs Double Quantum Dot. *Nano Letters*, 16(12):7685–7689, November 2016. ISSN 1530-6984, 1530-6992. doi:10.1021/acs.nanolett.6b03752. URL <http://pubs.acs.org/doi/abs/10.1021/acs.nanolett.6b03752>.
- [305] K. Wang, C. Payette, Y. Dovzhenko, P. W. Deelman, and J. R. Petta. Charge Relaxation in a Single-Electron Si/SiGe Double Quantum Dot. *Physical Review Letters*, 111(4):046801, July 2013. ISSN 0031-9007, 1079-7114. doi:10.1103/PhysRevLett.111.046801. URL <http://link.aps.org/doi/10.1103/PhysRevLett.111.046801>.
- [306] Ke Wang, Gang Xu, Fei Gao, He Liu, Rong-Long Ma, Xin Zhang, Zhanning Wang, Gang Cao, Ting Wang, Jian-Jun Zhang, Dimitrie Culcer, Xuedong Hu, Hong-Wen Jiang, Hai-Ou Li, Guang-Can Guo, and Guo-Ping Guo. Ultrafast coherent control of a hole spin qubit in a germanium quantum dot. *Nature Communications*, 13(1):206, January 2022. ISSN 2041-1723. doi:10.1038/s41467-021-27880-7.

- URL <https://www.nature.com/articles/s41467-021-27880-7>.
- [307] Lin-Jun Wang, Gang Cao, Tao Tu, Hai-Ou Li, Cheng Zhou, Xiao-Jie Hao, Zhan Su, Guang-Can Guo, Hong-Wen Jiang, and Guo-Ping Guo. A graphene quantum dot with a single electron transistor as an integrated charge sensor. *Applied Physics Letters*, 97(26): 262113, December 2010. ISSN 0003-6951, 1077-3118. doi:10.1063/1.3533021. URL <http://aip.scitation.org/doi/10.1063/1.3533021>.
- [308] R. Wang, R. S. Deacon, D. Car, E. P. A. M. Bakkers, and K. Ishibashi. InSb nanowire double quantum dots coupled to a superconducting microwave cavity. *Applied Physics Letters*, 108(20):203502, May 2016. ISSN 0003-6951, 1077-3118. doi:10.1063/1.4950764. URL <http://aip.scitation.org/doi/10.1063/1.4950764>.
- [309] T. F. Watson, B. Weber, M. G. House, H. Büch, and M. Y. Simmons. High-Fidelity Rapid Initialization and Read-Out of an Electron Spin via the Single Donor D - Charge State. *Physical Review Letters*, 115(16):166806, October 2015. ISSN 0031-9007, 1079-7114. doi:10.1103/PhysRevLett.115.166806. URL <https://link.aps.org/doi/10.1103/PhysRevLett.115.166806>.
- [310] T. F. Watson, S. G. J. Philips, E. Kawakami, D. R. Ward, P. Scarlino, M. Veldhorst, D. E. Savage, M. G. Lagally, Mark Friesen, S. N. Coppersmith, M. A. Eriksson, and L. M. K. Vandersypen. A programmable two-qubit quantum processor in silicon. *Nature*, 555(7698): 633–637, February 2018. ISSN 0028-0836, 1476-4687. doi:10.1038/nature25766. URL <http://www.nature.com/doifinder/10.1038/nature25766>.
- [311] Thomas F. Watson, Bent Weber, Yu-Ling Hsueh, Lloyd C. L. Hollenberg, Rajib Rahman, and Michelle Y. Simmons. Atomically engineered electron spin lifetimes of 30 s in silicon. *Science Advances*, 3(3):e1602811, March 2017. ISSN 2375-2548. doi:10.1126/sciadv.1602811. URL <http://advances.sciencemag.org/lookup/doi/10.1126/sciadv.1602811>.
- [312] Hannes Watzinger, Christoph Kloeffel, Lada Vukušić, Marta D. Rossell, Violetta Sessi, Josip Kukucka, Raimund Kirchschlager, Elisabeth Lausecker, Alisha Truhlar, Martin Glaser, Armando Rastelli, Andreas Fuhrer, Daniel Loss, and Georgios Katsaros. Heavy-Hole States in Germanium Hut Wires. *Nano Letters*, 16(11):6879–6885, November 2016. ISSN 1530-6984, 1530-6992. doi:10.1021/acs.nanolett.6b02715. URL <https://pubs.acs.org/doi/10.1021/acs.nanolett.6b02715>.
- [313] Hannes Watzinger, Josip Kukucka, Lada Vukušić, Fei Gao, Ting Wang, Friedrich Schäffler, Jian-Jun Zhang, and Georgios Katsaros. A germanium hole spin qubit. *Nature Communications*, 9(1):3902, September 2018. ISSN 2041-1723. doi:10.1038/s41467-018-06418-4. URL <http://www.nature.com/articles/s41467-018-06418-4>.
- [314] Bent Weber, Yu-Ling Hsueh, Thomas F. Watson, Ruoyu Li, Alexander R. Hamilton, Lloyd C. L. Hollenberg, Rajib Rahman, and Michelle Y. Simmons. Spin-orbit coupling in silicon for electrons bound to donors. *npj Quantum Information*, 4(1):61, November 2018. ISSN 2056-6387. doi:10.1038/s41534-018-0111-1. URL <http://www.nature.com/articles/s41534-018-0111-1>.
- [315] Anderson West, Bas Hensen, Alexis Jouan, Tuomo Tanttu, Chih-Hwan Yang, Alessandro Rossi, M. Fernando Gonzalez-Zalba, Fay Hudson, Andrea Morello, David J. Reilly, and Andrew S. Dzurak. Gate-based single-shot readout of spins in silicon. *Nature Nanotechnology*, 14:437–441, March 2019. ISSN 1748-3387, 1748-3395. doi:10.1038/s41565-019-0400-7. URL <http://www.nature.com/articles/s41565-019-0400-7>.
- [316] W. K. Wootters. Statistical distance and Hilbert space. *Physical Review D*, 23(2):357–362, January 1981. ISSN 0556-2821. doi:10.1103/PhysRevD.23.357. URL <https://link.aps.org/doi/10.1103/PhysRevD.23.357>.
- [317] X. Wu, D. R. Ward, J. R. Prance, D. Kim, J. K. Gamble, R. T. Mohr, Z. Shi, D. E. Savage, M. G. Lagally, M. Friesen, S. N. Coppersmith, and M. A. Eriksson. Two-axis control of a singlet-triplet qubit with an integrated micromagnet. *Proceedings of the National Academy of Sciences*, 111(33):11938–11942, August 2014. ISSN 0027-8424, 1091-6490. doi:10.1073/pnas.1412230111. URL <http://www.pnas.org/cgi/doi/10.1073/pnas.1412230111>.
- [318] M. Xiao, M. G. House, and H. W. Jiang. Measurement of the Spin Relaxation Time of Single Electrons in a Silicon Metal-Oxide-Semiconductor-Based Quantum Dot. *Physical Review Letters*, 104(9):096801, March 2010. ISSN 0031-9007, 1079-7114. doi:10.1103/PhysRevLett.104.096801. URL <https://link.aps.org/doi/10.1103/PhysRevLett.104.096801>.
- [319] Gang Xu, Yan Li, Fei Gao, Hai-Ou Li, He Liu, Ke Wang, Gang Cao, Ting Wang, Jian-Jun Zhang, Guang-Can Guo, and Guo-Ping Guo. Dipole coupling of a hole double quantum dot in germanium hut wire to a microwave resonator. *New Journal of Physics*, 22(8): 083068, August 2020. ISSN 1367-2630. doi:10.1088/1367-2630/aba85a. URL <https://iopscience.iop.org/article/10.1088/1367-2630/aba85a>.
- [320] X. Xue, T. F. Watson, J. Helsen, D. R. Ward, D. E. Savage, M. G. Lagally, S. N. Coppersmith, M. A. Eriksson, S. Wehner, and L. M. K. Vandersypen. Benchmarking Gate Fidelities in a Si / SiGe Two-Qubit Device. *Physical Review X*, 9(2):021011, April 2019. ISSN 2160-3308. doi:10.1103/PhysRevX.9.021011. URL <https://link.aps.org/doi/10.1103/PhysRevX.9.021011>.
- [321] Xiao Xue, Benjamin D’Anjou, Thomas F. Watson, Daniel R. Ward, Donald E. Savage, Max G. Lagally, Mark Friesen, Susan N. Coppersmith, Mark A. Eriksson, William A. Coish, and Lieven M. K. Vandersypen. Repetitive Quantum Nondemolition Measurement and Soft Decoding of a Silicon Spin Qubit. *Physical Review X*, 10(2):021006, April 2020. ISSN 2160-3308. doi:10.1103/PhysRevX.10.021006. URL <https://link.aps.org/doi/10.1103/PhysRevX.10.021006>.
- [322] Xiao Xue, Bishnu Patra, Jeroen P. G. van Dijk, Nodar Samkharadze, Sushil Subramanian, Andrea Corna, Brian Paquet Wuetz, Charles Jeon, Farhana Sheikh, Esdras Juarez-Hernandez, Brando Perez Esparza, Huzaifa Rampurawala, Brent Carlton, Surej Ravikumar, Carlos Nieva, Sungwon Kim, Hyung-Jin Lee, Amir Sammak, Giordano Scappucci, Menno Veldhorst, Fabio Sebastian, Masoud Babaie, Stefano Pellerano, Edoardo Charbon, and Lieven M. K. Vandersypen. CMOS-based cryogenic control of silicon quantum circuits. *Nature*, 593(7858):205–210, May 2021. ISSN 0028-0836, 1476-4687. doi:10.1038/s41586-021-03469-4. URL <http://www.nature.com/articles/s41586-021-03469-4>.
- [323] Xiao Xue, Maximilian Russ, Nodar Samkharadze, Brennan Undseth, Amir Sammak, Giordano Scappucci, and Lieven M. K. Vandersypen. Quantum logic with spin qubits crossing the surface code threshold. *Nature*, 601(7893):343–347, January 2022. ISSN 0028-0836, 1476-4687. doi:10.1038/s41586-021-04273-w. URL <https://www.nature.com/articles/s41586-021-04273-w>.
- [324] C. H. Yang, A. Rossi, R. Ruskov, N. S. Lai, F. A. Mohiyaddin, S. Lee, C. Tahan, G. Klimeck, A. Morello, and A. S. Dzurak. Spin-valley lifetimes in a silicon quantum dot with tunable valley splitting. *Nature Communications*, 4:2069, June 2013. ISSN 2041-1723. doi:10.1038/ncomms3069. URL <http://www.nature.com/doifinder/10.1038/ncomms3069>.

- [325] C. H. Yang, K. W. Chan, R. Harper, W. Huang, T. Evans, J. C. C. Hwang, B. Hensen, A. Laucht, T. Tanttu, F. E. Hudson, S. T. Flammia, K. M. Itoh, A. Morello, S. D. Bartlett, and A. S. Dzurak. Silicon qubit fidelities approaching incoherent noise limits via pulse engineering. *Nature Electronics*, 2(4):151–158, April 2019. ISSN 2520-1131. doi:10.1038/s41928-019-0234-1. URL <https://www.nature.com/articles/s41928-019-0234-1>. arXiv: 1807.09500.
- [326] C. H. Yang, R. C. C. Leon, J. C. C. Hwang, A. Saraiva, T. Tanttu, W. Huang, J. Camirand Lemyre, K. W. Chan, K. Y. Tan, F. E. Hudson, K. M. Itoh, A. Morello, M. Pioro-Ladrière, A. Laucht, and A. S. Dzurak. Operation of a silicon quantum processor unit cell above one kelvin. *Nature*, 580(7803):350–354, April 2020. ISSN 0028-0836, 1476-4687. doi:10.1038/s41586-020-2171-6. URL <http://www.nature.com/articles/s41586-020-2171-6>.
- [327] J. Yoneda, T. Otsuka, T. Nakajima, T. Takakura, T. Obata, M. Pioro-Ladrière, H. Lu, C. J. Palmstrøm, A. C. Gossard, and S. Tarucha. Fast Electrical Control of Single Electron Spins in Quantum Dots with Vanishing Influence from Nuclear Spins. *Physical Review Letters*, 113(26):267601, December 2014. ISSN 0031-9007, 1079-7114. doi:10.1103/PhysRevLett.113.267601. URL <https://link.aps.org/doi/10.1103/PhysRevLett.113.267601>.
- [328] J. Yoneda, K. Takeda, A. Noiri, T. Nakajima, S. Li, J. Kamioka, T. Kodera, and S. Tarucha. Quantum non-demolition readout of an electron spin in silicon. *Nature Communications*, 11(1):1144, March 2020. ISSN 2041-1723. doi:10.1038/s41467-020-14818-8. URL <http://www.nature.com/articles/s41467-020-14818-8>.
- [329] Jun Yoneda, Kenta Takeda, Tomohiro Otsuka, Takashi Nakajima, Matthieu R. Delbecq, Giles Allison, Takumu Honda, Tetsuo Kodera, Shunri Oda, Yusuke Hoshi, Noritaka Usami, Kohei M. Itoh, and Seigo Tarucha. A quantum-dot spin qubit with coherence limited by charge noise and fidelity higher than 99.9%. *Nature Nanotechnology*, 13:102–106, December 2017. ISSN 1748-3387, 1748-3395. doi:10.1038/s41565-017-0014-x. URL <http://www.nature.com/articles/s41565-017-0014-x>.
- [330] D. M. Zajac, T. M. Hazard, X. Mi, E. Nielsen, and J. R. Petta. Scalable Gate Architecture for a One-Dimensional Array of Semiconductor Spin Qubits. *Physical Review Applied*, 6(5):054013, November 2016. ISSN 2331-7019. doi:10.1103/PhysRevApplied.6.054013. URL <https://link.aps.org/doi/10.1103/PhysRevApplied.6.054013>.
- [331] D. M. Zajac, A. J. Sigillito, M. Russ, F. Borjans, J. M. Taylor, G. Burkard, and J. R. Petta. Resonantly driven CNOT gate for electron spins. *Science*, 359(6374):439–442, December 2017. ISSN 0036-8075, 1095-9203. doi:10.1126/science.aoa5965. URL <http://www.sciencemag.org/lookup/doi/10.1126/science.aoa5965>.
- [332] Xin Zhang, Rui-Zi Hu, Hai-Ou Li, Fang-Ming Jing, Yuan Zhou, Rong-Long Ma, Ming Ni, Gang Luo, Gang Cao, Gui-Lei Wang, Xuedong Hu, Hong-Wen Jiang, Guang-Can Guo, and Guo-Ping Guo. Giant Anisotropy of Spin Relaxation and Spin-Valley Mixing in a Silicon Quantum Dot. *Physical Review Letters*, 124(25):257701, June 2020. ISSN 0031-9007, 1079-7114. doi:10.1103/PhysRevLett.124.257701. URL <https://link.aps.org/doi/10.1103/PhysRevLett.124.257701>.
- [333] R. Zhao, T. Tanttu, K. Y. Tan, B. Hensen, K. W. Chan, J. C. C. Hwang, R. C. C. Leon, C. H. Yang, W. Gilbert, F. E. Hudson, K. M. Itoh, A. A. Kiselev, T. D. Ladd, A. Morello, A. Laucht, and A. S. Dzurak. Single-spin qubits in isotopically enriched silicon at low magnetic field. *Nature Communications*, 10(1):5500, December 2019. ISSN 2041-1723. doi:10.1038/s41467-019-13416-7. URL <http://www.nature.com/articles/s41467-019-13416-7>.
- [334] Guoji Zheng, Nodar Samkharadze, Marc L. Noordam, Nima Kalhor, Delphine Brousse, Amir Sammak, Giordano Scappucci, and Lieven M. K. Vandersypen. Rapid gate-based spin read-out in silicon using an on-chip resonator. *Nature Nanotechnology*, 14(8):742–746, August 2019. ISSN 1748-3387, 1748-3395. doi:10.1038/s41565-019-0488-9. URL <http://www.nature.com/articles/s41565-019-0488-9>.
- [335] A. M. J. Zwerver, T. Krähenmann, T. F. Watson, L. Lampert, H. C. George, R. Pillarisetty, S. A. Bojarski, P. Amin, S. V. Amitonov, J. M. Boter, R. Caudillo, D. Correas-Serrano, J. P. Dehollain, G. Droulers, E. M. Henry, R. Kotlyar, M. Lodari, F. Lüthi, D. J. Michalak, B. K. Mueller, S. Neyens, J. Roberts, N. Samkharadze, G. Zheng, O. K. Zietz, G. Scappucci, M. Veldhorst, L. M. K. Vandersypen, and J. S. Clarke. Qubits made by advanced semiconductor manufacturing. *Nature Electronics*, 5(3):184–190, March 2022. ISSN 2520-1131. doi:10.1038/s41928-022-00727-9. URL <https://www.nature.com/articles/s41928-022-00727-9>.